IOWA STATE UNIVERSITY
Digital Repository

2001

Embankment foundation reinforcement using rammed aggregate piers in Iowa soils

Aaron Jon Gaul
Iowa State University

Follow this and additional works at: https://lib.dr.iastate.edu/rtd

Part of the Construction Engineering and Management Commons, Geotechnical Engineering Commons, and the Structural Engineering Commons

Recommended Citation

Gaul, Aaron Jon, "Embankment foundation reinforcement using rammed aggregate piers in Iowa soils" (2001). *Retrospective Theses and Dissertations*. 16901.
https://lib.dr.iastate.edu/rtd/16901

Embankment foundation reinforcement using

rammed aggregate piers in Iowa soils

by

Aaron Jon Gaul

A thesis submitted to the graduate faculty

in partial fulfillment of the requirements for the degree of

MASTER OF SCIENCE

Major: Civil Engineering (Geotechnical Engineering)

Major Professor: John M. Pitt

Iowa State University

Ames, Iowa

2001

Graduate College
Iowa State University

This is to certify that the Master's thesis of

Aaron Jon Gaul

has met the thesis requirements of Iowa State University

Signatures have been redacted for privacy

TABLE OF CONTENTS

LIST OF FIGURES

LIST OF TABLES

INTRODUCTION

Background

Constructing embankments and infrastructure on soft foundation soils can have problematic and costly effects during both the construction phase and thereafter, e.g. total and differential settlement, insufficient bearing capacity and slope failures. Despite the fact that engineers have been familiar with the problems inherent in building on soft soils for many years, improvement techniques remain costly and limited (Hughes and Withers, 1974). Alternatives to traditional improvement techniques such as deep foundations, preloading (preconsolidation) methods and overexcavation and replacement methods are continually sought after in hopes of gaining more options when encountering soft soils.

As an alternative to long-established soil improvement techniques rammed aggregate piers (Geopier™ foundation elements) have been installed within and around the Ramp "C" abutment footprint for the I-35 overpass at the Hwy 5/I-35 interchange in Des Moines, IA. The rammed aggregate piers were installed in an effort to reduce total settlement and increase the rate of consolidation settlement in the soft alluvial clay. The primary goal of the pier installation was to reduce the construction delay between embankment and abutment construction. The area of the abutment is a staged earthwork construction. The initial four to five meters of fill was placed in July 2000 and the final four to five meters of fill will be placed during spring or summer 2001. At the adjacent Ramp "B" bridge abutment stone columns were installed in the foundation soils to increase slope stability at the interface between the silty alluvium and weathered shale. Seven to eight meters of fill was placed during July 2000 and abutment construction has begun. Although the main focus of this investigation is to evaluate embankment foundation reinforcement using rammed aggregate

piers, the stone column reinforced soil was investigated for a comparative analysis to the rammed aggregate pier reinforced soil.

Objectives/Scope of Study

The primary objective of this research is to investigate embankment foundation reinforcement using rammed aggregate piers in Iowa soils. Stone columns were also investigated in a similar application and compared to rammed aggregate piers. The IA Hwy 5/I-35 overpass project site was the primary research site for this investigation.

In-situ testing including piezocone penetrometer (CPTU), pressuremeter (PMT), K_o-stepped blade and borehole shear (BST) tests as well as extensive laboratory testing have been conducted to investigate rammed aggregate piers' and stone columns' effects on lateral stress, settlement, stress concentrations and rate of consolidation settlement. Comparative stiffness and densities of rammed aggregate piers and stone columns were also evaluated based on full-scale load tests and standard penetration (SPT) tests. Vibrating wire instrumentation including settlement cells and total pressure cells were installed for continuous and long-term (5 year) monitoring of the piers, columns and embankments. Settlement plates were installed and monitored by conventional survey methods.

Rammed aggregate piers encompass a relatively simple concept, nevertheless, recent case histories have shown that some structures constructed on aggregate pier reinforced soils have performed considerably better than predicted (Lawton and Fox, 1994; Lawton et al., 1994; Handy et al., 1999). The use of rammed aggregate piers has increased since their introduction in 1988, yet their behavior under load is not thoroughly understood. Research on rammed aggregate piers is necessary to better understand the complex pier-soil matrix

interaction under load. A better understanding of the load transfer mechanism of the piers and the pier-soil matrix interaction is hoped to be gained through the investigation described herein.

REVIEW OF LITERATURE

Review of Construction Processes

Rammed aggregate piers may appear similar to stone columns in many ways, but the characteristics unique to the rammed aggregate pier foundation system have resulted in an award of a U.S. patent, with international patents pending (Fox and Lawton, 1993). These unique characteristics are summarized as follows:

1. The piers are designed primarily to stiffen the subgrade soil. Strengthening of the subgrade soil and increased drainage are secondary considerations.

2. Aggregate piers are short, typically only two to three times as tall as they are wide. The piers are not typically extended to stronger, deeper soil zones.

3. Construction of aggregate piers involves the formation of a cavity by removal of matrix soil, rather than by lateral or vertical soil displacement. To a large extent the soil's natural cementation and fabric are preserved.

4. Aggregate piers are constructed using impact densification methods with relatively high impact frequency, rather than vibratory methods.

5. Aggregate piers are densified in thin lifts, prestraining, prestressing, and densifying adjacent matrix soils and producing very dense and very stiff foundation elements, thereby reducing vertical displacements upon application of structural loads (Lawton and Fox, 1994).

Rammed aggregate pier construction process

The major steps in the construction process of a rammed aggregate pier within a soil matrix are illustrated in Figure 1 and are summarized as follows:

1. A cylindrical or rectangularly prismatic cavity is formed in the soil by using either an auger or a backhoe.

2. The soils at the bottom of the cavity are densified and prestressed by repeated impact from a specially designed tamper with a beveled head.

3. Typically well-graded aggregate (normally highway base course stone) is placed loosely at the bottom of the cavity in a thin lift.

4. The aggregate is highly densified by repeated ramming from the tamper, which also prestresses the soil laterally.

5. Compacted lifts are added until the desired height is achieved (Lawton and Fox, 1994).

Reportedly, the result is a composite reinforced aggregate pier-soil matrix of improved modulus, stiffness, and capacity to control settlement (Lawton and Fox, 1994). Figure 2 shows a photograph of an auger removing saturated clay from the cavity (step 1). Figure 3 shows a photograph of aggregate being placed into the cavity and the beveled tamper is also shown (step 3).

Stone column construction process

The major steps in the construction process of a stone column within a soil matrix are illustrated in Figure 4 and are described as follows:

1. A cylindrical cavity is formed by inserting a long (10 m) thin (0.5 m diameter) vibrating tube into the soil. The vibrating tube is suspended from a crane and is known as a vibroflot.

2. Air or water at high pressure is forced out of the bottom of the tube. This combination of vibration and jetting forms the cavity in a matter of minutes. No excavation is necessary as the cavity is formed by soil displacement.

(a)

(b)

(c)

(d)
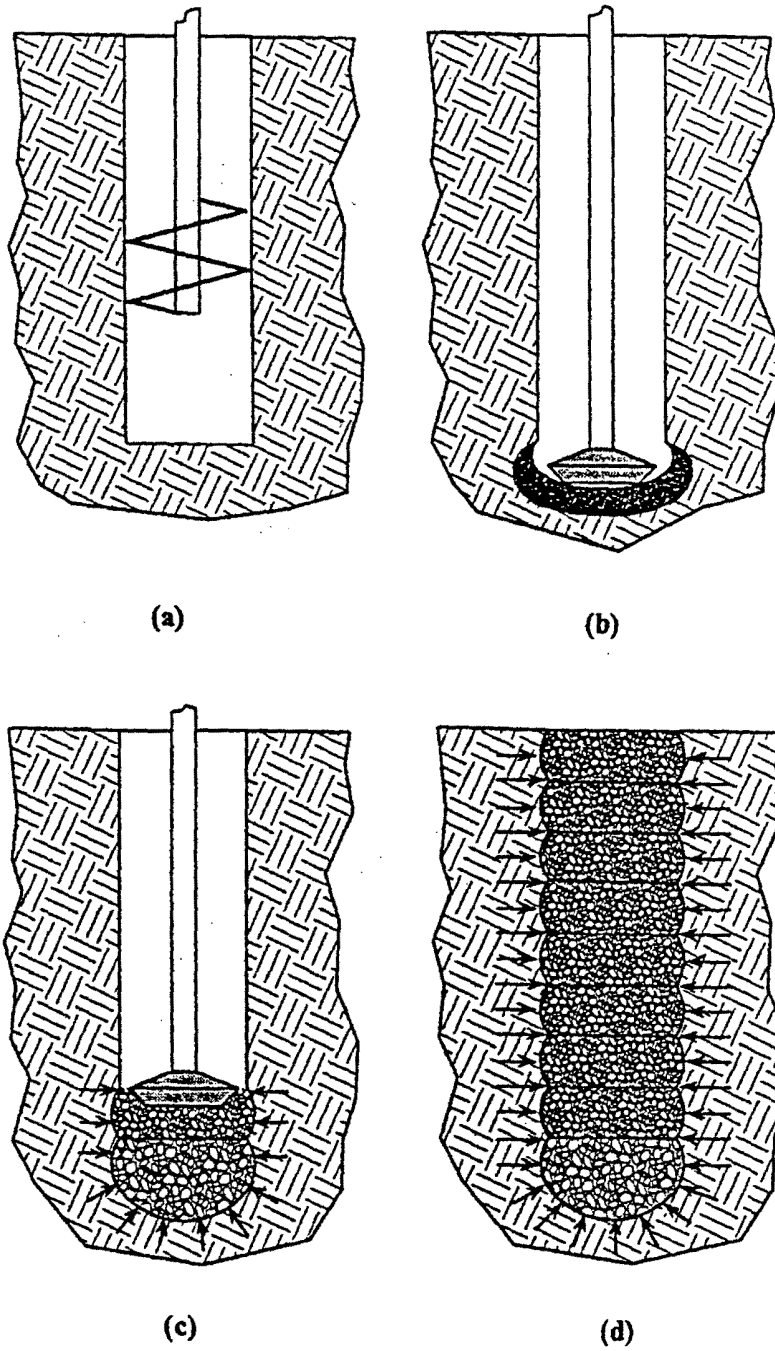
Figure 1. Construction process of a rammed aggregate pier

Figure 2. Auger removing saturated clay from cavity (step 1)

Figure 3. Aggregate placed into cylindrical cavity (beveled tamper also shown) (step 3)
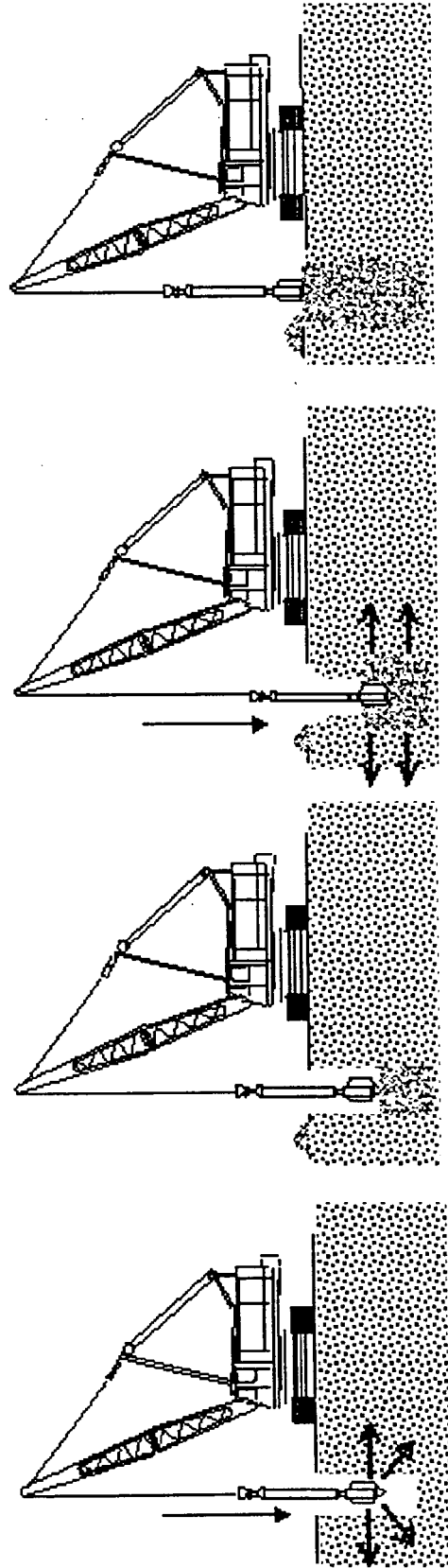
Figure 4. Construction process of a stone column (from www.menard-soltraitement.com)

3. The instrument is withdrawn partially and the hole is backfilled with granular material fed through the tube.

4. The backfilling is typically done in layers and the granular backfill is compacted by lowering the vibroflot on to the top of the granular backfill.

5. Alternating backfilling and compacting are done to form a continuous column (Hughes and Withers, 1974).

Figure 5 shows a photograph of the vibroflot suspended from a crane (step 1). Figure 6 shows the vibroflot penetrating the ground creating a cavity by vibration and air jetting (step 2).

Review of Design Methodology

Tributary area concept

The analysis presented for the comparison of rammed aggregate piers and stone columns will utilize the unit cell concept. It should be noted that the proprietors of rammed aggregate piers (Geopier^{TM} foundation elements) utilize their own design method for the design of rammed aggregate pier reinforced foundations. The unit cell, which includes the aggregate elements and the surrounding matrix soil, is approximated by a cylinder with an effective diameter dependent upon the spacing of the columns or piers. The unit cell is illustrated in Figure 7. Goughnour (1983) stated that the effective diameter, D_e, of the unit cell is chosen so that the cross-sectional area of the unit cell is equal to that of the tributary area per column, i.e. $D_e = 1.05s$ for a triangular pattern and $D_e = 1.13s$ for a square pattern, where "s" is the distance center to center between columns or piers. The tributary area per column is shown in Figure 8 for triangular and square pattern arrangements.

Figure 5. Vibroflot suspended from a crane (step 1)
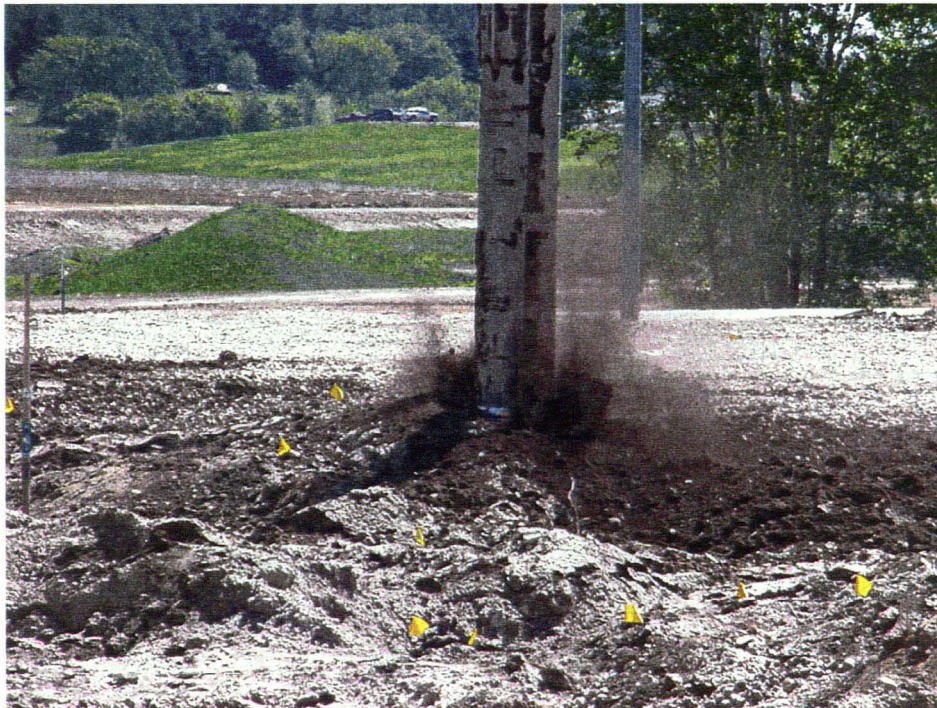
Figure 6. Vibroflot penetrating the ground creating a cavity by vibration and air jetting (step 2)
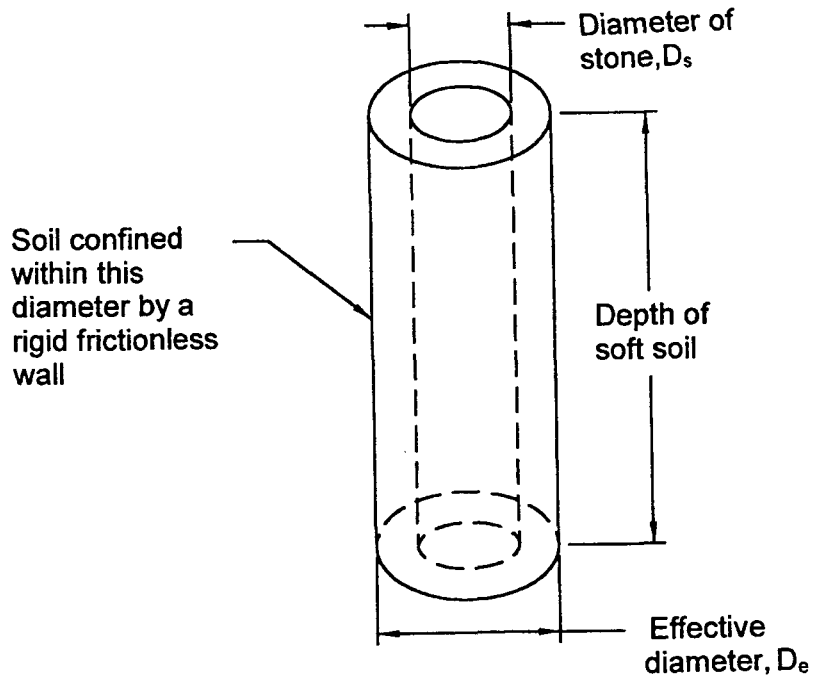
Figure 7. Assumed unit cell (after Goughnour, 1983)
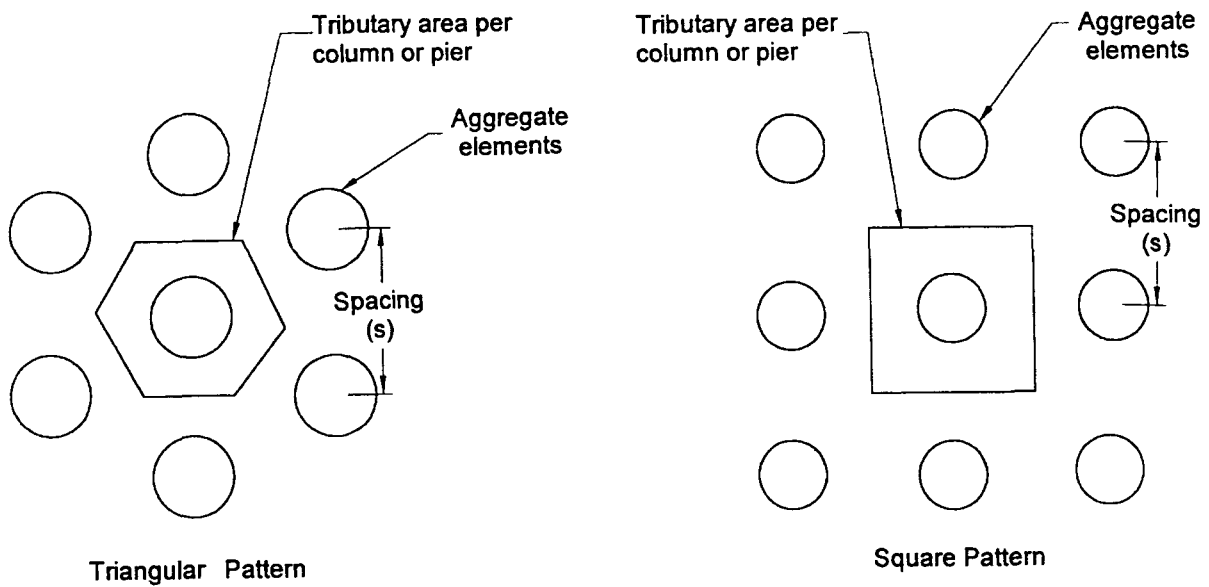
Figure 8. Tributary area definition (after Goughnour, 1983)

Barksdale and Brachus (1983) have presented a method for analyzing stone columns applying the unit cell concept. This methodology will be utilized to compare stress concentrations and settlement reductions of rammed aggregate pier and stone column reinforced soils.

An essential parameter in the analysis is the ratio of aggregate area to the total cross sectional area of the unit cell. This parameter is known as the area replacement ratio, a_s, and will later be related to key factors used to compare rammed aggregate piers and stone columns. The area replacement ratios for triangular and square arrangements are as follows, respectively:

$$a_s = 0.907 \left(\frac{D_s}{s} \right)^2 \tag{1}$$

$$a_s = 0.785 \left(\frac{D_s}{s} \right)^2 \tag{2}$$

where D_s is the diameter of the aggregate foundation.

Geopier™ foundation design methodology

The proprietors of rammed aggregate piers (Geopier Foundation Company) utilize a different design method than the tributary area concept. A major difference in the method is that the design of a Geopier reinforced soil is typically controlled by settlement criteria rather than bearing capacity criteria. Geopier foundation design methodology is not described in detail in published literature and the design is typically done under the supervision of Geopier foundation engineers.

Review of Reinforcement Evaluation

This review will define several key factors for a comparative evaluation of the effects stone columns and rammed aggregate piers have on matrix soils. Key factors used to evaluate and compare the behavior of rammed aggregate piers and stone columns include their effects on settlement, stress concentrations, rate of consolidation, and the influence of lateral stress on the surrounding soils.

Settlement effects

Settlement is a primary concern in nearly all types of construction on soils, e.g. highways, bridges, storage structures, buildings, embankments, etc. When tolerable levels of settlements are exceeded, structures can fail structurally despite large factors of safety against shear failure used in foundation design (See Lambe and Whitman, 1969, p. 199-202 for general guidance on allowable total and differential settlements for various structures). Structural damage is not the only concern when dealing with settlement; settlements must also be minimized to not detract from the appearance of a structure causing unsightly cracks and tilting as a result of differential settlements. Lambe and Whitman (1969) have listed a number of ways in which settlements can interfere with the function of a structure, e.g. cranes and other equipment may not operate correctly; pumps, compressors, etc., may get out of line; tracking units such as radar may become inaccurate; and utilities such as gas, water, or sewage may become disconnected. Even though settlement has long been an issue in foundation design, techniques to reduce settlements continue to be costly and limited.

Hughes and Withers (1974) have summarized common settlement reduction techniques as follows:

1. Piling, using friction alone in deep deposits or point bearing on hard stratum underlying the soft clay.

2. Preloading (preconsolidation), to reduce settlements.

3. Sand drains, to accelerate consolidation settlements.

4. Replacing the soft soils, either with stronger material or a buoyant foundation.

5. Stone columns.

And in recent years, the use of rammed aggregate piers.

The first four methods have been well understood for quite some time, but the behaviors under load of stone columns and rammed aggregate piers are not yet thoroughly understood. Continued research on stone columns and rammed aggregate pier foundation elements is necessary for a better understanding of the complex pier-soil matrix interaction under loads.

Although stone columns and rammed aggregate piers are different in many ways as previously mentioned, the proprietors of both make similar claims as to the many roles each play in reinforcing soft soils. The following list summarizes the primary and secondary roles the proprietors of rammed aggregate piers and stone columns have claimed to be inherent within the improvement system:

1. Increased bearing capacity (Lawton and Fox, 1994; Hughes and Withers, 1974).

2. Increased subgrade drainage, thus increasing the rate of consolidation (Stewart and Martin, 1984; Lawton and Fox, 1994; Hughes and Withers, 1974).

3. Initial compaction of the matrix soils during installation (Lawton and Fox, 1994; Hughes and Withers, 1974).

4. Increased lateral stresses upon installation and loading (Lawton and Fox, 1994; Hughes and Withers, 1974).

5. Partial replacement of softer soils by a stronger material (Lawton and Fox, 1994; Hughes and Withers, 1974).

Ground settlements under load in unreinforced and reinforced soils depend not only on the composition of the soil and of the aggregate foundation, but also in the complex interaction between the two. As a measure of effectiveness of settlement reduction we will consider the ratio of settlement of the reinforced soil, S_r, to the settlement of the unreinforced soil, S_u. The inverse of the settlement ratio is known as the improvement factor. The settlement ratio and improvement factor will be denoted as follows, respectively:

$$SR = \frac{S_r}{S_u} \qquad (3)$$

$$IF = \frac{1}{SR} \qquad (4)$$

Recent case histories and laboratory tests have demonstrated rammed aggregate piers to be several times as effective at reducing settlements as stone columns. Table 1 displays a summary of SR and IF values measured from recent case histories, laboratory model tests and estimates from theory for both stone column and rammed aggregate pier reinforced soils.

Stress concentrations

Reportedly, when rammed aggregate piers and stone columns are introduced into soft soils, the result is an increase in bearing capacity of the natural soils (Lawton and Fox, 1994). Although not a primary function of stone columns and rammed aggregate piers, additional drainage is provided by the aggregate foundation. By reducing the drainage length, soft soils

Table 1. Summary of settlement ratios (SR) for stone column and rammed aggregate pier reinforced soils

Foundation Type	SR	IF	Obtained From	Reference
Stone Columns	0.5	2.0	Elastic Theory	Buggy, Martinez, Hussin, and Deschamps (1994)
Stone Columns	0.5	2.0	Load Tests	Brinoli, Garassino, and Renzo (1994)
Stone Columns	0.6	1.7	Laboratory Models	Stewart and Fahey (1984)
Stone Columns	0.4	2.5	Est. Method-Elastic	Balaam and Booker (1985)
Stone Columns	0.7	1.4	Est. Method-Plastic	Balaam and Booker (1985)
Stone Columns	0.75	1.3	Estimation	Greenwood (1970)
Stone Columns	0.8	1.3	Estimation	Van Imp (1989)
Rammed Aggregate Piers	0.2	5.0	Case History [b]	Lawton, Fox, and Handy (1994)
Rammed Aggregate Piers	0.17	5.9	Load Tests	Lawton and Fox (1994)
Rammed Aggregate Piers	0.10[a]	10[a]	Case Histories [b]	Lawton and Fox (1994)
Rammed Aggregate Piers	0.17[a]	5.9[a]	Predicted [c]	Lawton and Fox (1994)

[a] Average values of SR and IF from 10 case histories presented by Lawton and Fox (1994).
[b] Settlements of S_u were estimated using Bowels (1988) and Schmertmann (1970) and values of S_r were attained by means of field surveys.
[c] Settlements of S_u and S_r were estimated using Bowels (1988), Schmertmann (1970), and Schmertmann et al. (1978).

will consolidate more rapidly upon loading and the result will be a load transfer to the stone (Goughnour, 1983; Lawton et al., 1994). As consolidation continues, a substantial portion of the bearing load is transferred to the dense, stiff elements of the aggregate reinforcement. The result is a concentration of stress occurring in the aggregate elements and a stress reduction in the matrix soils, which may inhibit settlement. The significance of this load transfer is evident by the ratio of bearing stress applied to the piers to the bearing stress

applied to the adjacent matrix soil. This is known as the stress concentration ratio, n, defined as:

$$n = \frac{\sigma_f}{\sigma_s} \qquad (5)$$

where σ_f and σ_s are the total vertical stresses in the aggregate foundation and the surrounding soil, respectively.

Buggy et al., (1994) have presented a relationship between vertical loads and concentrations of stress on stone columns using the unit cell concept. For equilibrium of vertical forces, the stresses in the aggregate foundation and the surrounding soil, σ_f and σ_s, are related to a_s and "n" by the following relationships:

$$\sigma_f = \frac{n\sigma}{1+(n-1)a_s} \qquad (6)$$

$$\sigma_s = \frac{\sigma}{1+(n-1)a_s} \qquad (7)$$

where σ is the average vertical stress over the unit cell. Although the unit cell concept was originally used to describe the load transfer mechanism in stone column reinforced soils, Lawton and Fox display an agreement to equations (6) and (7) for rammed aggregate pier reinforced soils with the following statement, "The percentage of the foundation load carried by the aggregate piers is primarily a function of two factors - the areal coverage of the piers within the footprint of the footing and the relative stiffness of the piers compared to the matrix soil" (1994, p.964).

The unit cell concept can be used to design stone column or rammed aggregate pier arrangements. After choosing the pier or column diameter (D_s) and spacing (s) for a selected

arrangement pattern, a_s can be determined using equations (1) and (2). Equations (6) and (7)

can then be used to estimate the stresses on the aggregate foundation and surrounding soil by

assuming a reasonable stress concentration ratio based on previous measurements or

estimated from theory. The previous steps can be done in an iterative process until a safe

bearing load is determined. Stuart and Fayey (1984) state typical stress concentration ratios

of 3 or 4 in stone column reinforced soils while Lawton and Fox (1994) provide results of

static load tests yielding stress concentration ratios ranging from 10-20. Table 2 displays a

summary of stress concentration ratios obtained by methods of theory, laboratory models,

load tests and field measurements for both stone column and rammed aggregate pier

reinforced soils.

Influence of lateral stress

Although it has long been recognized that a variety of foundation systems such as

rammed aggregate piers, stone columns, tapered piles and other recent innovations can

induce lateral stress on adjacent soils (Hughes and Withers, 1974; Lawton and Fox, 1994), it

has not been until recent history that lateral stress has been recognized as a benefactor of the

performance of the system. Figure 9 illustrates the stresses (vertical and lateral) induced

Table 2. Summary of stress concentration ratios (n) for stone columns and rammed aggregate piers

Foundation Type	n	Obtained From	Overlying Material	Reference
Stone columns	3.8	Field measurements	N/A[a]	Greenwood and Kirsch (1983)
Stone columns	4.0	N/A[a]	N/A[a]	Mitchell (1981)
Stone columns	4.1	Laboratory models	Rigid plate	Stuart and Fahey (1984)
Rammed aggregate piers	10+	Load tests	Concrete	Lawton and Fox (1994)

[a] Information not available
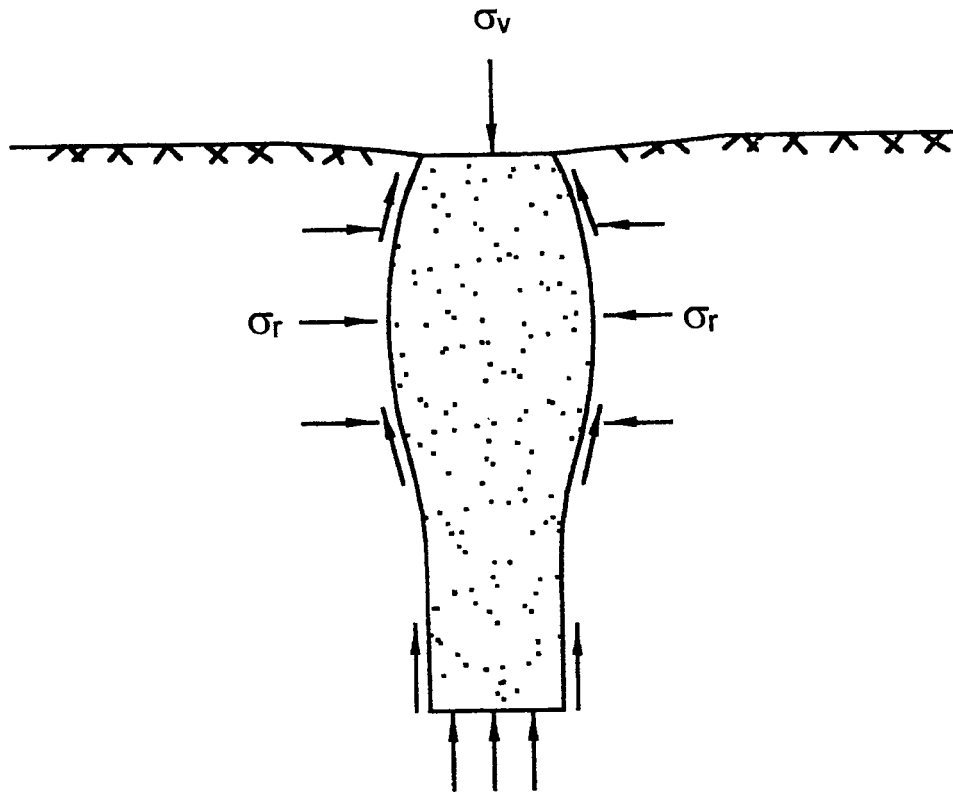
Figure 9. Stresses on a stone column under load (after Hughes and Withers, 1974)

by a loaded stone column and Figure 10 illustrates the stresses (vertical only) on a friction

pile for comparison. Figure 11 illustrates the stresses (vertical and lateral) induced into the

matrix soil as a result of impact ramming during installation of a rammed aggregate pier.

Hughes and Withers (1974) have suggested that in a stone column reinforced soil, significant

lateral stresses are not induced into the soil until the column is loaded and bulges into the

adjacent soil matrix, on the other hand, lateral stresses are induced during installation of a

rammed aggregate pier and lateral stresses are further increased in the event of deformation

and budging as settlement occurs under load (Lawton and Fox, 1994).
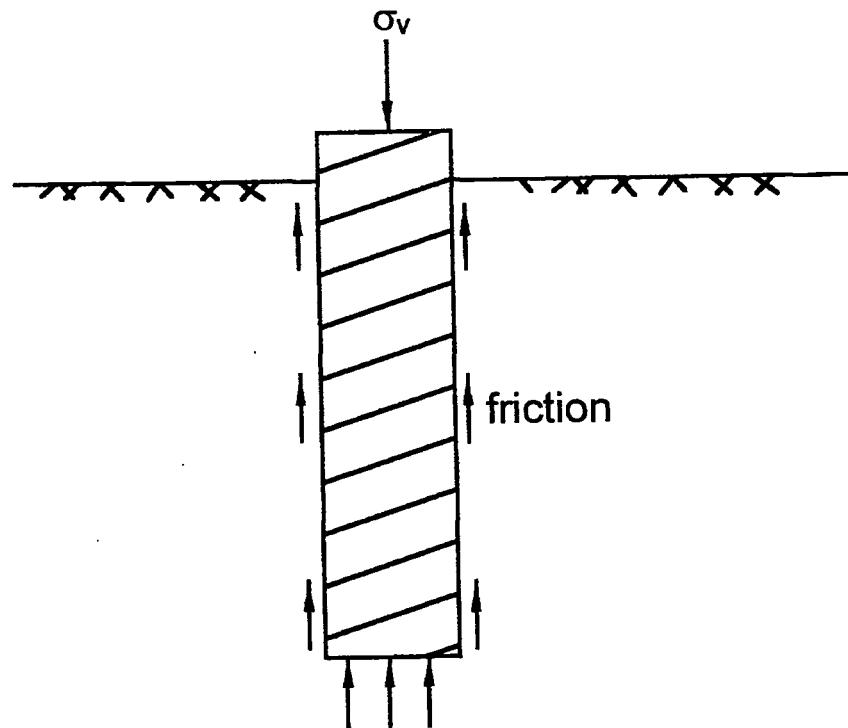
Figure 10. Stresses on a friction pile under load (after Hughes and Withers, 1974)

Recent measurements of surprisingly small settlements of structures supported by

aggregate pier reinforced soils have brought the phenomenon of induced lateral stress

inhibiting settlement into question (Lawton et al., 1994). Handy (2001) describes a

theoretical development explaining how inducing high lateral stress can reduce settlement.

The concept illustrates using elastic theory and Mohr diagrams that by imposing high lateral

stress the apparent preconsolidation pressure is increased, which in turn permits a

substantially larger applied vertical stress before consolidation will occur. Figure 12

illustrates Handy (2001). Handy (2001) explains why this phenomenon has previously not

been revealed in laboratory load testing. It is shown that this behavior cannot be revealed in
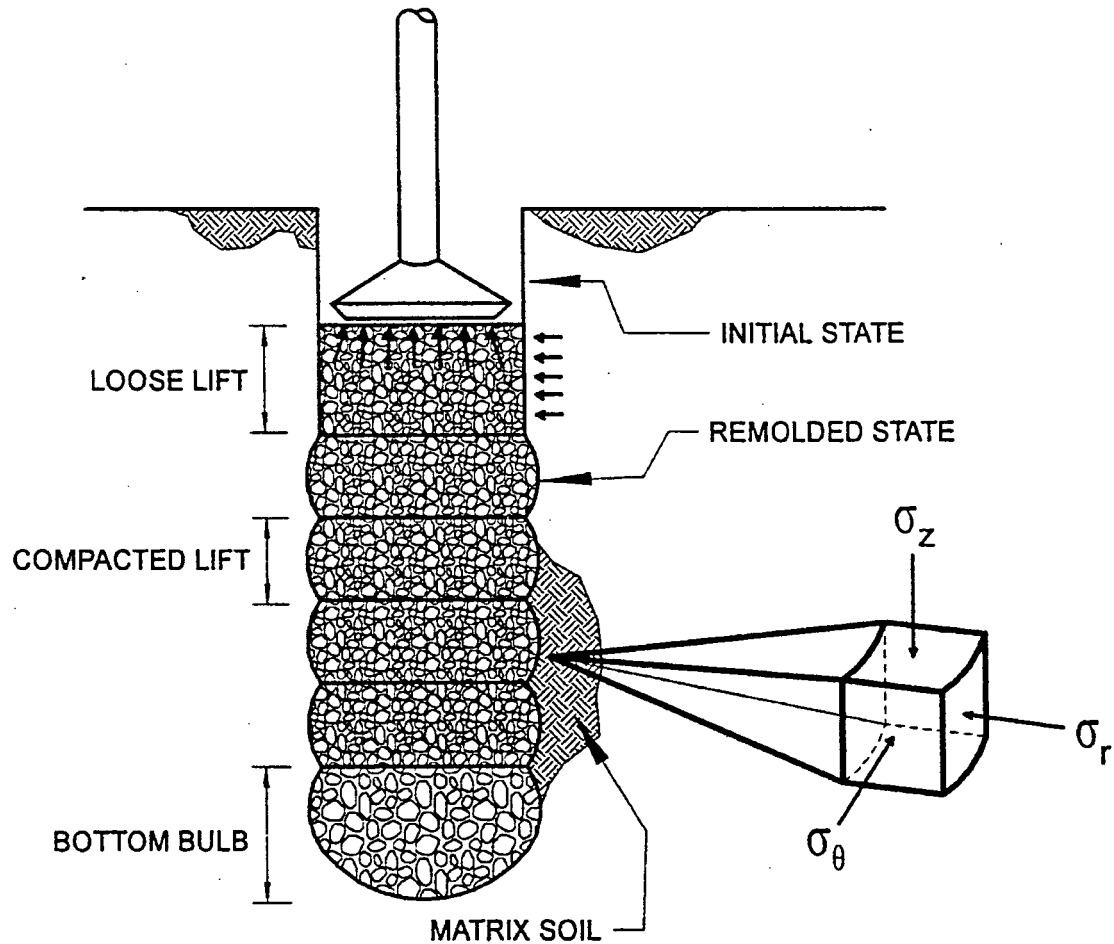
Figure 11. Stresses induced into the matrix soil as a result of impact ramming during installation of a rammed aggregate pier

ordinary consolidation testing because high lateral stresses cannot be induced before vertical loading. Handy (2001) also points out that conventional triaxial testing in which fluid pressure is applied to the top plate cannot duplicate a high initial lateral stress and low vertical stress scenario. Other considerations such as a lack of field data demonstrating a significant contribution to the performance of the foundation system have also prevented this phenomenon from being credited (White et al., 2000).
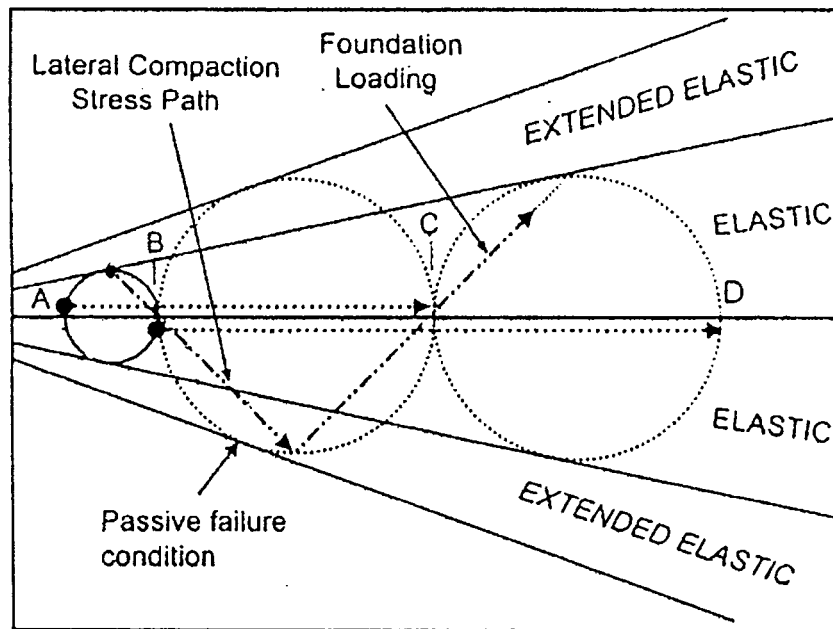
Figure 12. Mohr-Coulomb representation of Handy (2001) - Inducing lateral stress increases horizontal stress from A to C allowing vertical stress to increase from B to D before initiating consolidation (from Handy, 2001)

Rate of consolidation

Settlement is a primary concern in nearly all types of construction. In many cases the magnitude of settlement is not the only consideration, but the time for which it takes settlement to occur can also be of importance. As a load is placed on a saturated clay stratum, pore-water pressures increase proportionally to the stress increase on the surface, i.e. the load is initially carried by the pore-water. As excess pore-water pressures dissipate into more pervious stratum, the volume of voids in the soil mass is reduced, causing the soil to consolidate and settlement to occur. The time required for the pore-water pressures to dissipate is related to the permeability of the soil, i.e. more permeable soils dissipate pore-water pressures more rapidly than less permeable soils.

Additional drainage is provided by the aggregate in the rammed aggregate piers and

stone columns. The additional drainage enhances excess pore pressure dissipation and

thereby accelerates the rate of consolidation. As shown in Figure 13, Stewart and Fahey

(1984) demonstrated through laboratory experiments that the use of stone columns could

reduce the time for 50% of the excess pore pressure dissipation from 10 months to 6 months.

It is estimated that similar radial drainage contributions are made with the installation of

rammed aggregate piers.
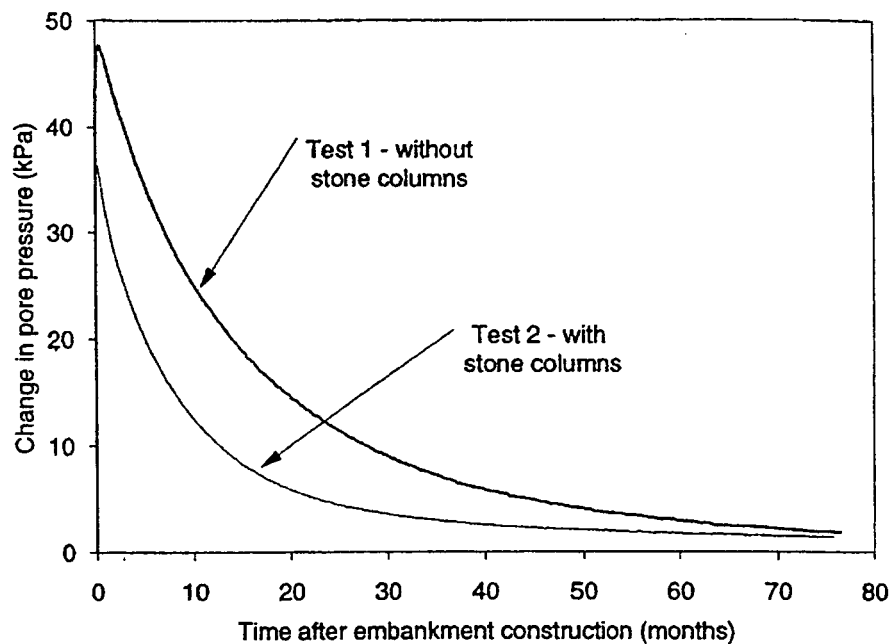
Figure 13. Pore pressure response in a clay stratum as a result of additional drainage provided by stone columns demonstrated through laboratory experiments (from Stewart and Fahey, 1984)

PROJECT LOCATION AND DESCRIPTION

At the IA Hwy 5/I-35 research site in Des Moines IA, rammed aggregate piers were installed within and around the Ramp "C" abutment footprint in an effort to reduce total settlement and increase the rate of consolidation in the soft foundation soils. Figure 14 shows location details for the research site. The primary goal of the pier installation was to reduce the construction delay between embankment and abutment construction. The area of the abutment is a staged earthwork construction. The initial four to five meters of fill was placed in July 2000 and the final four to five meters of fill will be placed during spring or summer 2001. Figure 15 is a representative cross-section of the Ramp "C" embankment.

In-situ testing was conducted prior to and following installation of the rammed aggregate piers in order to evaluate initial site conditions and the changes in matrix soil properties. Vibrating wire instrumentation was installed for continuous and long-term (5 year) monitoring of the embankment. Settlement plates were also installed and monitored by survey methods. Figure 16 shows the arrangement of rammed aggregate piers installed at Ramp "C" along with in-situ test and instrumentation locations. Table 3 lists the instrumentation and settlement plates monitored at Ramp "C" and the amount of fill placed on each following Stage 1 of embankment construction.

At the adjacent Ramp "B" bridge abutment stone columns were installed in the foundation soils to increase slope stability at the interface between the silty alluvium and weathered shale. Seven to eight meters of fill was placed during July 2000 and abutment construction has begun. The main focus of this investigation is to evaluate embankment foundation reinforcement using rammed aggregate piers, however, the stone column reinforced soil was investigated for a comparative analysis.

Stone column
reinforced zone

Rammed aggregate pier
reinforced zone

Ramp "C"

Ramp "B"

I-35

Existing IA Hwy 5
(Army Post Road)
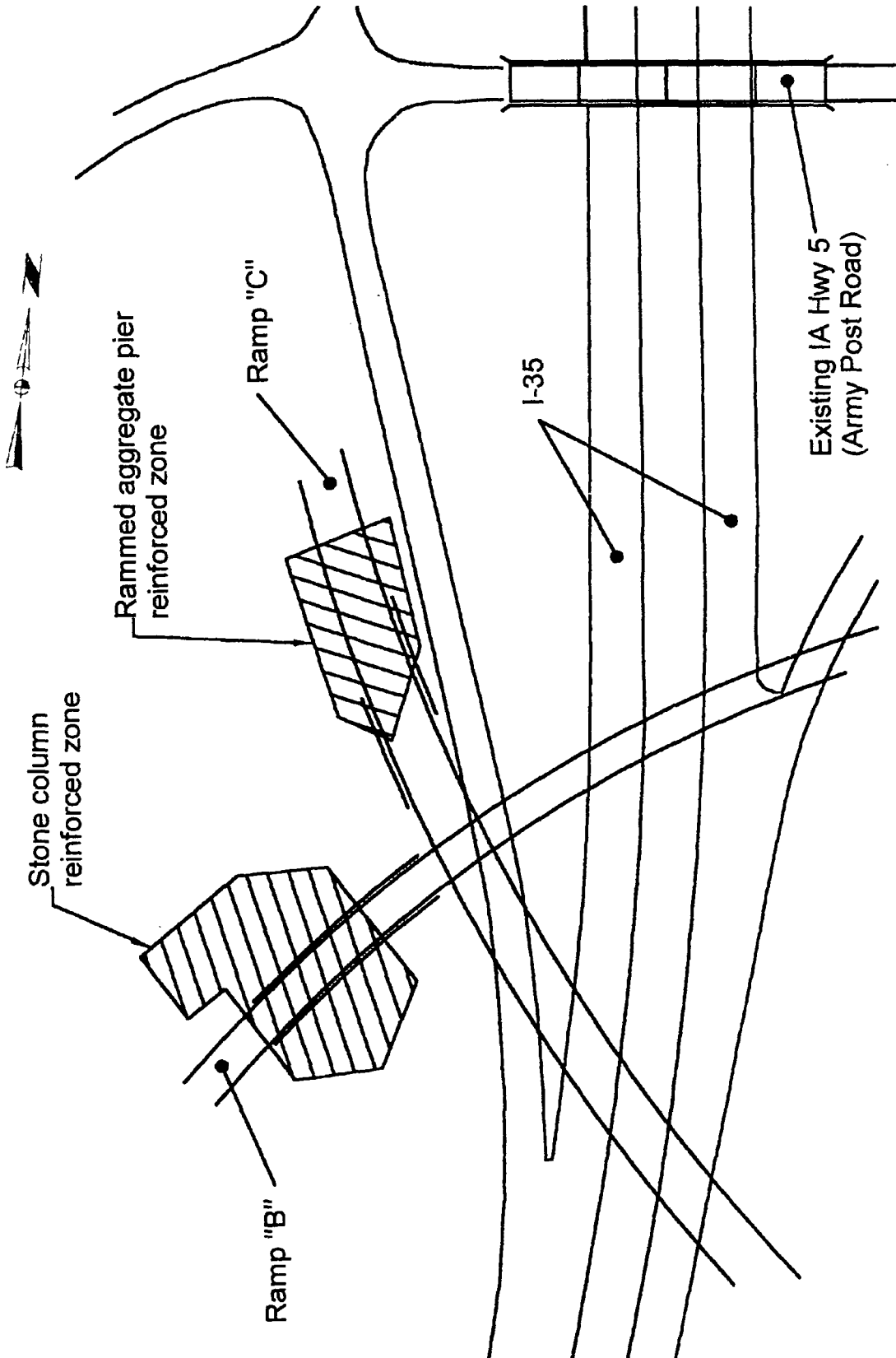
Figure 14. IA Hwy 5/I-35 research site location details
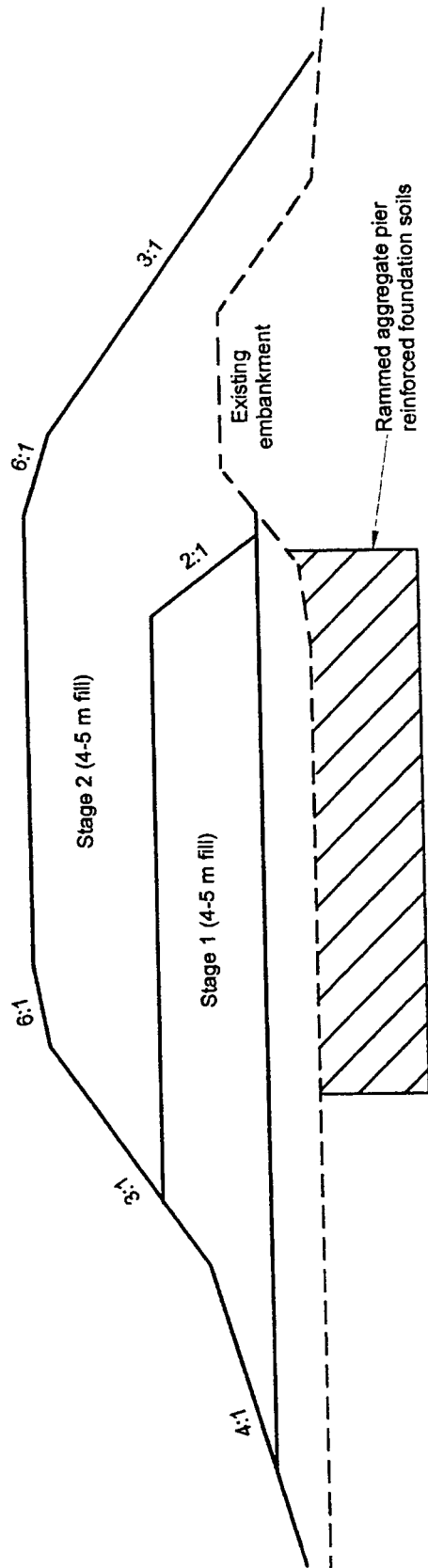
Figure 15. Ramp "C" embankment cross section

Labels within figure:
3:1
6:1
6:1
2:1
3:1
4:1
Existing embankment
Rammed aggregate pier reinforced foundation soils
Stage 2 (4-5 m fill)
Stage 1 (4-5 m fill)
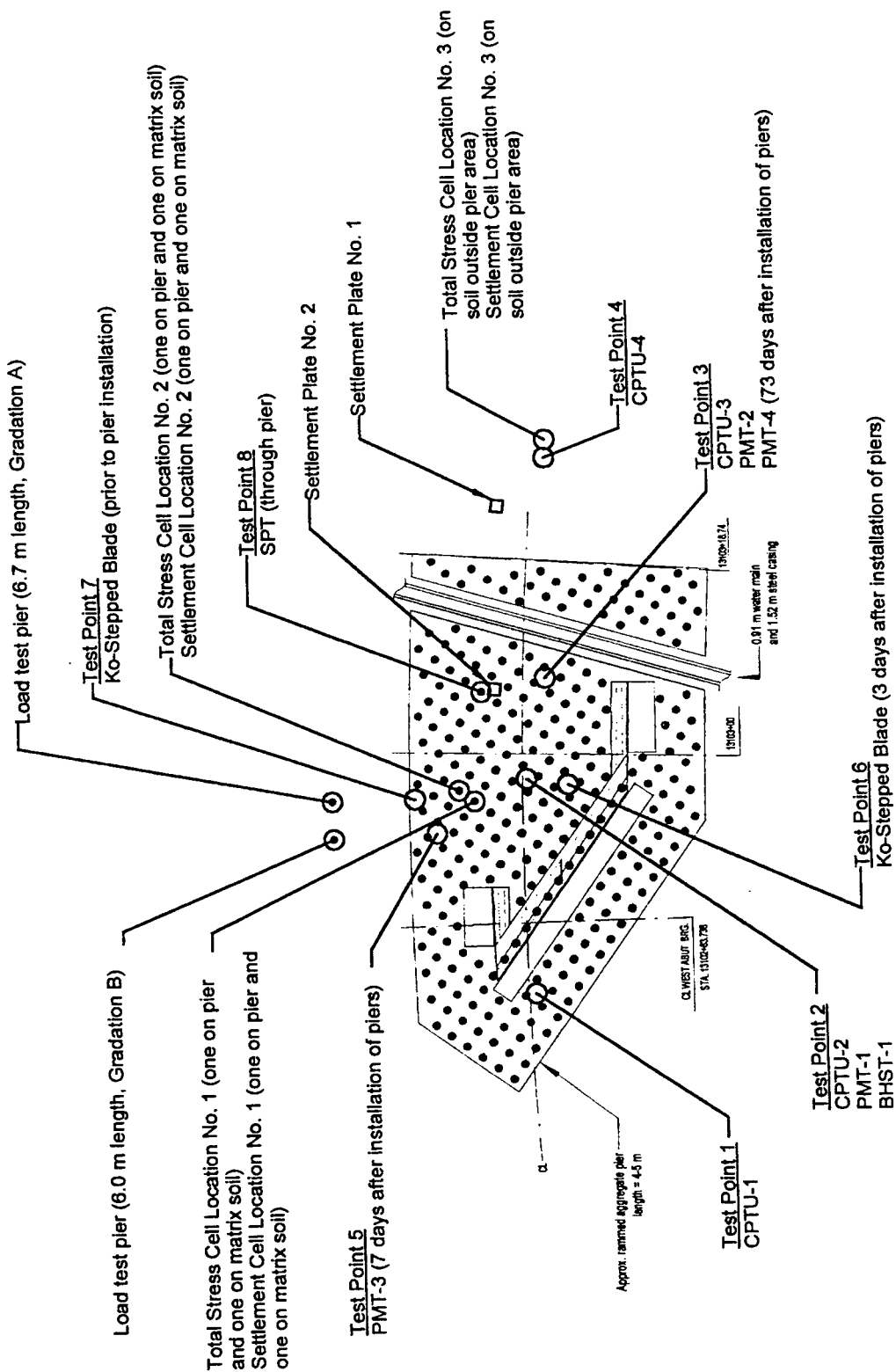
Figure 16. Ramp "C" test and instrumentation locations (black dots represent rammed aggregate piers)

Table 3. Ramp "C" instrumentation and settlement plates

Instrument Description	Fill Height (m)	Notes
Settlement Plate No. 1	5.7	Located outside rammed aggregate pier area
Settlement Plate No. 2	4.7	Located between rammed aggregate piers
Settlement cell location No. 1	2.4	One cell on and one adjacent to pier No. 105
Settlement cell location No. 2	2.4	One cell on and one adjacent to pier No. 106
Settlement cell location No. 3	5.7	Located outside rammed aggregate pier area
Total stress cell location No. 1	2.4	One cell on and one adjacent to pier No. 105
Total stress cell location No. 2	2.4	One cell on and one adjacent to pier No. 106
Total stress cell location No. 3	5.7	Located outside rammed aggregate pier area

Similar to Ramp "C", in-situ testing was conducted and vibrating wire instrumentation was monitored. Figure 17 shows the arrangement of stone columns installed at Ramp "B" along with in-situ test and instrumentation locations. Table 4 lists the instrumentation and settlement plates monitored at ramp "B" and the amount of fill placed on each. Figure 18 is a photograph of Ramp "C" looking from the south at Ramp "B" and Figure 19 is a photograph of Ramp "B" looking from the north at Ramp "C". Also shown in both photographs is the instrumentation console fenced in with orange construction fence.

Total Stress Cell Location No. 3 (one on column and one on matrix soil)

Settlement Plate No. 5 (between stone columns)

Settlement Plate No. 4 (between stone columns)

Total Stress Cell Location No. 2 (one on column and one on matrix soil)

Load test column (5.0m length, Gradation A)

Settlement Plate No. 3 (on a stone column)

Total Stress Cell Location No. 1 (one on column and one on matrix soil)

CPTU-5

Approx. stone column length = 4-6m

Approx. stone column length = 8-10m

Approx. stone column length = 2-4m

Approx. stone column length = 4-6m

Approx. stone column length = 2-4m

Ko-Stepped Blade (30 days after installation of columns)

Figure 17. Ramp "B" test and instrumentation locations (black dots represent stone columns)

Figure 18. Ramp "C" looking from the south

Figure 19. Ramp "B" looking from the north

.com

Table 4. Ramp "B" instrumentation and settlement plates

Instrument Description	Fill Height (m)	Notes
Settlement Plate No. 3	7.7	Positioned on a stone column
Settlement Plate No. 4	7.7	Located between stone columns
Settlement Plate No. 5	8.4	Located between stone columns
Total stress cell location No. 1	6.4	One cell on and one adjacent to a stone column
Total stress cell location No. 2	8.6	One cell on and one adjacent to a stone column
Total stress cell location No. 3	9.0	One cell on and one adjacent to a stone column

TESTING PROGRAM

To evaluate site conditions, in-situ and laboratory testing as well as field monitoring and verification were performed. In-situ tests were conducted prior to the installation of rammed aggregate piers (Ramp "C") and stone columns (Ramp "B") for an evaluation of pre-construction site conditions. In-situ testing was again conducted after the installation of rammed aggregate piers and stone columns for a comparative analysis of soil conditions. In addition to in-situ testing, laboratory testing was conducted on representative samples for verification of in-situ test results and to obtain additional soil strength parameters. Additional activities included observation and verification of rammed aggregate pier and embankment construction. Vibrating wire instrumentation was installed at Ramps "C" and "B" for continuous and long-term monitoring of the rammed aggregate pier and stone column reinforced foundations. The investigative procedures and results of the experiments are described herein.

Drilling and Sampling Procedures

The borings were performed with a truck-mounted, rotary drill rig using hollow-stem augers to advance the boreholes. Representative samples were obtained by 3 inch Shelby tube sampling procedures. The Shelby tube sampling procedure utilizes a thin walled, steel tube with a sharp cutting edge that is pushed hydraulically into the bottom of the boring to obtain relatively undisturbed samples of cohesive or moderately cohesive soils.

The samples were sealed and returned to the laboratory for further examination, classification and testing. Conditions encountered in each of the test borings were monitored and recorded by the drill crew.

In-Situ Testing Program and Procedures

In-situ tests have included piezocone penetrometer (CPTU), pressuremeter (PMT), standard penetration (SPT), K_o-stepped blade and borehole shear (BHST). The test procedures and results are provided herein.

Piezocone penetrometer (CPTU)

Originating and later modified by the Dutch, cone penetration soundings (CPT) are one of the most useful tests to generate a continuous subsurface profile (Riaund and Miran, 1992). According to Riaund and Miran (1992), no other conventional geotechnical tool can match the CPT for layer definition and low cost per foot. Data is obtained by means of a cone hydraulically pushed into the soil while continuous measurements of penetration resistance and friction resistance are taken. In addition to the standard cone, the piezocone measures pore-water pressures by means of a pore pressure sensor near the penetrometer tip. Figure 20 illustrates the main components of the cone penetrometer.

Penetration soundings generate data that can be used to infer soil type and can be correlated to produce a number of soil parameters such as friction angle (ϕ) and relative density (D_r).

CPTU data

Electric piezocone (CPTU) sounding were performed at 5 points across the IA Hwy 5/I-35 site prior to the construction of rammed aggregate piers and stone columns. CPTU-1 through 4 were performed at Ramp "C" and CPTU-5 was performed at Ramp "B". CPTU-1 through 4 are located in the rammed aggregate pier reinforced area and CPTU-5 is located in the stone column reinforced area. The piezocone soundings were made at the locations

u_3 →

Pore pressure
filter location

Friction
sleeve

Cone
penetrometer

u_2 →

Cone

u_1 →
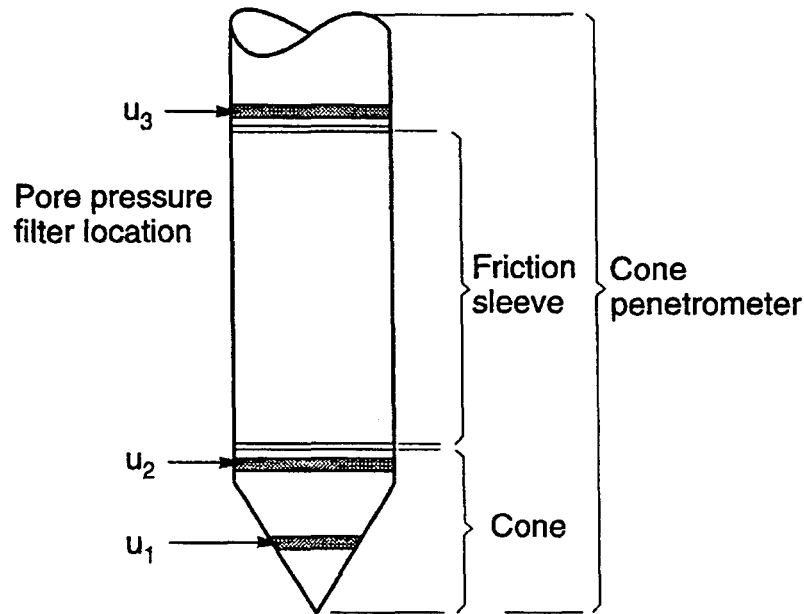
Figure 20. Main components of the cone penetrometer (from Lunne et al., 1997)

shown in Figures 16 and 17. The CPTU data was obtained using an electric subtraction cone with a pore pressure sensor near the tip. The cone was pushed hydraulically and data was collected at 5 cm intervals. Data was reported as an average over a 25 cm depth interval.

Piezocone data for Ramp "C" (CPTU-2) and Ramp "B" (CPTU-5) are presented in Figures 21 and 22 where q_T is the corrected tip resistance (q_c corrected for pore pressure effects), f_s is the sleeve friction, R_f is the friction ratio (f_s / q_c x 100%), and μ is the penetration pore-water pressure. From this data, it can be determined that the stone column upper zone soils are approximately 1.2 times stiffer than the rammed aggregate pier upper zone soils. This was calculated based on the average tip resistance q_c, since q_c is directly proportional to E_s, i.e. E_s = 3 to 8 q_c (Bowles, 1996). The assumption is that the empirical correlation factor (3 to 8) for the alluvial clay (Ramp "C") and silty alluvium (Ramp "B") is

similar. A full presentation of the CPTU data in both graphical and tabular form is shown in Appendix A. The soil was classified based on the Simplified Soil Classification Chart for the Standard Electronic Friction cone by Robertson and Campanella (1986) and Robertson et al. (1986). The relative density (D_r) was determined using a correlation proposed by Jamiolkowski et al. (1985). The drained friction angle (ϕ) was determined using a correlation proposed by Kulhawy and Mayne (1990).

Results of CPTU-1 through 4 indicate natural alluvial clay and sand formations overlaying stiff weathered shale. CPTU-1 through 4 indicate similar deposits at each point; however, the soundings revealed that the sediment to shale interface dips to the south. As a result of the dipping interface, the compressible layer increases in thickness from north to south (CPTU-4 to CPTU-1). CPTU points 1-4 encountered 0.5 to 1 meters of medium to stiff clay underlain by a compressible alluvial clay layer varying from 3 to 6 meters in thickness. Underlying the alluvial clay is a stratum of fine-grained alluvial sand and silty sand deposits varying from 4 to 4.5 m thickness. Underlying the alluvial sand is stiff weathered shale encountered at depths of 8.5 meters at CPTU-4 to 11 meters at CPTU-1.

Results of the CPTU-5 indicate alluvial silts over interbedded alluvial silts and clays over alluvial clay underlain by the stiff weathered shale. CPTU-5 encountered 2.8 meters of fill underlain by 3 meters of alluvial silt. Underlying the alluvial silt is a 2.5 meter thick layer of interbedded alluvial silts and clays. Underlying the interbedded silts and clays is a compressible alluvial clay layer of 3.5 meter thickness. The stiff weathered shale was encountered at a depth of 12 meters.
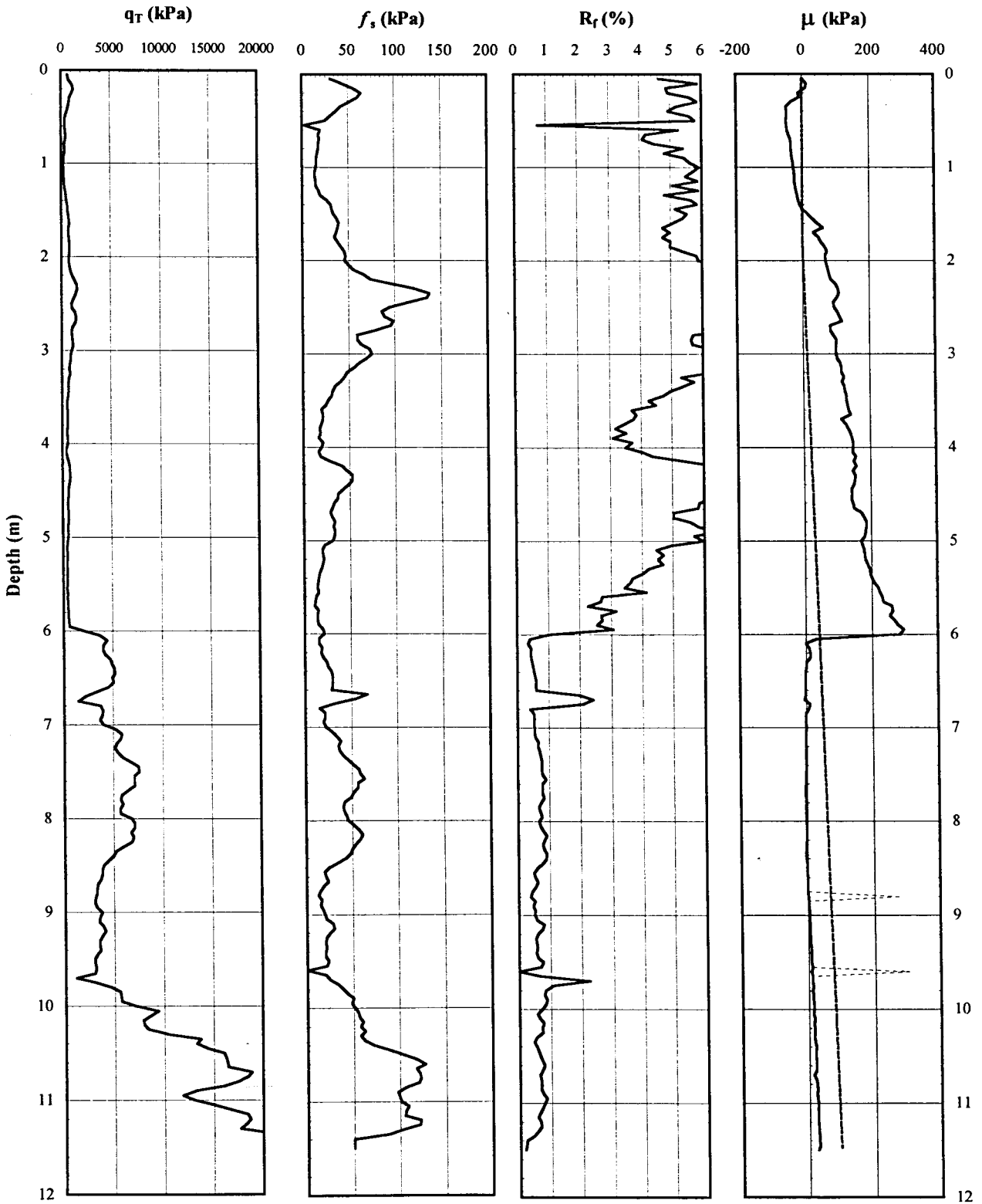
Figure 21. Piezocone penetration data for Ramp "C" (CPTU-2)
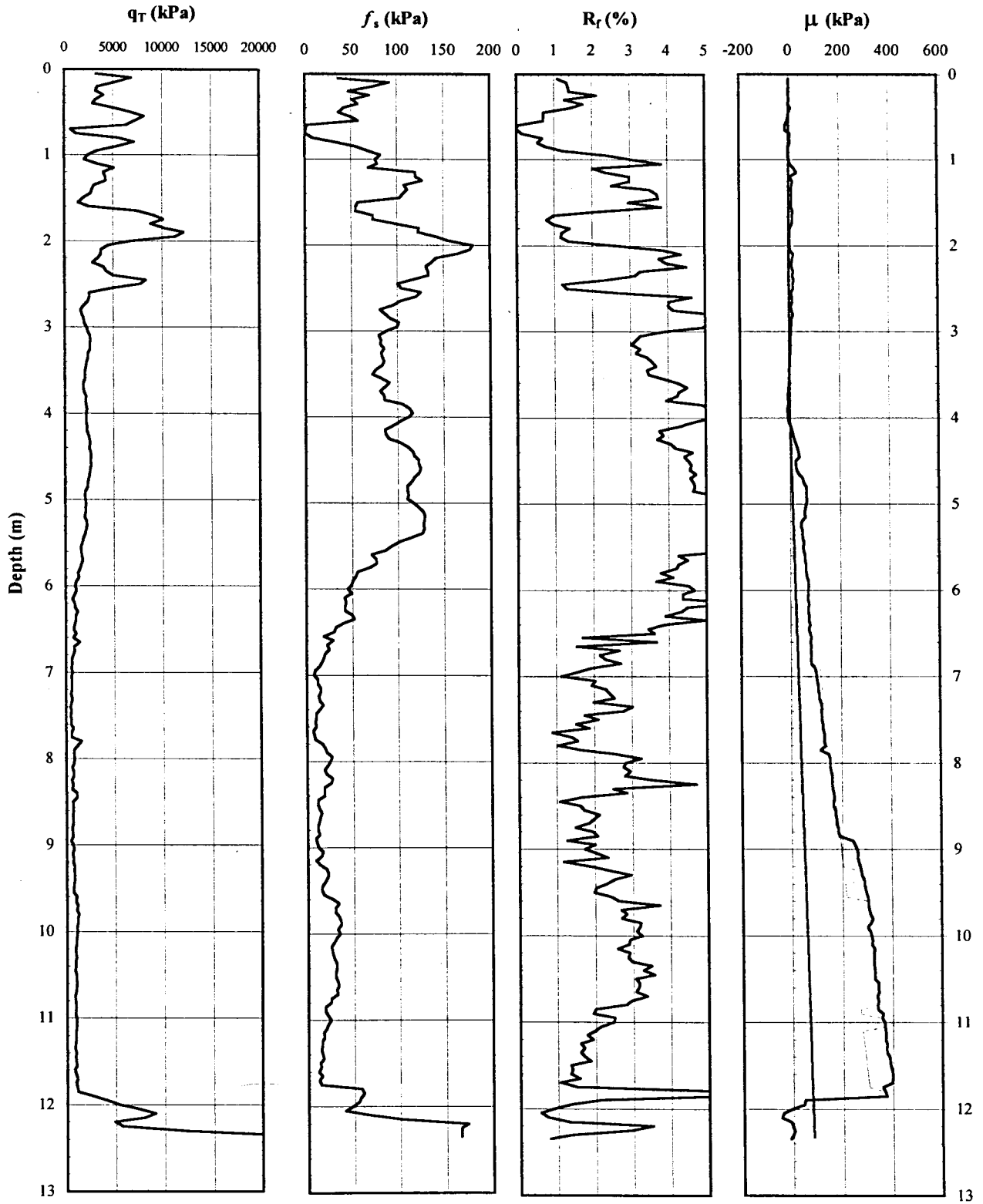
Figure 22. Piezocone penetration data for Ramp "B" (CPTU-5)

Settlement estimates using CPTU data

Applying a method proposed by Sanglerat (1972) settlements were estimated for

Ramp "C". CPTU-2 data was used to predict the total settlement under the center of the

embankment following Stage 1 (4.6 m fill) and Stage 2 (4.6 m fill) of the embankment

construction. Details of these calculations are in Appendix B. Influence factors from

Winterkorn and Fang were used to determine the changes in stress following embankment

construction (1975, p. 167). The soil compressibility coefficient α was determined by

dividing the average pressuremeter modulus (discussed later) by the average q_c for the

compressible layer. The resulting α value of 5.8 seems reasonable since it is in the mid range

of α values recommended by Sanglerat (1972) for this type of soil (low to medium plasticity

clay).

The results of these calculations indicate 12.0 cm (4.7 inch) following Stage 1 and an

additional 10.0 cm (4 inch) following Stage 2 for a total settlement of 22.1 cm (8.7 in).

These calculations are estimates of total settlement had the foundation soils not been

reinforced by rammed aggregate piers. Riaund and Miran (1992) provided information

evaluating the precision of Sanglerat's method from 17 different sites in France. It was

determined that the method over predicted settlement by an average of 47% for this database.

It is noteworthy that the inaccuracy is largely due to the difficulty in determining α. Local

experience based on settlement observations as well as prior knowledge of modulus values

on site can help to adjust the soil compressibility coefficient to achieve accurate settlement

estimates.

Standard penetration (SPT)

Originating in the late 20's in the USA, the standard penetration test (SPT) is one of

the oldest and simplest forms of subsurface exploration (Nagaraj, 1993). Because of its

simplicity, the SPT continues to be one of the most readily used in-situ tests. The test

consists of driving a 35 mm (1.4 inch) inside diameter split sampling tube into the ground by

repeated blows of a hammer. Figure 23 illustrates the sampling tool used for the SPT.

The split tube is connected to a drill rod and is hammered into undisturbed soil in the

bottom of a borehole. The driving force is a 63 kg (140 lb) hammer with a free fall of 762

mm (30 in). The test is performed by driving the split tube into undisturbed soil in three

successive increments of 150 mm (6 in). The first increment is regarded as seating and the
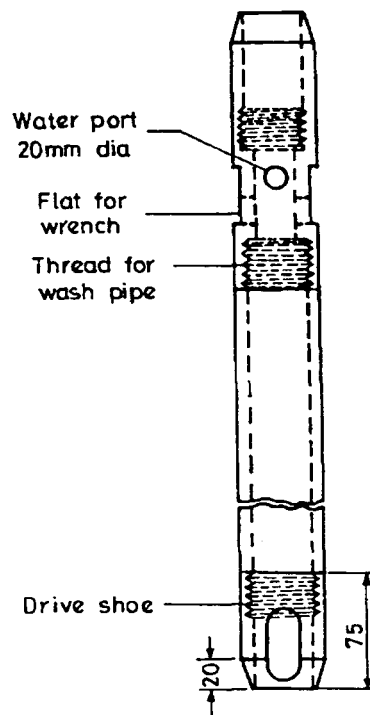
Figure 23. Sampling tool used for the SPT (from Nagaraj, 1993)

number of blows is discarded. The number of blows for the final two increments (300 mm

penetration) is regarded as the SPT or "N" value at the mid elevation of the test. Through

correlation, density and compressibility of the soils can be estimated with SPT-N values.

SPT data

SPT soundings were performed after installation of stone columns and rammed

aggregate piers at the IA Hwy 5/I-35 site. The tests were performed in stone columns and

rammed aggregate piers constructed with the same aggregate type and gradation (Gradation

A). N-values through the stone columns averaged 10.6 ± 5.0 for 42 tests. In comparison N-

values through rammed aggregate piers averaged 16.7 ± 7.7 for 6 tests. The rammed

aggregate piers averaged 58% higher N-values, which indicates a stiffer, denser composite

material.

Pressuremeter (PMT)

Originating in Germany and later developed in France, the prebored pressuremeter

(PMT) test is a widely used device for measuring in-situ soil strength. The prebored

pressuremeter test consists of inserting a cylindrical probe into a borehole and expanding the

cylinder to pressurize the soil horizontally as shown in the schematic in Figure 24. The

radial pressure exerted onto the soil and the relative increases in cavity radius are measured

to give an in-situ pressure-volume (stress-strain) curve of the soil. The pressuremeter test is

repeated at a range of depths in order to obtain a profile of soil parameters. From the

pressure-volume curve (referred to as the pressuremeter curve), the pressuremeter modulus,

E_o, and the limit pressure at failure, p_L, which can be correlated to many other soil

parameters, are obtained (Briaud, 1989).
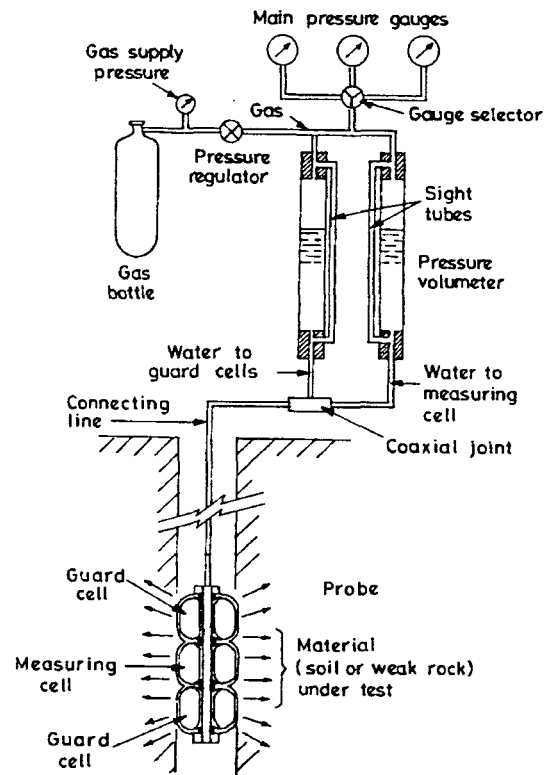
Figure 24. Schematic of the PMT (from Nagaraj, 1993)

PMT data

Prebored pressuremeter tests were conducted at two points at Ramp "C" prior to the

installation of rammed aggregate piers. Pressuremeter tests were again conducted 7 and 73

days after construction of rammed aggregate piers. The purpose of repeating the tests after

construction of the piers was to provide an assessment of the lateral stress induced during

pier installation and of further changes in lateral stress as consolidation occurs. The prebored

pressuremeter tests were conducted at the locations shown in Figure 16. All pressuremeter

tests were conducted within the alluvial clay stratum with the exception of the 5.9 and 6.1

meter depth tests where sand may have been encountered. All pressuremeter tests were

conducted within a 7 meter radius of each other, for this reason it is assumed that tests at like depths within this region encountered similar material.

Figure 25 show a profile of the results of pressuremeter tests prior to and following installation of rammed aggregate piers. Appendix C shows the pressuremeter curve and creep curve for each test. PMT-1 and PMT-2 were conducted prior to the installation of the rammed aggregate piers. E_o was calculated using the slope of the straight-line portion of the pressuremeter curve. The recommended procedure for determining p_L is to extend the curve manually and read the limit pressure based on the extrapolated curve (Briaud, 1989). As shown in the creep volume curves in Appendix C, the creep volume rapidly increases as the soil exceeds the elastic portion of the curve and increases asymptotically at p_L.

PMT-3 and 4 were conducted 7 and 73 days after installation of the rammed aggregate piers, respectively. No significant changes in E_o or p_L were evident from these tests. Future PMT testing should be conducted to evaluate the long-term effects rammed aggregate piers have on E_o and p_L.

Borehole shear (BHST)

The borehole shear (BHST) test was originated and developed at Iowa State University over 30 years ago and has received considerable popularity and attention in the last twenty-five years (Nagaraj, 1993). The BHST is a simple experiment that can be used to determine the cohesion intercept (c) and friction angle (ϕ) of in-situ soils. The test replaces the need for traditional laboratory testing such as consolidated drained (CD) and consolidated undrained (CU) triaxial testing saving considerable time and money. Several studies have compared the BHST to CD and CU triaxial tests (Wineland, 1976; Schmertmann, 1976) supporting a previous assessment that the BHST is usually a drained test (Handy, 1976).
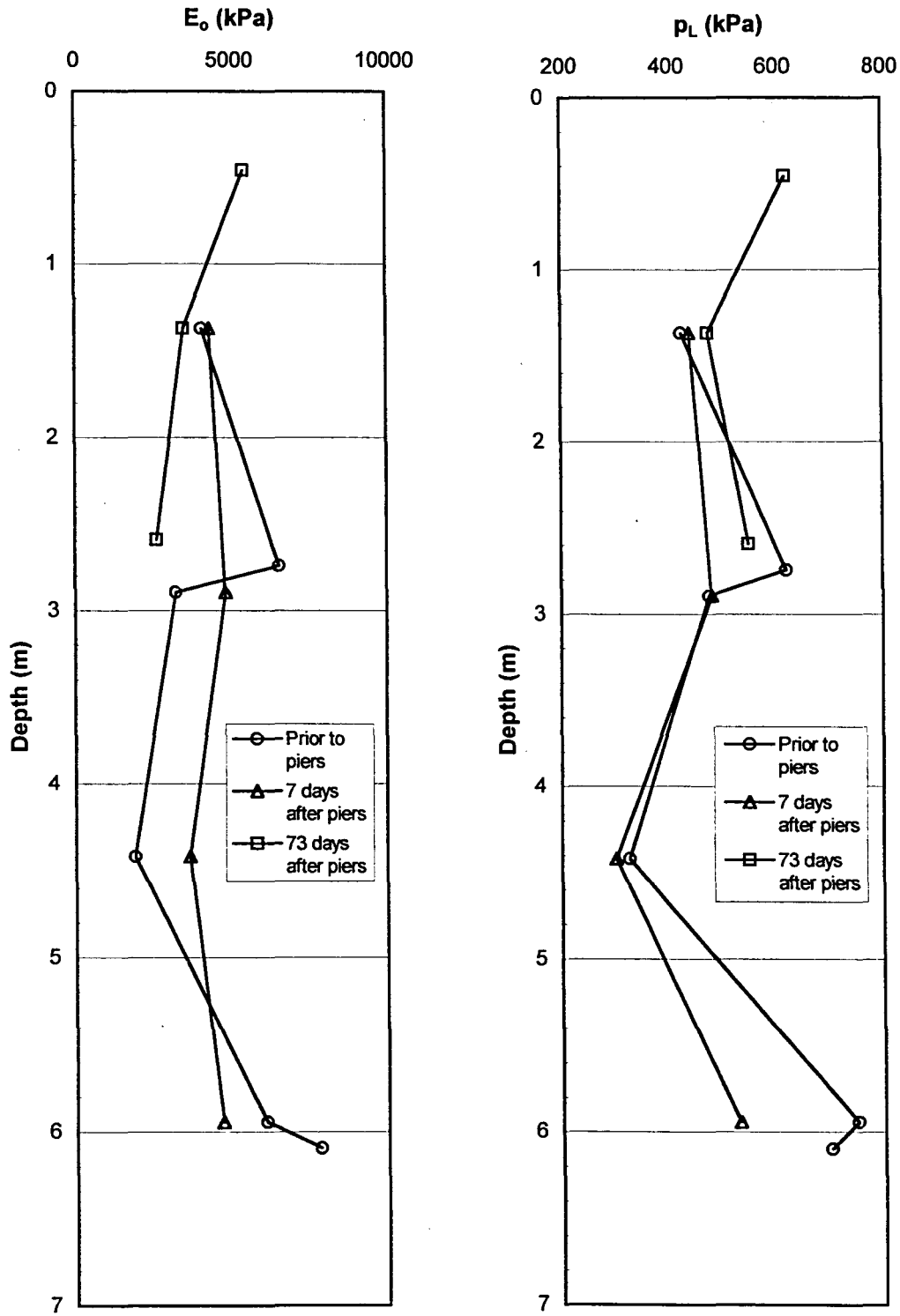
Figure 25. Pressuremeter test results prior to and following installation of rammed aggregate piers (left) pressuremeter modulus, E_o, (right) limit pressure, p_L

The test consists of lowering an expandable shear head into a borehole, laterally expanding the shear head against the walls under a constant normal stress (σ), allowing the soil to consolidate, and pulling vertically on the shear head measuring shear resistance (τ). Points are produced on the Mohr-Coulomb shear envelope by measuring the maximum shear resistance at successive increments of normal stress applied against the walls of the borehole (White and Handy, 2001). The simple apparatus for the test consists of three parts, the shear head, the pulling assembly and the control console. A schematic of the borehole shear tester is shown in Figure 26.

BHST data

Borehole shear tests were performed at Ramp "C" prior to the construction of the rammed aggregate piers. The borehole shear tests were conducted at the approximate location shown in Figure 16.

A profile of the results of BHST-1 is shown in Figure 27. Mohr-Coulomb shear envelopes for BHST-1 are presented in Appendix D. The initial points displayed as hollow points in Figures D1 through D4 are indicative of inadequate shear plate seating, these outliers were ignored in the regression. The final points displayed as hollow points in Figures D4 and D5 indicate full expansion of the shear head and these points were also ignored in the regression. The coefficient of correlation, R^2, ranged from 0.992 to 0.999 for each of the tests conducted at BHST-1. The near unity values of R^2 indicate an almost perfect association between shear strength and normal stress signifying low apparatus and operator variability.
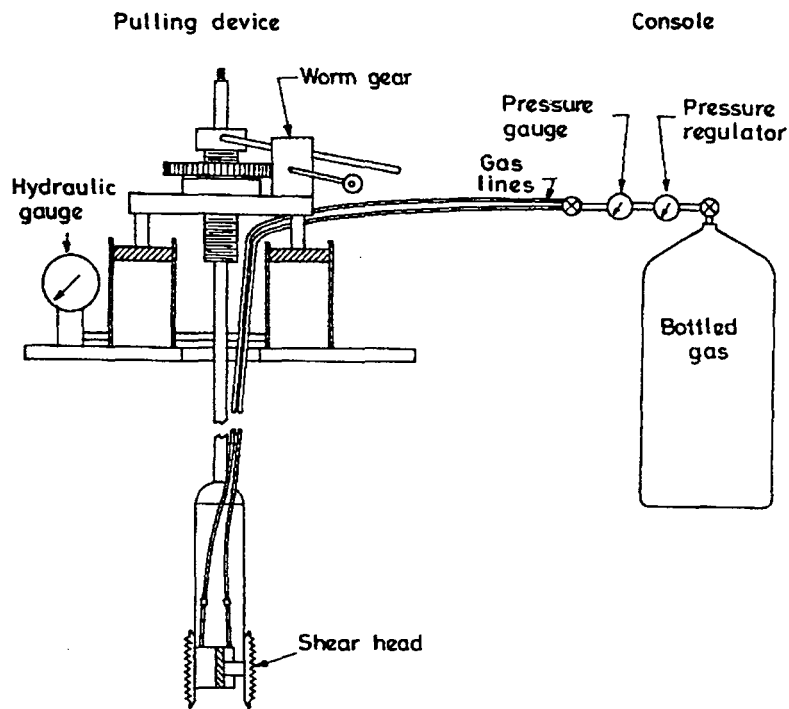
Figure 26. Borehole shear apparatus (from Nagaraj, 1993)

K_o-stepped blade

The K_o-stepped blade, designed over twenty years ago at Iowa State University, is the

most recently developed instrument for the measurement of in-situ lateral stress. The test

consists of inserting a thin blade into the bottom of a borehole and measuring the amount of

disturbance caused by successive increases in blade thickness; 3.0, 4.5, 6.0 and 7.5 mm.

The inspiration was to develop an instrument that would account for the inevitable

soil disturbance caused by the insertion of a measuring device into in-situ soil. By

introducing known levels of disturbance caused by the thickness of the blades, a relationship
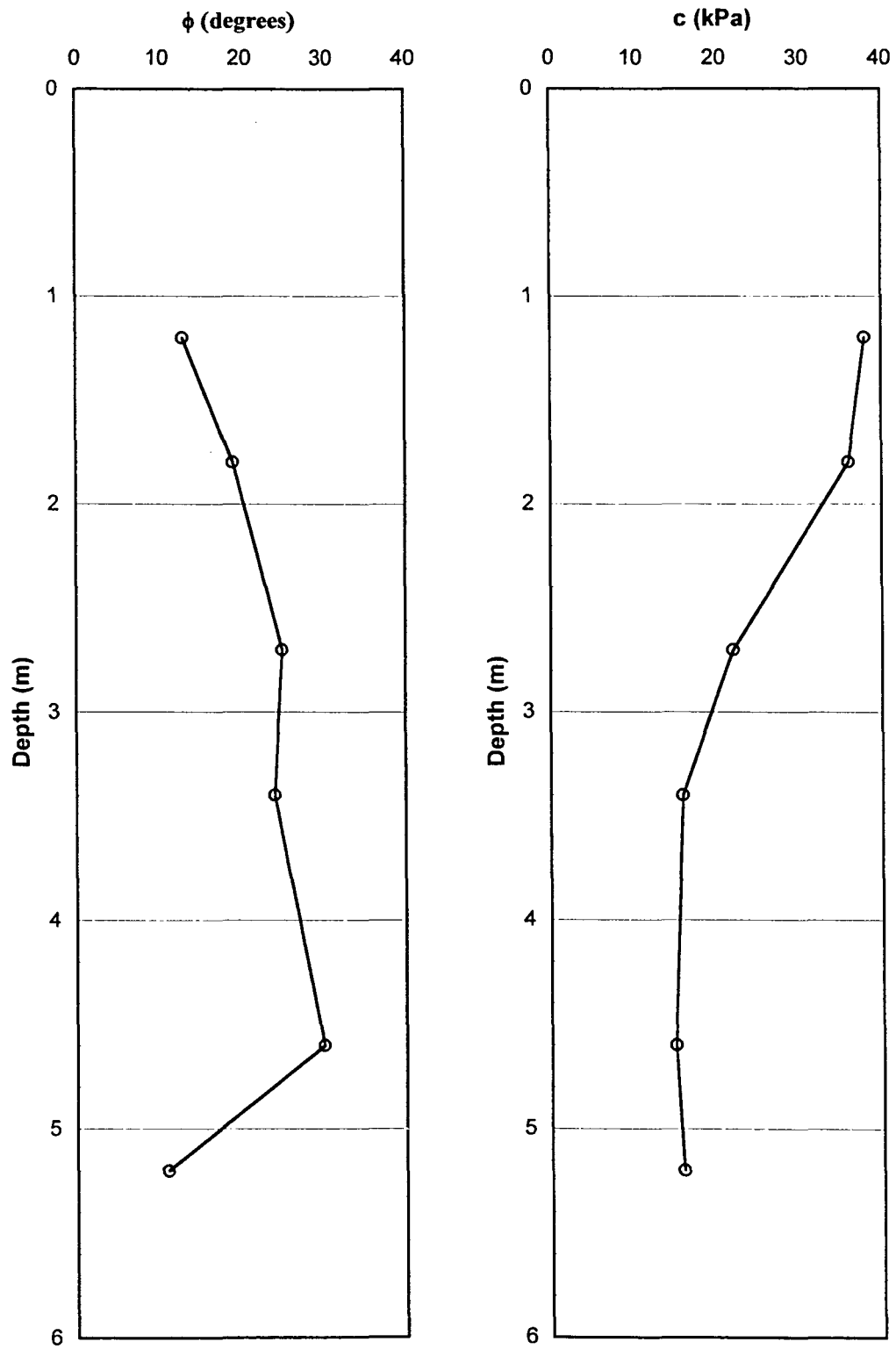
Figure 27. BHST-1 results (left) angle of internal friction, ϕ, (right) cohesion, c

between measured stress and disturbance is produced. This relationship when extrapolated to zero thickness results in a measure of in-situ lateral stress. Figure 28 illustrates the extrapolation principle of the K_o-stepped blade. Although an exponential relationship was not anticipated, Handy et al. (1982) reported the following relationship between blade thickness and measured stress:

$$p_1 = p_0 ae^{bt} \tag{8}$$

where p_0 and p_1 are mold stresses prior to and after the insertion of the blade, respectively, "t" is the blade thickness, and "a" and "b" are regression coefficients. The value of "a" is assumed to be 1.0, which gives $p_1 = p_0$ when $t = 0$. The value of the "b" coefficient represents a stiffness response of the soil to blade intrusion (Handy et al., 1982).

Stepped blade data

K_o-stepped blade tests were conducted to determine the influence rammed aggregate piers and stone columns have on lateral stress. Initially, tests were conducted in the far field condition to determine in-situ lateral stress conditions. Tests were again conducted in the radial stress direction (σ_r) and in the tangential stress direction (σ_θ) following installation of rammed aggregate piers and in the radial stress direction following installation of stone columns. K_o-stepped blade data is presented in the "Field Investigation Results and Discussion."
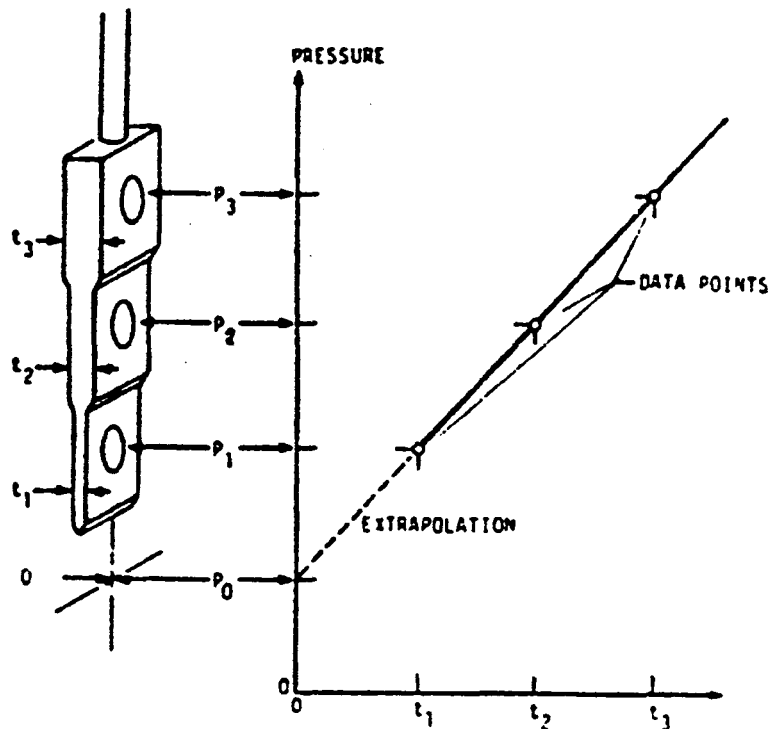
Figure 28. Extrapolation principle of the K_o-stepped blade (from Handy et al., 1989)

Laboratory Testing Program and Procedures

Consolidated drained (CD) triaxial compression tests, consolidated undrained (CU) triaxial compression tests, unconfined compression tests, confined compression (oedometer) tests, and Atterberg limit tests were performed on representative portions of undisturbed samples obtained by Shelby tube sampling procedures. A standard proctor compaction test was performed on the embankment fill. Aggregate particle-size distribution tests were performed on the aggregates used to construct the rammed aggregate piers and stone columns. The laboratory tests were conducted to provide verification of in-situ test results

and to obtain additional soil strength parameters. The laboratory procedures and results are described herein.

Consolidated drained (CD) triaxial compression

A series of consolidated drained (CD) triaxial compression tests was conducted to determine the approximate shear strength of the soil in terms of effective stresses. Four CD tests were conducted on alluvial clay obtained at a depth of 2.7 m from Ramp "C". Tests were conducted at confining pressures (σ_3) of 69, 138, 159 and 276 kPa.

The CD test results were analyzed by plotting the stress path of each specimen to failure. By evaluating the stress conditions at failure, the soil's strength parameters cohesion, c', and angle of internal friction, ϕ', were determined in terms of effective stresses (' denotes effective stress).

Relatively undisturbed cohesive samples of approximate height-to-diameter ratios of 2.0 were confined (σ_3) permitting drainage. Specimens were then axially loaded ($\sigma_1 - \sigma_3$) at a deflection rate slow enough to allow pore pressures to dissipate as load was applied. Load measurements were recorded for every corresponding deflection of 0.01 inch. Failure of each specimen was determined by a significant drop in axial stress.

The stress-strain behavior and corresponding changes in volume for the series of CD triaxial tests are shown in Figures 29 and 30. As to be expected, higher confining stresses resulted in a stiffer material (steeper stress-strain slopes) with greater peak strengths. The volume response of all four clay samples was an increase in volume (shown as negative volume change in Figure 30). This volumetric expansion during triaxial loading suggests the alluvial clay is in an overconsolidated stress state (Lambe and Whitman, 1969). The stress paths for the CD tests are shown in the p'-q diagram in Figure 31. A linear regression on the

peak stress values generated the K_f-line. The K_f-line is related to the Mohr-Coulomb failure

envelope by the following relationships:

$$\sin (\phi) = \tan (\alpha) \tag{9}$$

$$c = \frac{a}{\cos(\alpha)} \tag{10}$$

where, α is the angle of the K_f-line, ϕ is the shear failure angle of a Mohr-Coulomb failure

envelope, , "a" is the K_f-line intercept on the "q" axis and "c" is the shear stress intercept of a

Mohr-Coulomb failure envelope. Hence, as determined from the p'-q diagram in Figure 31,

$\phi' = 23°$ and c' = 7 kPa.
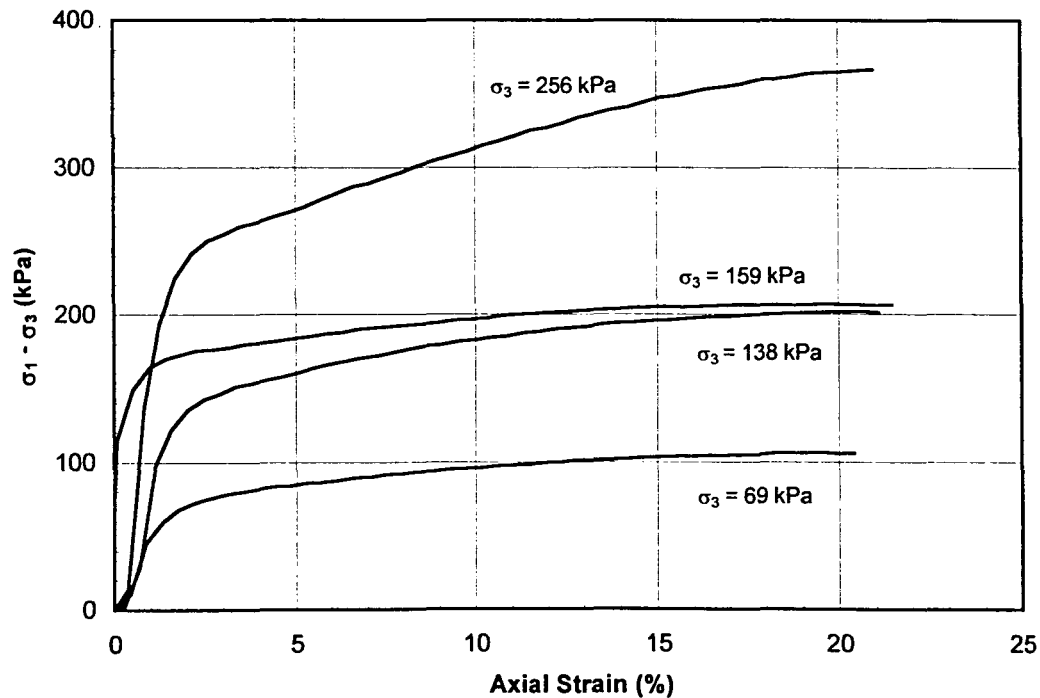
Figure 29. Stress-strain behavior of CD triaxial tests from depth 2.7 m
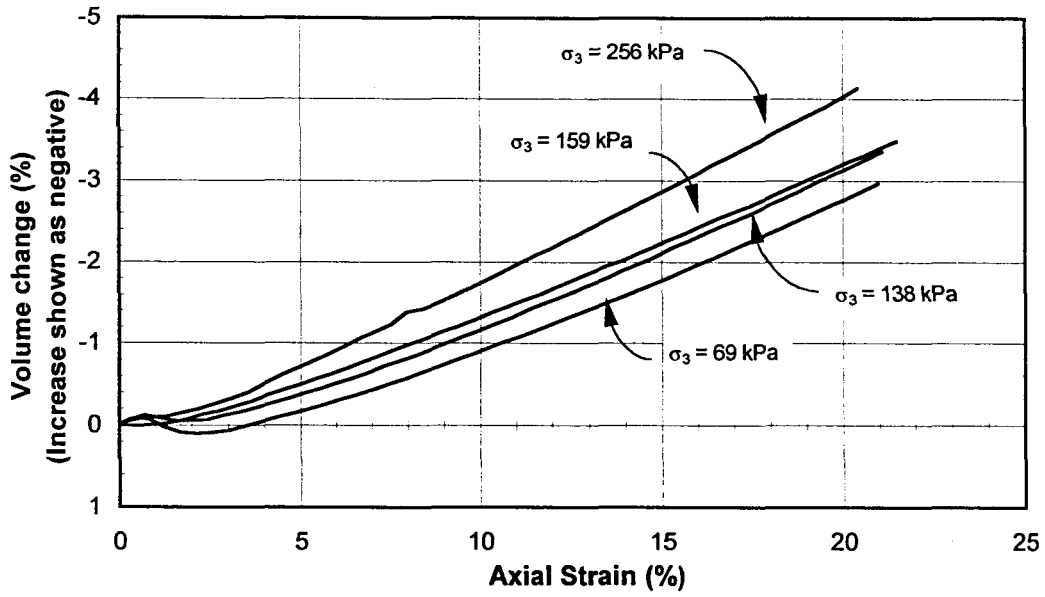
Figure 30. Volumetric change for CD triaxial tests from depth 2.7 m
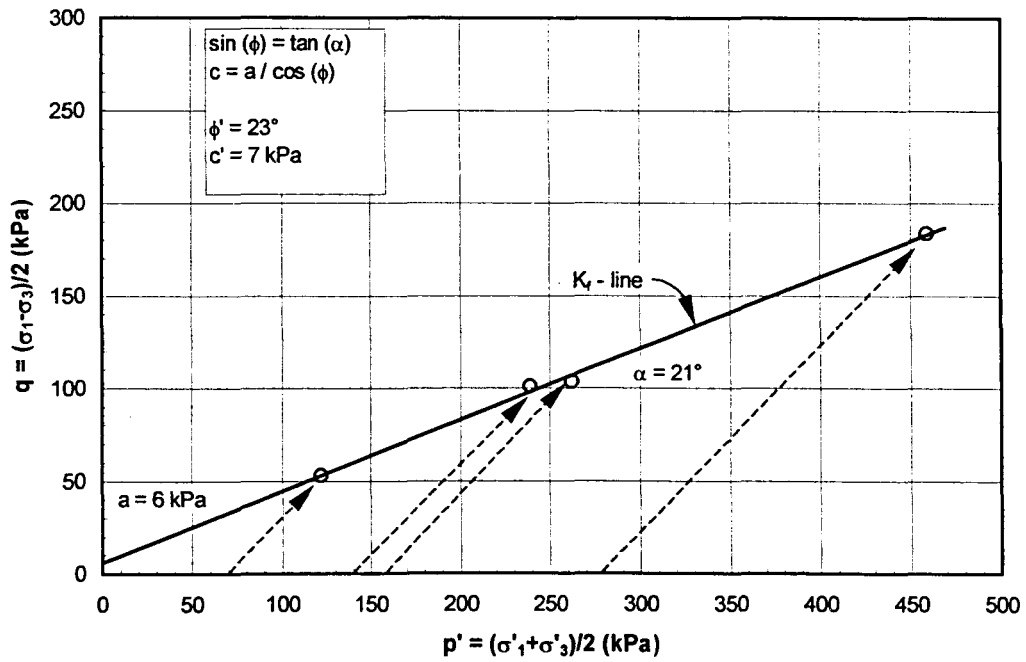
Figure 31. Stress paths for the loadings of CD triaxial tests from depth 2.7 m

Consolidated undrained (CU) triaxial compression

A series of consolidated undrained (CU) triaxial compression tests was conducted to determine the approximate shear strength of the soil in terms of total stresses. Three CU tests were conducted on alluvial clay obtained at a depth of 3.4 m from Ramp "C". Tests were conducted at confining pressures (σ_3) of 10, 41 and 69 kPa.

The CU test results were analyzed by plotting the stress path of each specimen to failure. By evaluating the stress conditions at failure, the strength parameters cohesion, c, and angle of internal friction, ϕ, were determined in terms of total stresses.

Relatively undisturbed cohesive samples of approximate height-to-diameter ratios of 2.0 were confined (σ_3) permitting drainage. Specimens were then axially loaded ($\sigma_1 - \sigma_3$) at a deflection rate of approximately 0.2% per min preventing drainage. Load measurements were recorded for every corresponding deflection of 0.01 inch. Failure of each specimen was determined by a drop in deviator stress.

The stress-strain behavior for the series of CU triaxial tests is shown in Figure 32. The similarity in the resulting peak shear strengths suggests that all three specimens were subjected to the same stress history prior to loading. This indicates that consolidation may not have occurred as confining pressures were applied. Two reasons why consolidation may not have occurred are (1) selected chamber pressures were not sufficient enough to surpass the effective stresses of the specimens prior to the application of chamber pressures or (2) complete drainage did not occur while initial consolidation pressures were applied. As a result, all three specimens were subjected to the same effective stress state prior to axial loading. Because all three specimens were subjected to the same effective stress prior to loading, the results resemble that of unconsolidated undrained (UU) triaxial compression

tests. This is shown by the "ϕ = 0 concept" illustrated by the stress paths for the CU tests

shown in Figure 33. This concept states that specimens of like material subjected to

equivalent effective stresses prior to loading will result in equivalent shear failure strengths

(Lambe and Whitman, 1969). The K_f-line generated by the peak stress values has a nearly

zero slope resulting in ϕ = 0°. The resulting "c" of 28 kPa for the undrained loading situation

is actually undrained cohesion (c_u), also commonly referred to as the undrained shear

strength (s_u) of the soil (Lambe and Whitman, 1969).
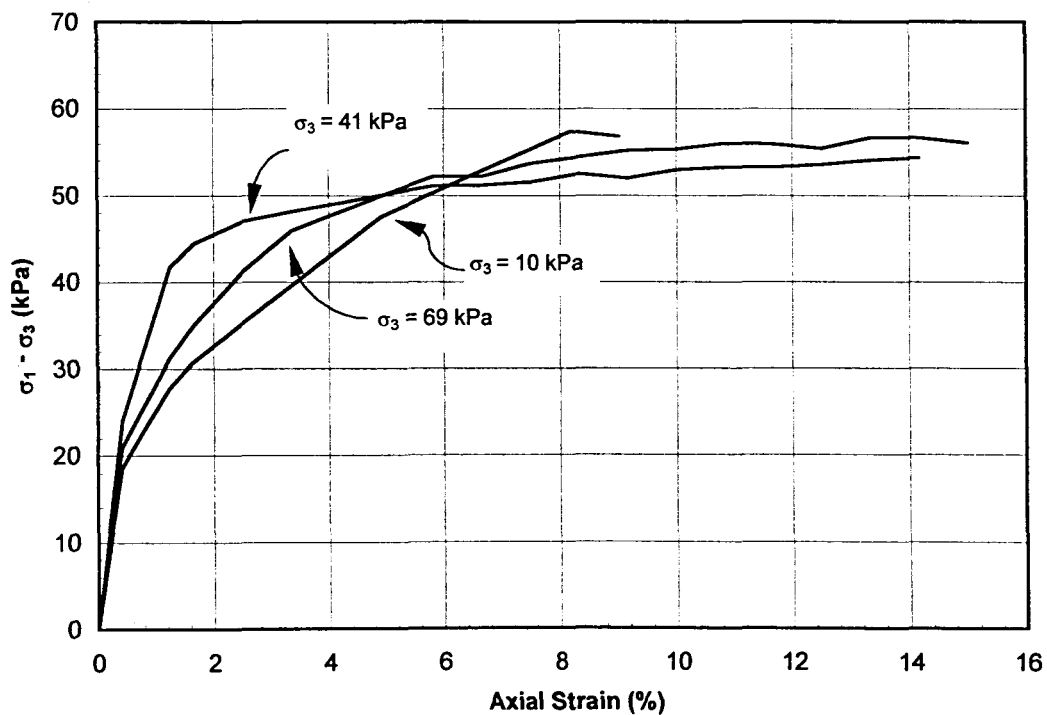
Figure 32. Stress-strain behavior of CU triaxial tests from depth 3.4 m
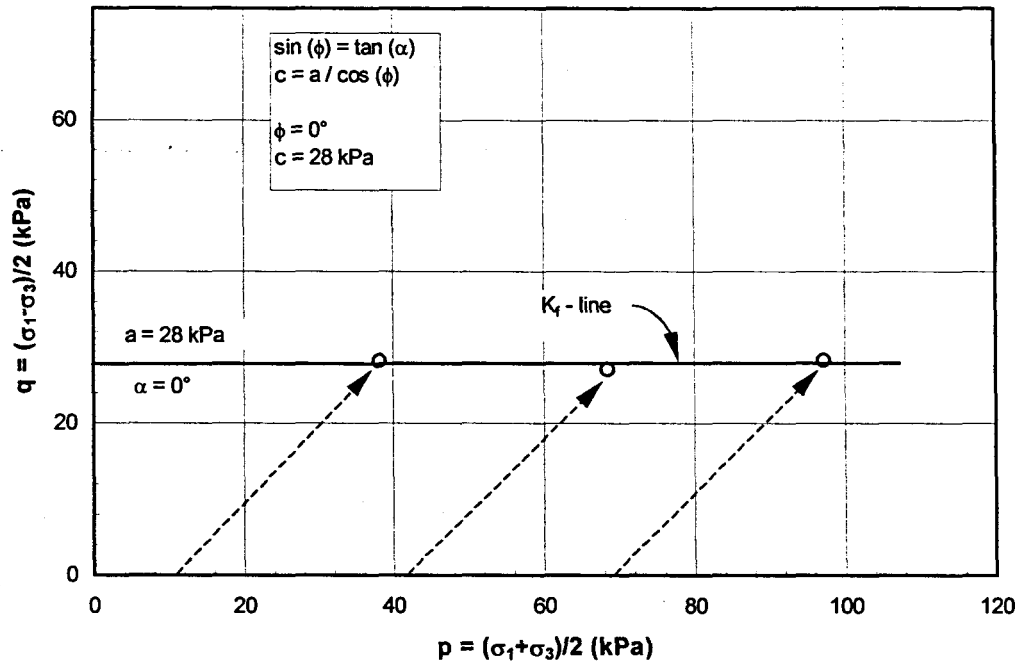
Figure 33. Stress paths for the loadings of CU triaxial tests from 3.4 m

Unconfined compression

A series of unconfined compression tests was conducted to determine the

approximate shear strength of the soil in terms of total stress (undrained condition, $\phi = 0$).

Nineteen tests were performed on relatively undisturbed samples obtained from Ramp "C".

Samples were obtained from three locations across the site; Test Points 2, 3 and 5 as shown

in Figure 16. Tests were conducted on samples taken from depths of 1 to 6 meters.

The unconfined compression test is a special case of the triaxial compression test in

which the confining pressure is zero, i.e. $\sigma_3 = 0$. The parameters determined from the series

of unconfined compression tests were the unconfined compressive strength of the soil, q_u,

and undrained cohesion, c_u ($c_u = q_u/2$).

Relatively undisturbed cohesive samples of approximate height-to-diameter ratios of 2.0 were axially loaded at a deflection rate of approximately 2% per min. Load measurements were recorded for every corresponding deflection of 0.01 inch. Failure of each specimen was determined by a significant drop in axial stress.

The resulting unconfined compressive strength, q_u, is a measure of the load per unit area at which the specimen failed. The unconfined compressive strength decreased with depth with the exception of a slight increase just shallow of 3 m. This is similar to the relative strength conditions indicated by CPT and PMT data. A profile of the results of the nineteen unconfined compression tests is shown in Figure 34.

Confined compression (oedometer)

A one-dimensional confined compression test was conducted to determine the compressibility of the alluvial clay at Ramp "C". The test was conducted to provide information for a primary consolidation settlement estimate. The test was conducted on a sample obtained from a depth of 2.7 m and is assumed to be representative of the entire alluvial clay layer.

For this test, a relatively undisturbed soil specimen of approximate height-to-diameter ratio of 0.3 was restrained laterally and loaded axially. Each stress increment was maintained until excess pore-water pressures were dissipated (time t_{90}). During the consolidation process the change in specimen height was recorded as a function of time. The consolidation test results were analyzed by plotting void ratio, e, verses the logarithm of pressure applied to the sample, this is commonly referred to as the e-log-p curve. The e-log-p curve for this test is shown in Figure 35.
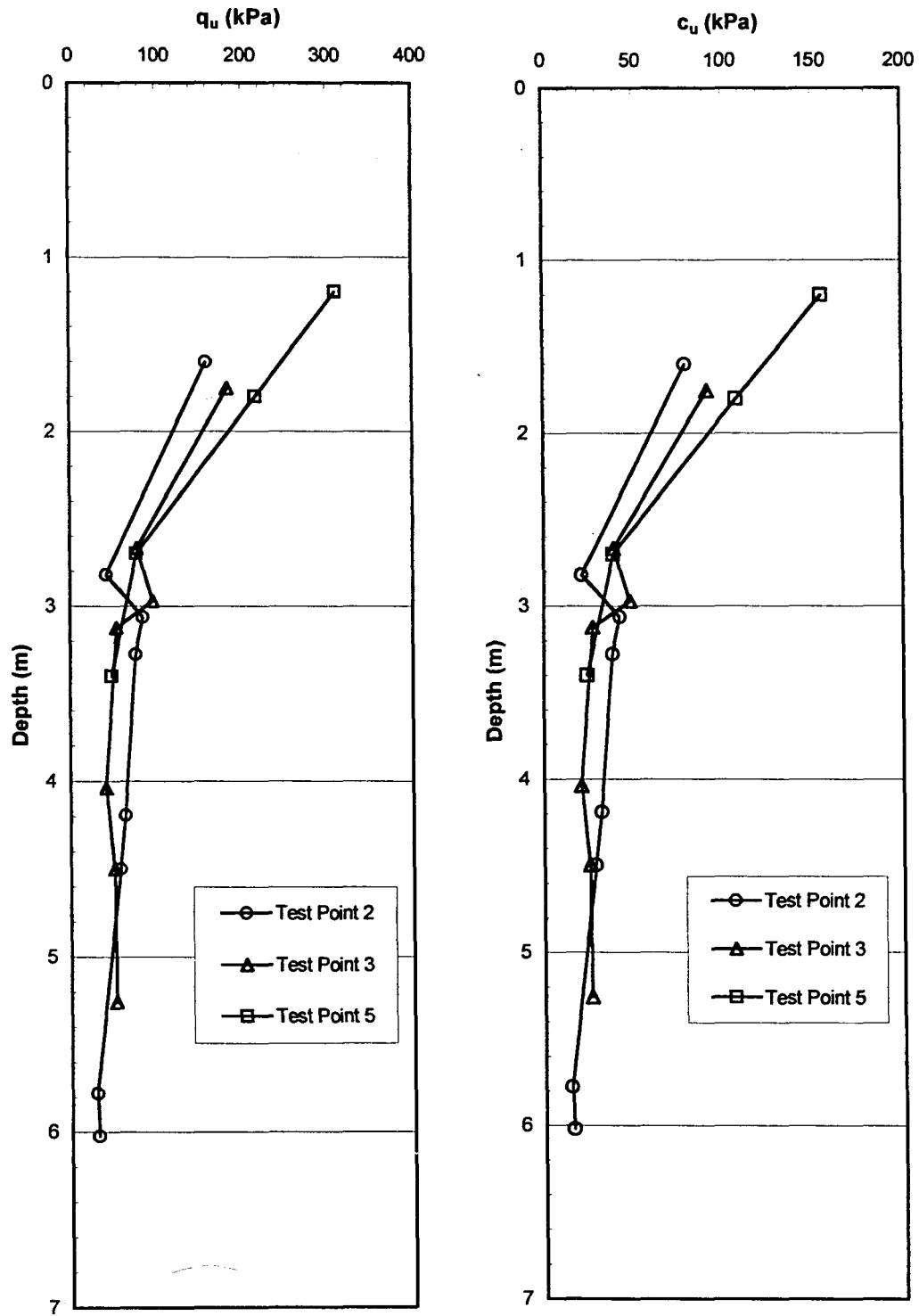
Figure 34. Unconfined compression test results (left) unconfined compressive strength, q_u, (right) undrained cohesion, c_u

$e_o = 0.863$

$w_o = 31.0\%$

$w_f = 23.3\%$

$c_c = 0.313$

$c_s = 0.031$
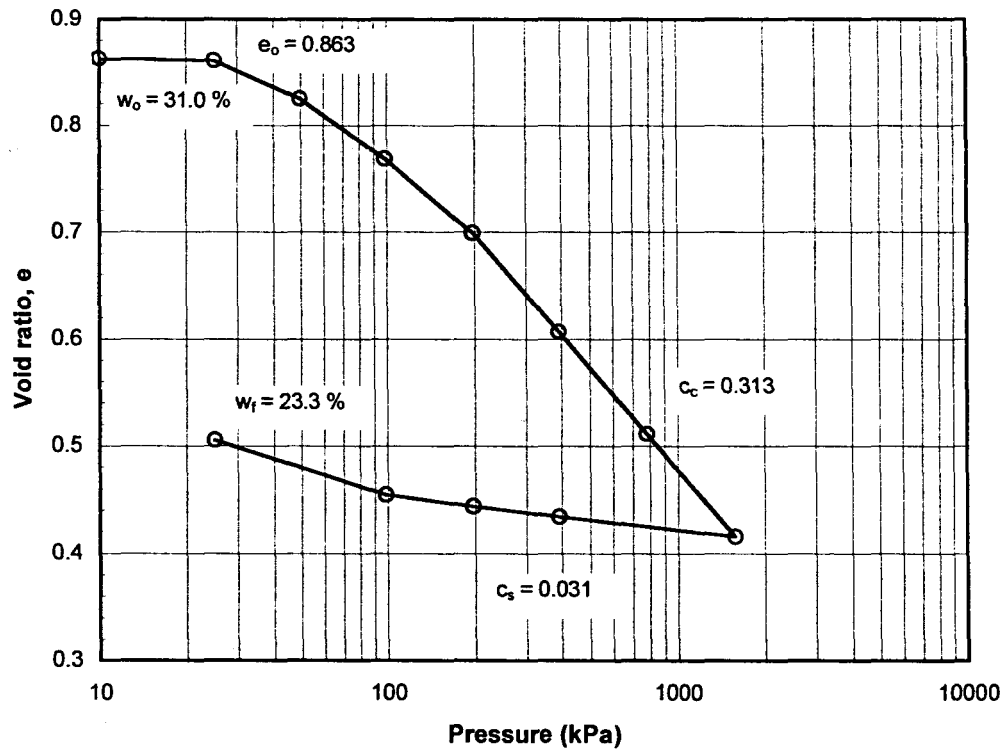
Figure 35. e-log-p curve for the compressible clay at depth 2.7 m

For rate of settlement analysis the square-root-of-time compression curves

(compression verses $\sqrt{t_{90}}$) were plotted for several pressure increments. By applying the

square-root-of-time-method, the coefficient of consolidation, c_v, was calculated and time-

settlement relationships were established. The square-root-of-time compression curves are

shown in Appendix E. Table 5 lists a summary of average c_v values obtained from this test

along with two confined compression tests conducted by the Iowa DOT. The average c_v

value from the three tests was used to establish predicted time-settlement relationships.

Table 5. Summary of coefficients of consolidation (c_v)[a]

Test No.	c_v (m²/day)	AASHTO Classification	Depth (m)	Moisture Content (%)	Source
1	0.232	A-6 (19)	1.0	32	IDOT
2	0.074	A-6	2.7	31	ISU
3	0.130	A-6 (15)	4.0	29	IDOT

[a] Average c_v = 0.145 m²/day used for time-settlement calculations

Settlement estimates using confined compression data

Primary consolidation settlements of up to 25 cm (9.7 in) following Stage 1 (4.6 m fill) and an additional 14 cm (5.6 in) following Stage 2 (4.6 m fill) of embankment construction have been estimated. The settlement estimates are based on the e-log-p curve shown in Figure 35. The effective stress was calculated at mid-depth of the consolidating layer before construction and after Stages 1 and 2 of embankment construction. The settlement estimates are based on a 5.6 m thick consolidating layer (one-dimensional drainage). Stress calculations for the compressible layer as well as details of the primary consolidation settlement estimates are shown in Appendix F.

Atterberg limits

Atterberg limits were conducted on samples obtained from Test Point 3 at Ramp "C". The liquid limit test determines the moisture content at which a fine-grained soil will change from a plastic to liquid state; the plastic limit test determines the moisture content at which a fine-grained soil will change from a semisolid to a plastic state. The difference between the liquid limit and the plastic limit is the plasticity index. These tests provide information on the plasticity of the soil, which is a basis for soil classification.

The liquid limit test consists of a brass cup that is dropped onto a base plate by cranking the cam. Soil is placed in the brass cup and a groove is placed in the center. The moisture content required to close the groove 0.5 inches at 25 blows is defined as the liquid limit. Several tests are performed with increasing moisture contents and the results are plotted on a log scale to determine the liquid limit.

The equipment used for the plastic limit test consists of a smooth rolling plate, which is typically glass, and a source of water. The plastic limit is the moisture content at which rolling a 1/8-inch thick thread of soil will crumble.

Dry density values and moisture contents were determined from samples obtained from Test Points 2 and 3. Dry density values were determined by measurements of sample weight, volume and moisture content.

The results of the classification tests for Ramp "C" indicate fat clay of high plasticity underlain by clay of low to medium plasticity. Moisture contents, dry densities and Atterberg limits of the soils encountered at Ramp "C" are shown in Figure 36.

Standard proctor compaction

A standard proctor compaction test was conducted on the embankment fill used at Ramp "C". This test determines the maximum dry unit weight of compaction and the corresponding optimum moisture content.

The compaction curve is shown in Figure 37. From this graph, the optimum moisture content is determined to be 12.5% and the maximum dry unit weight is 18.6 kN/m^3 (118.3 lb/ft^3).
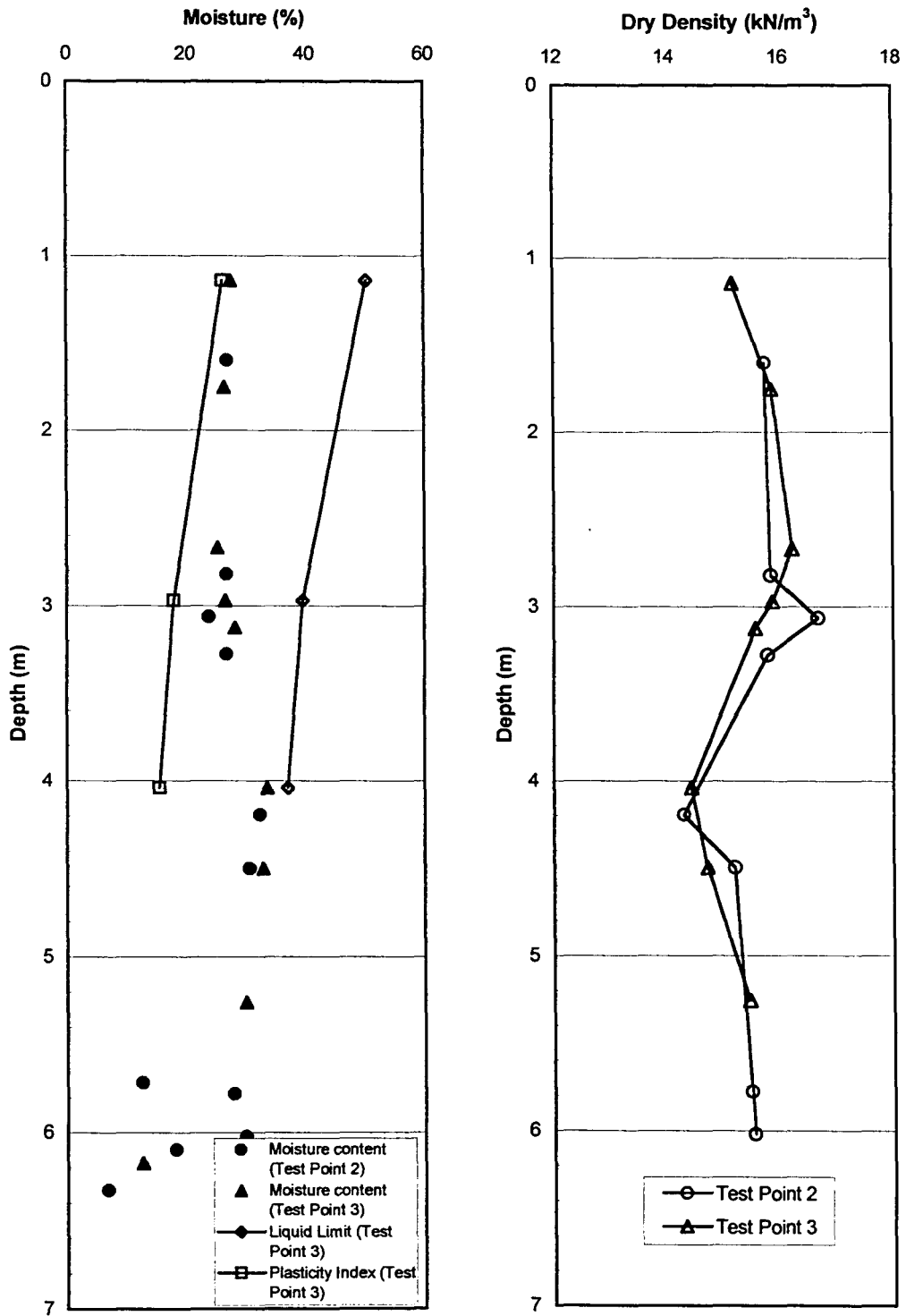
Figure 36. Atterberg limits, moisture content and dry density test results (left)
Atterberg limits and moisture content (right) dry density
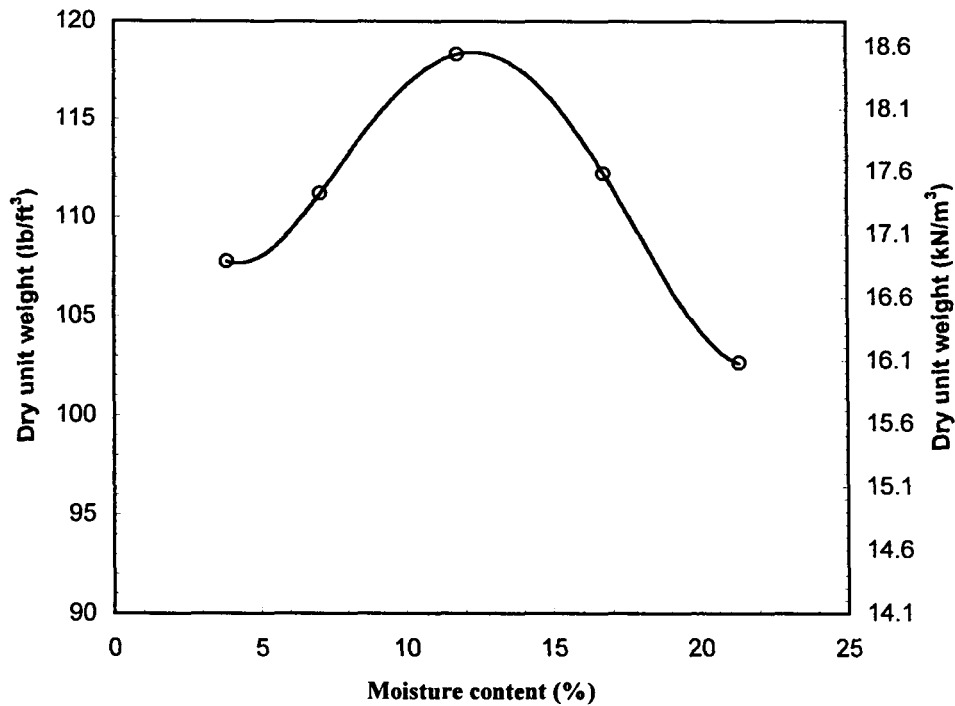
Figure 37. Standard proctor curve for the embankment fill

Aggregate particle-size distribution

A particle-size analysis was conducted on the aggregate used to construct the rammed aggregate piers and stone columns at the IA Hwy 5/I-35 site. The piers at Ramp "C" and the columns at Ramp "B" were constructed of 1.5 inch open-graded aggregate. Although rammed aggregate piers are typically constructed of a conventional roadstone, open-graded aggregate was used at this site due to the high phreatic surface in an effort to maximize drainage of the compressible soils. For load test comparisons, a single rammed aggregate pier was constructed with conventional roadstone.

The open-graded aggregate will be referred to as Gradation A and is classified as a poorly graded gravel (GP) by the Unified Soil Classification System. The roadstone will be

referred to as Gradation B and is classified as well-graded gravel with silt and clay (GW-GM). Figure 38 shows the grain-size distributions of Gradations A and B.

Long-Term Monitoring Program

Vibrating wire settlement cells and total stress cells have been installed at Ramp "C" for continuous and long-term monitoring of the rammed aggregate pier reinforced foundation soils and supported embankment. Total stress cells were installed at Ramp "B" for monitoring of the stone column reinforced foundation soils and supported embankment. The total stress cells are used to study stress concentrations on rammed aggregate piers and stone
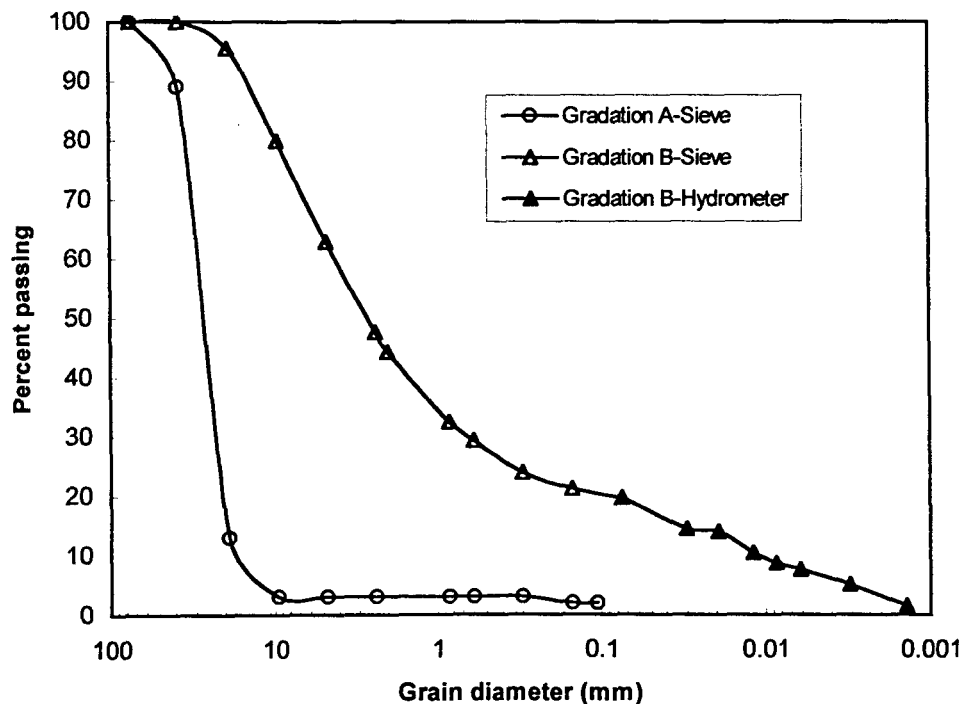
Figure 38. Aggregate particle-size distributions for the aggregate used in construction of stone columns (Gradation A) and rammed aggregate piers (Gradations A and B)

columns under an embankment load. In addition to the vibrating wire instrumentation, settlement plates have been installed at both ramps for additional settlement monitoring by survey methods. The vibrating wire instrumentation and settlement plates were monitored continuously during construction of the embankments and will be monitored for the next five years. Figures 16 and 17 show the instrumentation and settlement plate locations for Ramp "C" and "B", respectively. Figure 39 is a photograph of a group of settlement cells and total pressure cells at Ramp "C". Figure 40 is a photograph of the instrument console where the data logger is attached and readings are taken.

Figure 39. Settlement cells and total stress cells at Ramp "C"
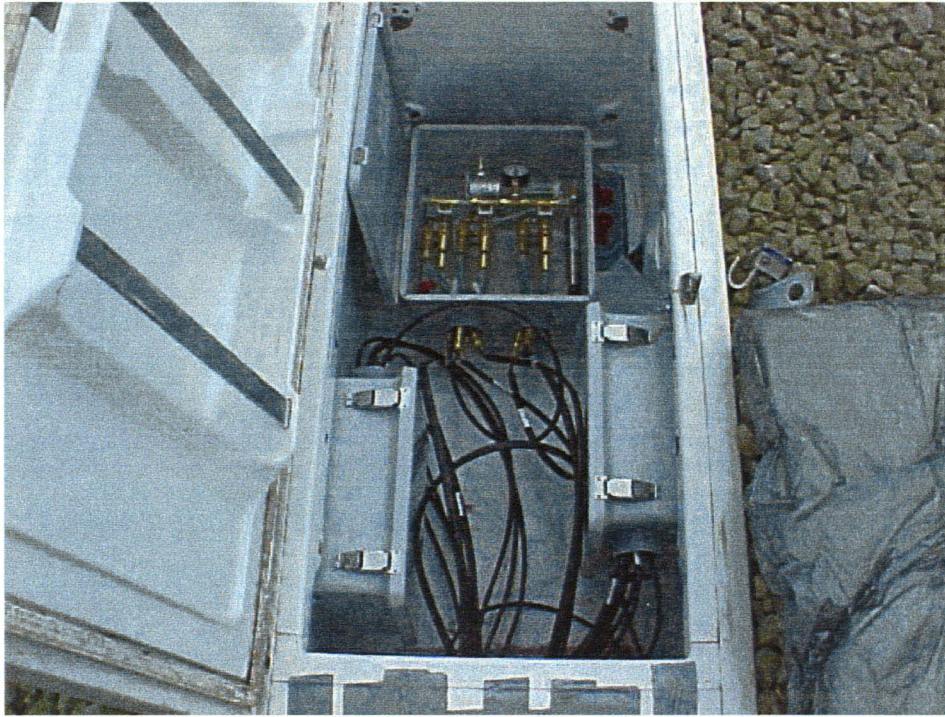
Figure 40. Instrumentation console

Settlement

Instrumentation

Three groups of vibrating wire settlement cells were installed at Ramp "C" prior to embankment construction. Settlement cell locations 1 and 2 each include a cell positioned on a rammed aggregate pier and a cell positioned on the adjacent matrix soil. Settlement cell location number 3 is located outside the rammed aggregate pier reinforced foundation area for comparison.

Survey

Two settlement plates were installed at Ramp "C" prior to embankment construction. Plate number 1 is located outside the rammed aggregate pier area and plate number 2 is positioned between rammed aggregate piers. Three settlement plates were installed at Ramp

"B" prior to construction of the embankment. Plate number 3 is positioned on a stone column and plate numbers 4 and 5 are positioned between stone columns.

Stress concentrations

Instrumentation

Five vibrating wire total stress cells were installed at Ramp "C" prior to embankment construction. Stress cell locations 1 and 2 each include a stress cell positioned on top of a rammed aggregate pier and a cell positioned on the adjacent matrix soil. Stress cell location number 3 is located outside the rammed aggregate pier reinforced area and includes a single stress cell positioned on the foundation soil.

Six vibrating wire total stress cells were installed at Ramp "B". Each stress cell location includes a cell positioned on top of a stone column and a cell positioned on the adjacent matrix soil.

FIELD INVESTIGATION RESULTS AND DISCUSSION

Site Conditions

At Ramp "C" foundation soils consist of approximately 0.5 to 1 meter of medium to stiff clay underlain by a compressible alluvial clay layer varying from 4 to 6 meters in thickness. Underlying the alluvial clay is a stratum of fine-grained alluvial sand and silty sand deposits varying from 4 to 4.5 meters in thickness. Underlying the alluvial sand is stiff weathered shale at depths of 8.5 to 11 meters.

At Ramp "B" foundation soils consist of approximately 2.8 meters of fill underlain by 3 meters of alluvial silt. Underlying the alluvial silt is a 2.5 meter thick layer of interbedded alluvial silts and clays. Underlying the interbedded silts and clays is a compressible alluvial clay layer of 3.5 meter thickness. Weathered shale was encountered at a depth of 12 meters.

From piezocone penetration soundings it was determined that the stone column upper zone soils are approximately 1.2 times stiffer than the rammed aggregate pier's. This was calculated based on the average tip resistance, q_c, since q_c is directly proportional to E_s (Bowles, 1996).

Layout

Rammed aggregate piers

The rammed aggregate pier layout was designed as a square layout pattern as shown in Figure 41. The piers were designed with a spacing (s) of 1.82 m (6 ft) and a diameter (D_s) of 0.76 m (2.5 ft). The area replacement ratio for this arrangement is therefore:

$$a_s = 0.785 \left(\frac{D_s}{s} \right)^2 = 0.137,$$ i.e., 13.7 % of the reinforced area was replaced by rammed

Ø 0.76m — Rammed aggregate piers

1.8m

1.8m
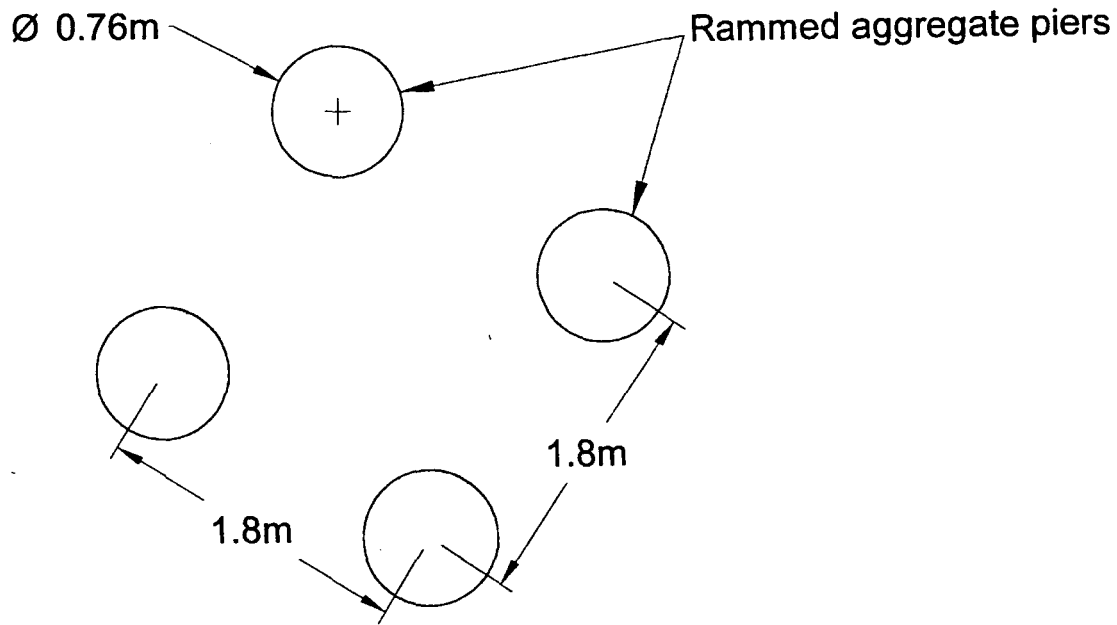
Figure 41. Rammed aggregate pier layout detail (Ramp "C")

aggregate piers elements. The length of the piers varied from 5-6 m (16.4-19.7 ft) at the

south edge of the reinforced area to 4.5-5.5 m (14.8-18 ft) at the north edge of the

reinforcement area depending on the depth of the alluvial clay.

Stone columns

The stone column layout was designed as an equilateral triangle layout pattern as

shown in Figure 42. Like the rammed aggregate pier layout, the stone column layout was

designed with a spacing (s) of 1.82 m (6 ft); however, the stone columns were designed

slightly larger with a diameter (D_s) of 0.91 m (3 ft). The area replacement ratio for the stone

column arrangement is therefore: $a_s = 0.907\left(\dfrac{D_s}{s}\right)^2 = 0.227$, i.e., 22.7% of the reinforced

area was replaced by stone column elements. The length of the stone columns varied from 2-
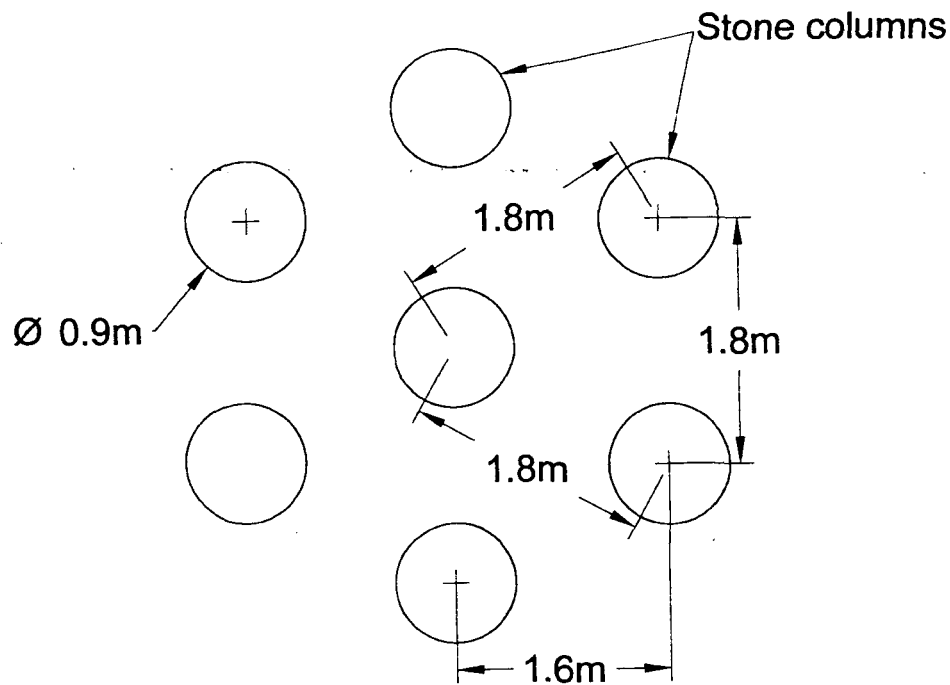
Figure 42. Stone column layout detail (Ramp "B")

4 m (6.6-13.1 ft) at the south edge of the reinforced area to up to 14 m (32.8 ft) at the north

edge of the reinforcement area depending on the depth of the sediment-shale interface.

Results

Several key factors were previously defined in the "Review of Literature" and will be

used to evaluate and compare the performance of rammed aggregate piers and stone columns.

The results of their effects on settlement, stress concentrations, rate of consolidation and their

influence of lateral stress on the surrounding soil matrix are included herein. Load tests were

performed on rammed aggregate piers of two aggregate gradations and a single load test was

performed on a stone column. The results of the load tests and an evaluation of comparative

stiffness are included herein.

Settlement

Foundation settlements were continuously monitored during embankment

construction and thereafter using conventional surveying techniques for both ramps. In

addition to surveys, vibrating wire settlement cell instrumentation was installed under Ramp

"C" for continuous, long-term monitoring.

Ramp "C"

Predicted settlement. Settlements of 12 to 25 cm (4.7 to 9.7 in) following Stage 1

and an additional 10 to 14 cm (4 to 5.6 in) following Stage 2 of embankment construction

have been estimated using CTPU and confined compression (oedometer) data. Details of the

settlement estimates using CPTU and confined compression (oedometer) data are shown in

Appendix B and F, respectively.

Using the average of the two settlement estimates, time-settlement relationships were

computed by Terzaghi's consolidation equation:

$$t = \frac{TH^2}{c_v} \tag{11}$$

where "t" is the elapsed time in which a fraction of settlement occurs, "T" is a time factor

relating the percentage of settlement complete, "H" is the maximum distance through which

pore-water must flow in order to escape the consolidating layer, and c_v is the coefficient of

consolidation established from confined compression (oedometer) testing. The time-

settlement relationships were calculated based on the assumption that an average c_v of 0.145

m^2/day represents the entire compressible layer (average determined from 3 confined

compression tests).

Time-settlement relationships for the scenarios of (1) an unreinforced foundation and (2) a rammed aggregate pier reinforced foundation were calculated assuming drainage was not allowed through the embankment soils. A one-dimensional drainage distance of 5.6 m was used for the unreinforced embankment foundation scenario. The rammed aggregate pier reinforced foundation experiences double-drainage with a maximum drainage distance of 0.9 m (half the distance between piers). Actual foundation settlements for the rammed aggregate pier reinforced area measured less than 4 cm (1.6 in) as determined from settlement plate surveys (discussed later). An additional 4 cm (1.6 in) of settlement is anticipated following Stage 2. Figure 43 shows predicted time-settlement relationships for the nonreinforced condition along with measured (Stage 1) and predicted (Stage 2) settlements for the reinforced foundation. Figures 44 and 45 show more detailed plots of the time-settlement relationships for Stages 1 and 2 of embankment construction. As illustrated by the time-settlement relationships the time frame to reach approximately 95% primary consolidation is about 10 days for the rammed aggregate pier reinforced foundation compared to about 250 days had the foundation not been reinforced with rammed aggregate piers. Because of this significant increase in time-rate of consolidation, time delays for subsequent bridge construction can be significantly reduced.

Actual settlement. Two settlement plates were installed under Ramp "C" prior to embankment construction. Plate number 1 is located outside the rammed aggregate pier area and is covered by approximately 5.7 m of fill as shown in Table 3. Located near plate number 1 is a vibrating wire settlement cell (location number 3) intended for continuous and long-term settlement monitoring, also covered by 5.7 meters of fill. Plate number 2 is
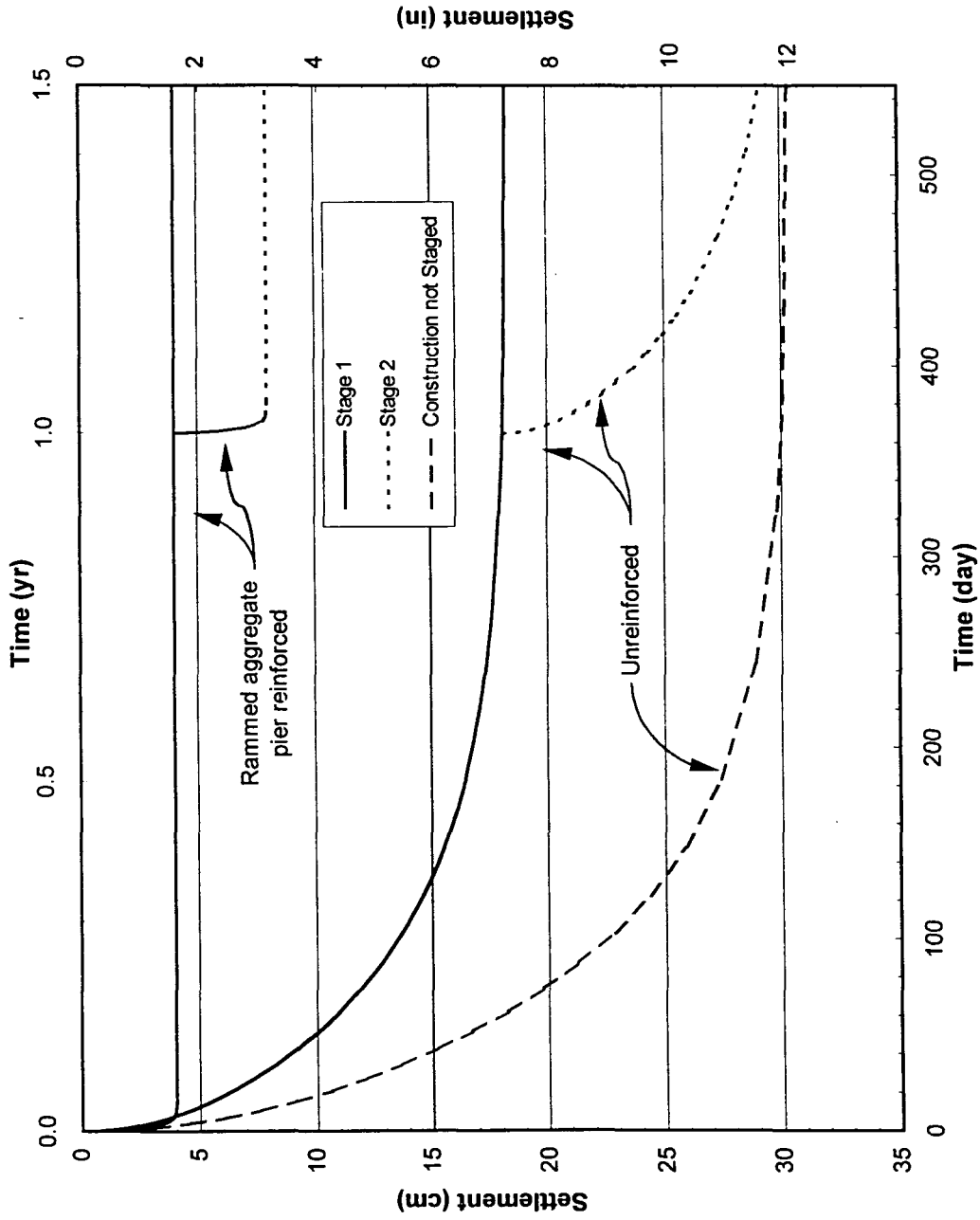
Figure 43. Predicted time-settlement relationships for Ramp "C"
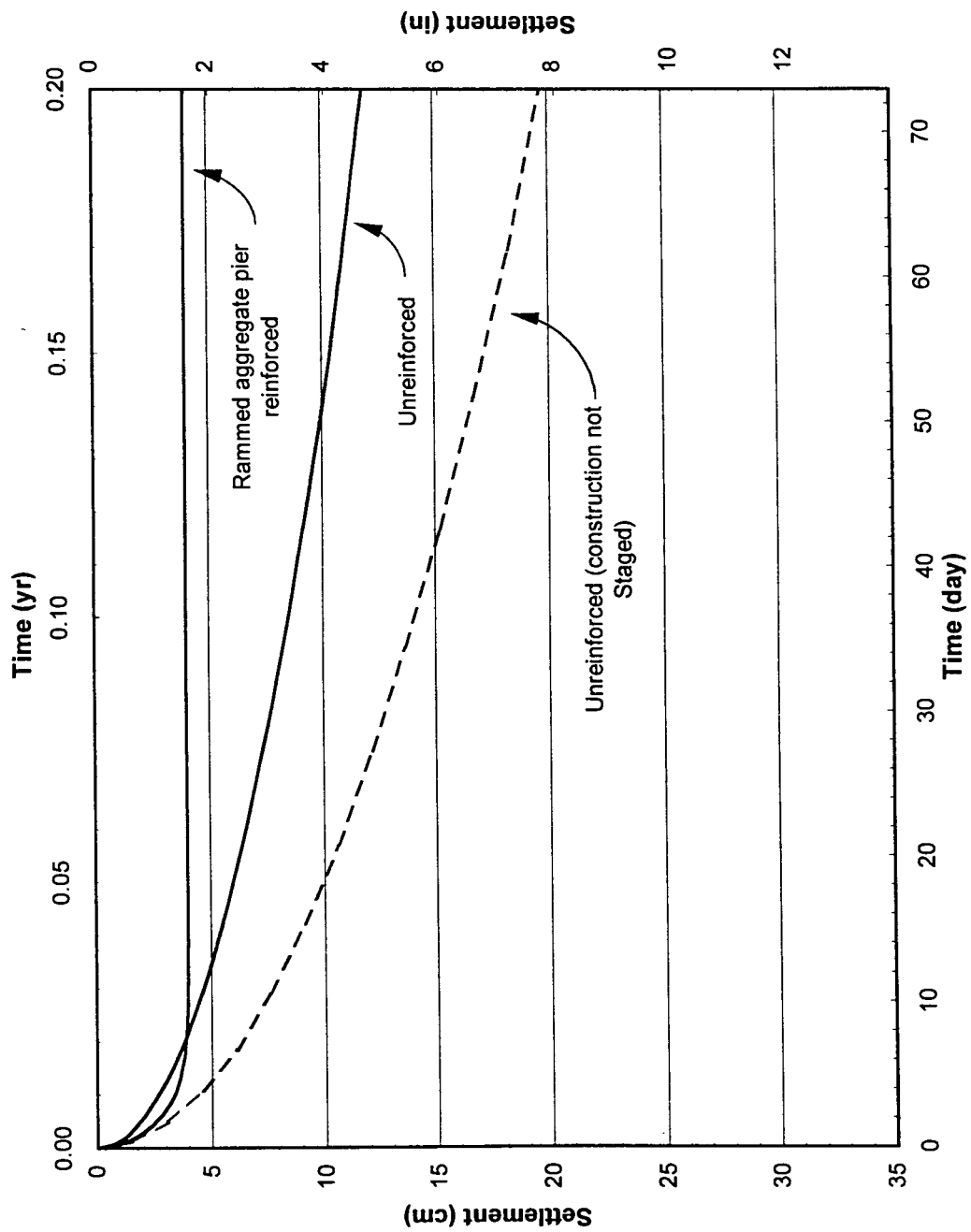
Figure 44. Predicted time-settlement relationships for Stage 1 embankment construction (Ramp "C")
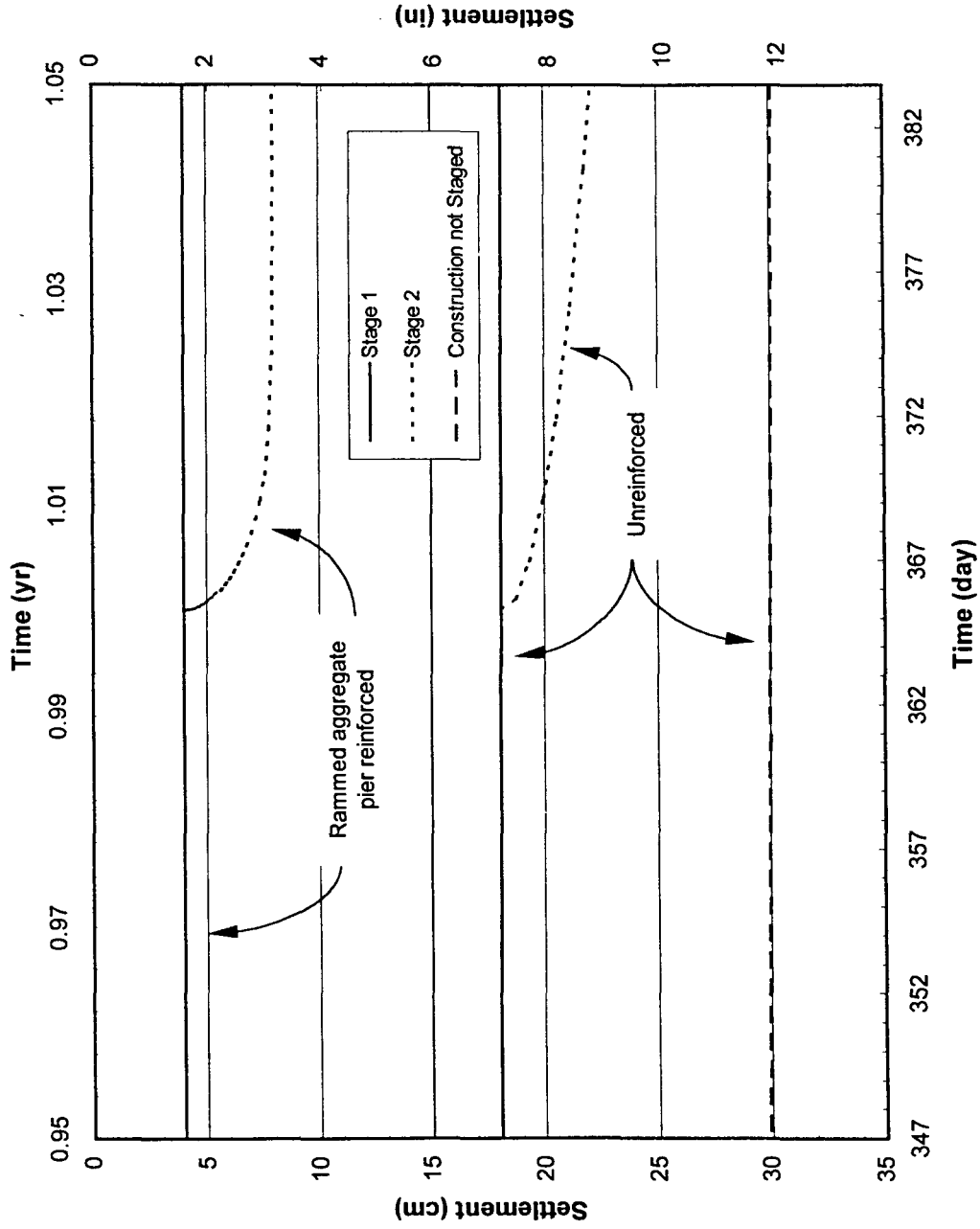
Figure 45. Predicted time-settlement relationships for Stage 2 embankment construction (Ramp "C")

positioned between rammed aggregate piers and is covered by approximately 4.7 m of fill.

Two groups of vibrating wire settlement cells (locations 1 and 2) are located in the rammed

aggregate pier reinforced area. Each group contains a cell positioned on a rammed aggregate

pier and a cell positioned on the adjacent matrix soil. During Stage 1 the settlement cells

were covered by only 2.4 m of fill, however, they will be covered to full fill height (9 m

total) during Stage 2.

Figure 46 shows the results of settlement plates 1 and 2 as a function of fill height and

Figure 47 shows the same results as a function of time. Each plot shows considerable scatter,

however, settlement trends are apparent. Settlement of the reinforced foundation (S_r) was

approximately 2.5 cm (1.0 in) and settlement of the unreinforced foundation (S_u) was

approximately 6.5 cm (2.6 in). From this settlement data, the settlement ratio for Stage 1 is

$0.38 \left(SR = \dfrac{S_r}{S_u} \right)$ and the improvement factor is 2.3 $\left(IF = \dfrac{1}{SR} \right)$, i.e., rammed aggregate piers

reduced settlement by a factor of 2.3 times that of the unreinforced foundation.

Stage 1 of embankment construction was completed by the beginning of August

2000. The time-settlement relationship shown in Figure 47 shows that foundation settlement

in the rammed aggregate pier reinforced area was nearly complete by the middle of the

August. As predicted, time delays for subsequent bridge construction could be significantly

reduced.

Figure 48 shows the results of vibrating wire settlement cell locations 1 and 2 as a

function of time. The settlement cells show movements of over 20 cm (7.9 in) in the rammed

aggregate pier reinforced foundation. These results compared to the results of the settlement

plates (approximately 2 cm) indicate that one of the methods is yielding erroneous results. If
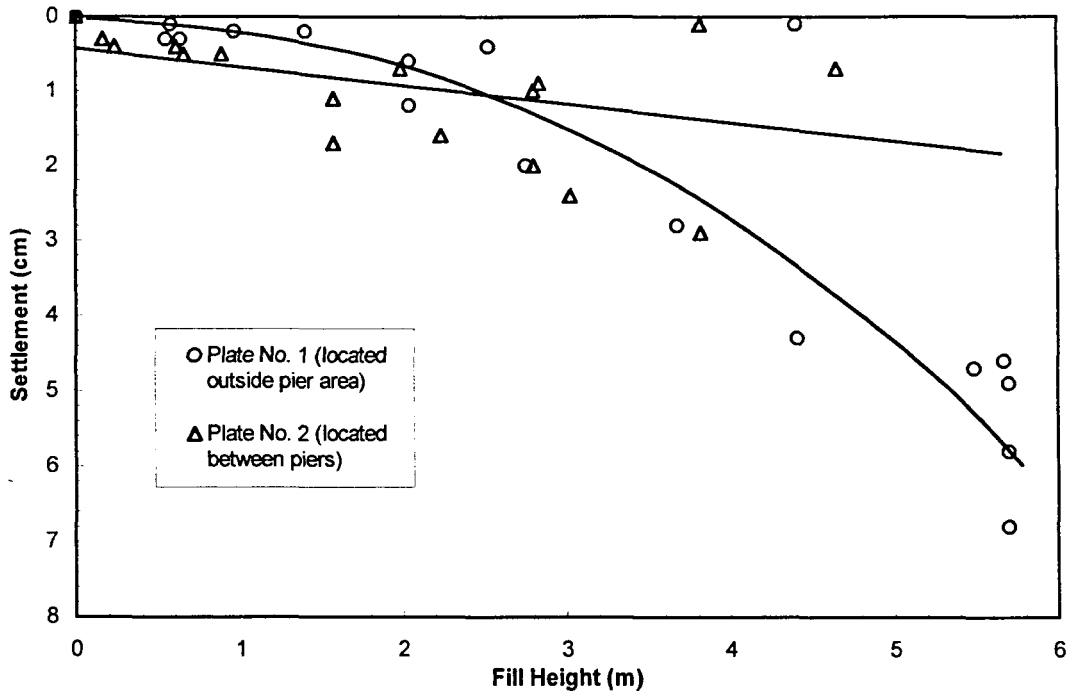
Figure 46. Ramp "C" (Stage 1) settlement plate measurements as a function of fill height
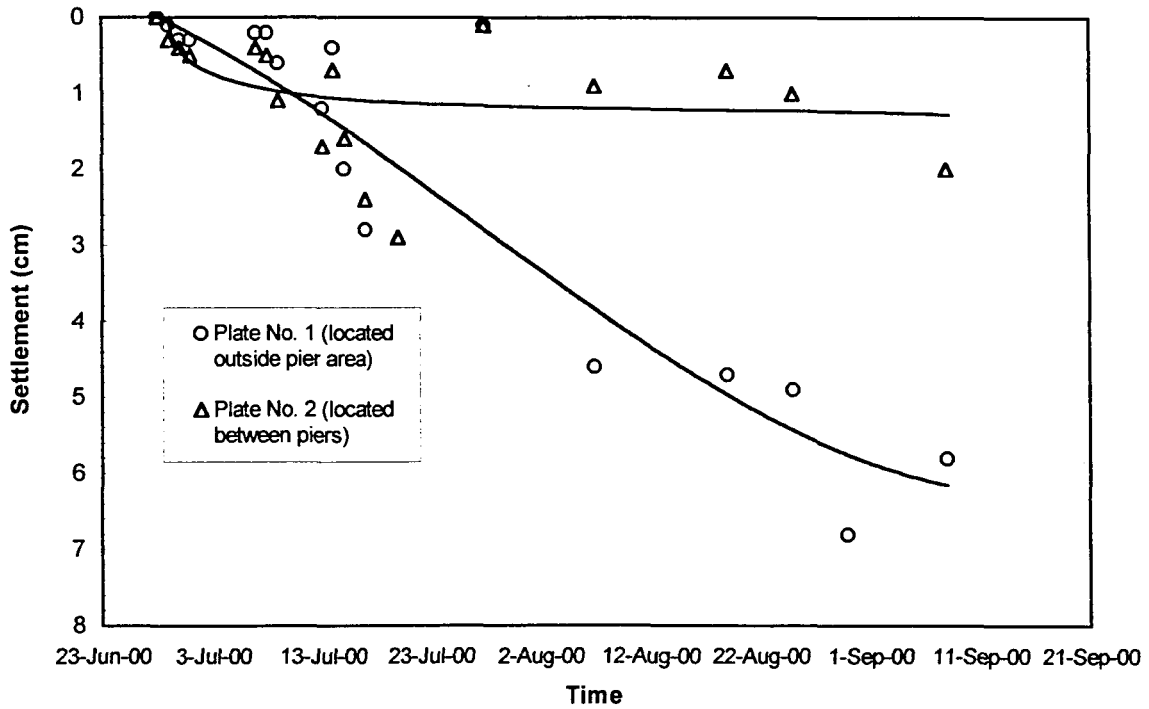
Figure 47. Ramp "C" (Stage 1) settlement plate measurements as a function of time
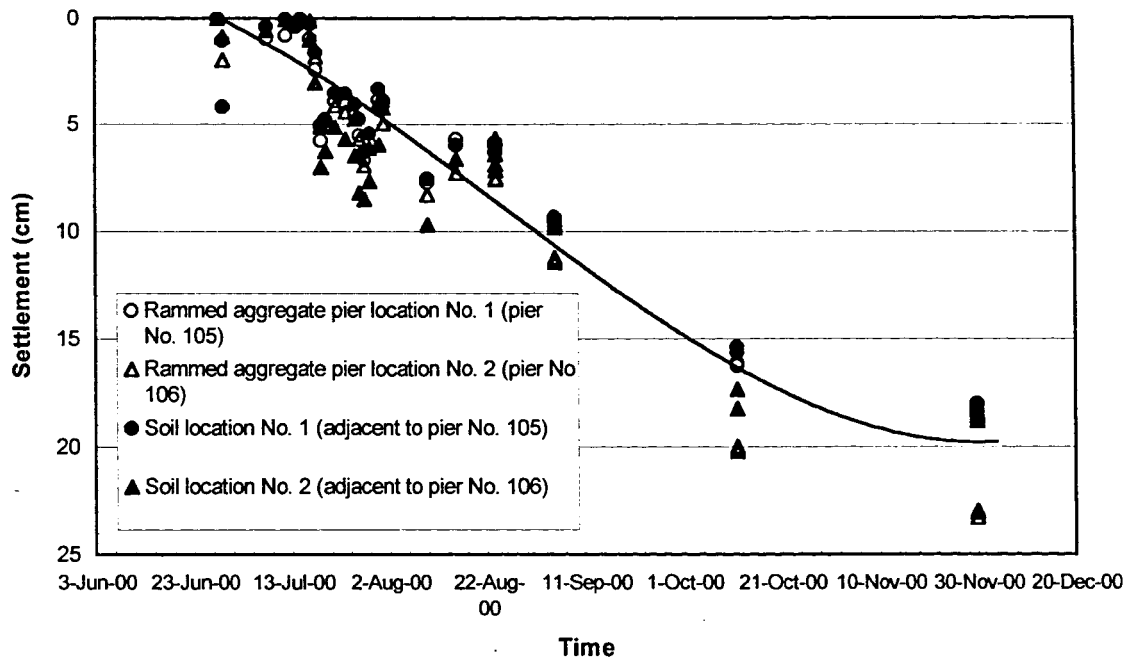
Figure 48. Ramp "C" (Stage 1) settlement cell readings as a function of time (locations 1 and 2)

the movements of cell locations 1 and 2 (20+ cm) are compared to the movement of cell location 3 (13 cm) shown in Figure 49, it is suggested that the error is most likely associated with settlement cell locations 1 and 2. The rationale for this deduction is that it is highly unlikely that the reinforced matrix soils settled nearly twice as much as the unreinforced soils. The nature of the error at settlement cell locations 1 and 2 is unknown at this time.

Although there may be significant error in the magnitude of the settlement deduced from settlement cell locations 1 and 2, a significant observation can be made from the data. As shown by the significant overlap of the markers of the settlement plot in Figure 48, it appears that the rammed aggregate pier elements and the soft adjacent matrix soils settled nearly identical amounts. This suggests that the rammed aggregate piers may be confining the adjacent soil matrix preventing excessive settlement.
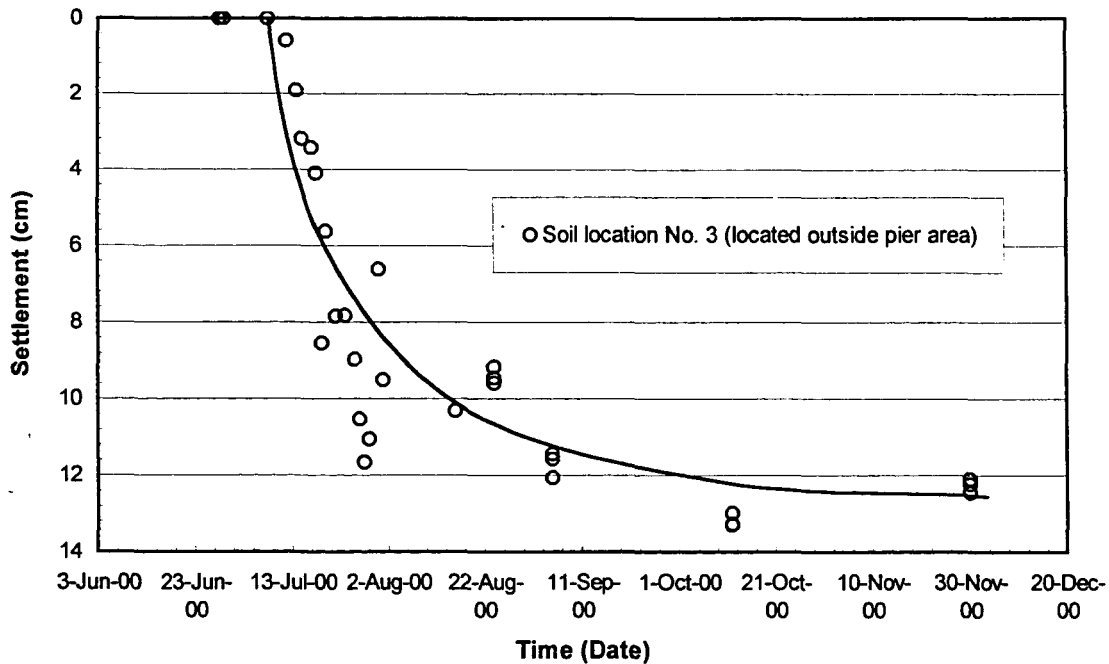
Figure 49. Ramp "C" (Stage 1) settlement cell readings as a function of time (location 3)

Ramp "B"

Three settlement plates were installed under Ramp "B" prior to embankment construction. Plate number 3 is positioned on top of a stone column and plates 4 and 5 are positioned between stone columns. As shown in Table 4, settlement plates 3, 4 and 5 are covered by approximately 7.7, 7.7 and 8.4 m of fill, respectively.

Figure 50 shows the results of settlement plates 3, 4 and 5 as a function of fill height and Figure 51 shows the settlement plate results as a function of time. Plate number 3 settled approximately 10 cm (3.9 in) while plates 4 and 5 experienced significantly greater settlements of up to 65 cm (25.6 in). From this it can be determined that the soil matrix surrounding the stone columns is settling independently from the stone columns. The fact
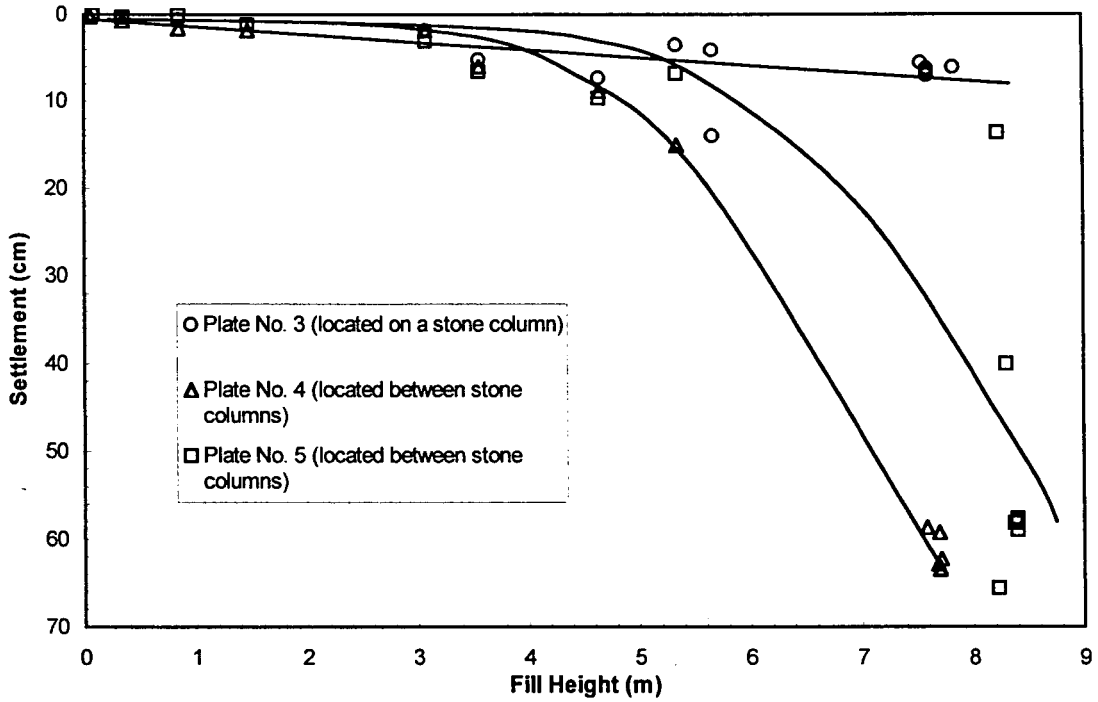
Figure 50. Ramp "B" settlement as a function of fill height
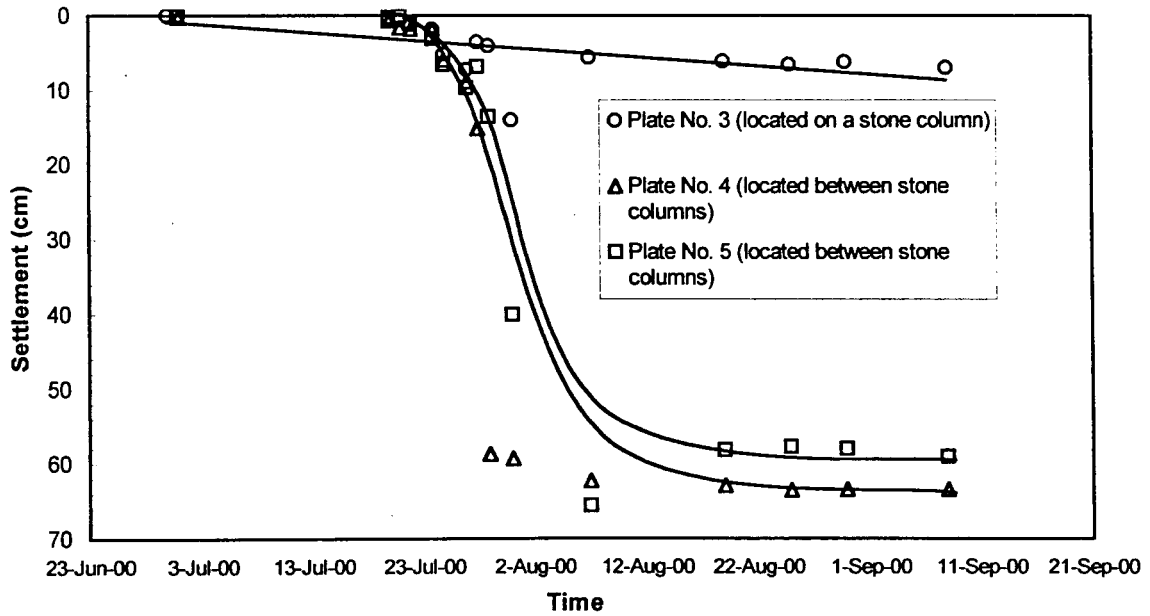
Figure 51. Ramp "B" settlement as a function of time

that the matrix soil and stone columns are acting independent of each other suggests that the matrix soil is shearing along the perimeter of the stone columns.

Ramp "B" embankment construction was completed by the middle of August 2000. The time-settlement relationship shown in Figure 51 shows that foundation settlement was nearly complete by the end of the month. Similar to Ramp "C", time delays for subsequent bridge construction could be significantly reduced.

Stress concentrations

Ramp "C"

Five vibrating wire total stress cells were installed at Ramp "C" prior to embankment construction. Stress cell locations 1 and 2 as shown in Figure 16 include a cell positioned on top of a rammed aggregate pier and a cell positioned on the adjacent matrix soil, each covered by approximately 2.4 m of fill. Stress cell location number 3 is located outside the rammed aggregate pier reinforced area and includes a single stress cell positioned on the unreinforced foundation soil. Stress cell location number 3 is currently covered by approximately 5.7 m of embankment fill.

Figure 52 shows readings of stress cell locations 1 and 2 as a function of embankment fill height. As a frame of reference the theoretical vertical stress was plotted based on an assumed unit weight (γ) of 20.42 kN/m^3 (130 lb/ft^3) for the embankment soils. Although it was expected that the stiffer elements of the rammed aggregate piers carry a larger percentage of the theoretical total vertical stress, it was not expected that the soft clay surrounding the piers carry a larger percentage of the theoretical vertical stress as well (Fox and Lawton, 1994; Stewart and Fahey, 1984). All four stress cells at locations 1 and 2
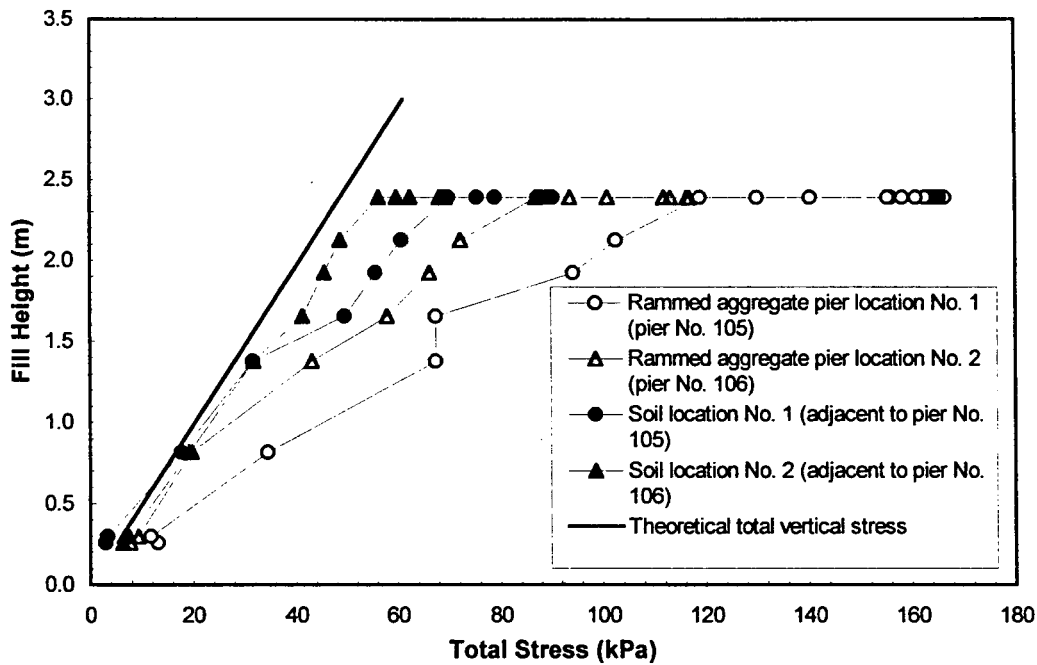
Figure 52. Ramp "C" total stress cell locations 1 and 2

measure increasing stress with time, with greater stress increases on the rammed aggregate

piers.

Figure 53 shows the ratio of the load carried by the piers to the load carried by the

adjacent soil matrix referred to as the stress concentration ratio (stress on the aggregate

elements/stress on the soil). Stress concentration ratios greater than one indicate that the

rammed aggregate piers are bearing more load than the adjacent matrix soil. As expected, as

consolidation continues, a greater portion of the bearing load is transferred to the stiff

elements of the rammed aggregate piers and the stress concentration ratio increases with time

(Fox and Lawton, 1994). The average stress concentration ratio at Ramp "C" is 1.7.

Figure 54 shows data for stress cell location number 3 as a function of fill height.

Again the theoretical vertical stress was plotted based on an assumed unit weight (γ) of 20.42
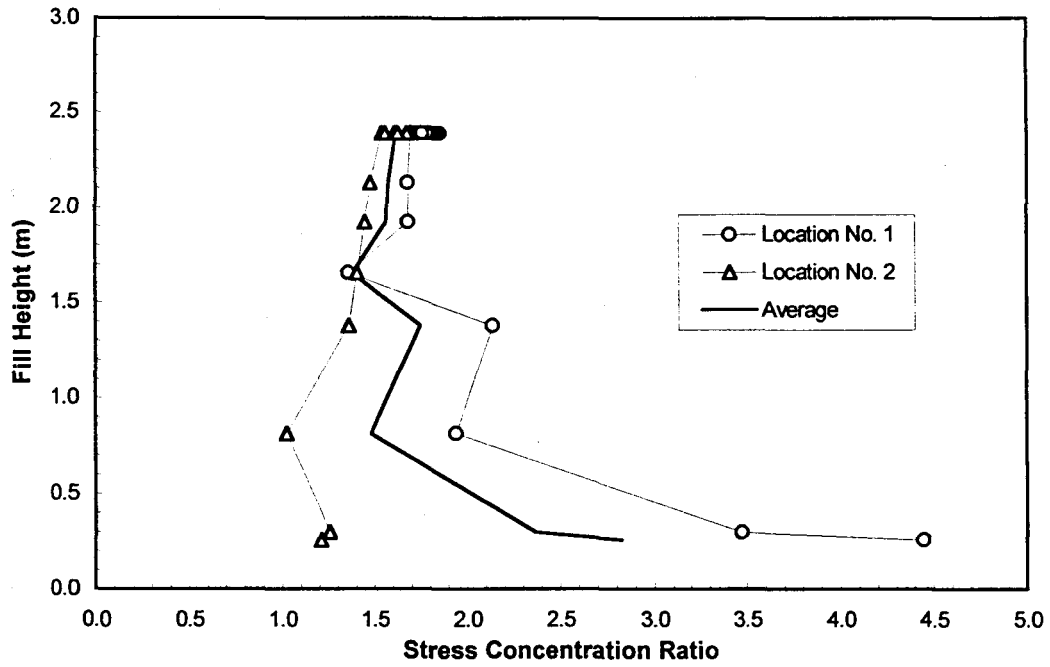
Figure 53. Rammed aggregate pier stress concentration ratios (Ramp "C")
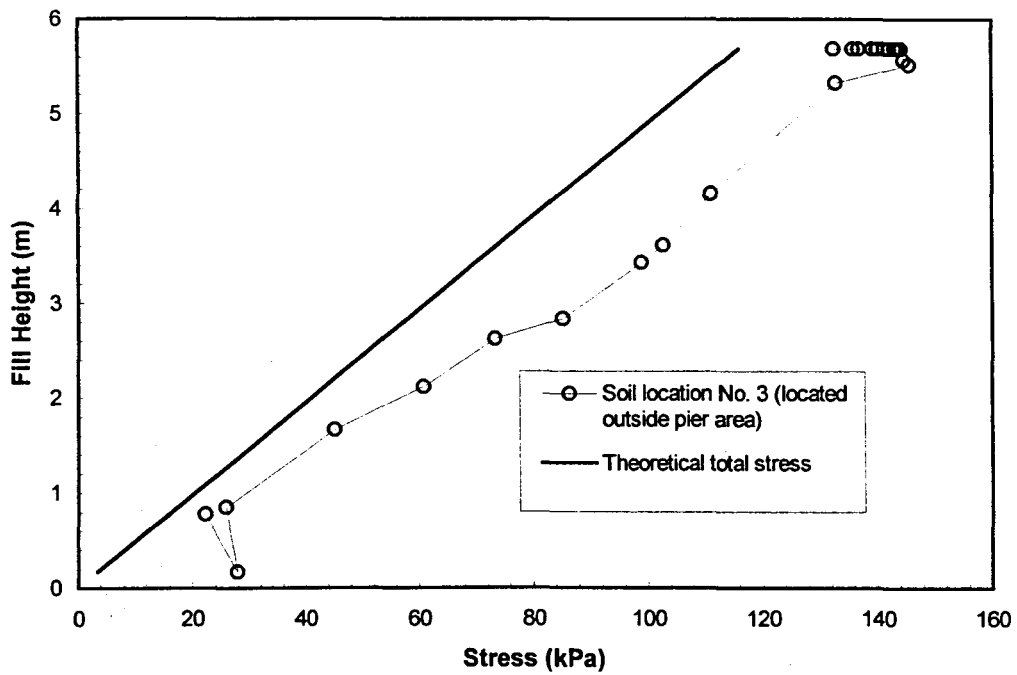
Figure 54. Ramp "C" total stress cell location No. 3

kN/m³ (130 lb/ft³) for the embankment soils. Similar to stress cell locations number 1 and 2, the soil is carrying a larger vertical stress than the calculated theoretical. This was unexpected considering the maximum dry unit weight of the fill soil as determined from a standard proctor compaction test is 18.6 kN/m³ (118.3 lb/ft³). Unlike stress cell locations 1 and 2, the total stress at cell location 3 is decreasing with time. This is presumed to be because the soils at location number 3 are not confined as they are at locations 1 and 2.

Ramp "B"

Six vibrating wire total stress cells were installed at Ramp "B" prior to embankment construction. Figure 17 shows the locations of the total stress cells at Ramp "B". Each stress cell location includes a cell positioned on top of a stone column and a cell positioned on the adjacent soil matrix of the stone column. 6.4, 8.6 and 9.0 m of fill cover stress cell locations 1, 2 and 3, respectively.

Figure 55 shows the total stress cell readings as a function of fill height. As a frame of reference the theoretical geostatic vertical stress was plotted based on an assumed unit weight (γ) of 20.42 kN/m³ (130 lb/ft³) for the embankment soil. Similar to the rammed aggregate piers the stone columns are carrying a larger portion of the surface load and the stresses are further increasing with time. Unlike the surrounding soil matrix of the rammed aggregate piers the load carried by the stone column soil matrix is not increasing with time. As previously shown, settlement results have indicated that the rammed aggregate piers and their matrix soils experienced similar magnitudes of settlements while stone columns and their matrix soils experienced greatly different magnitudes of settlement. It was previously indicated that the rammed aggregate pier matrix soils are confined by the piers and are
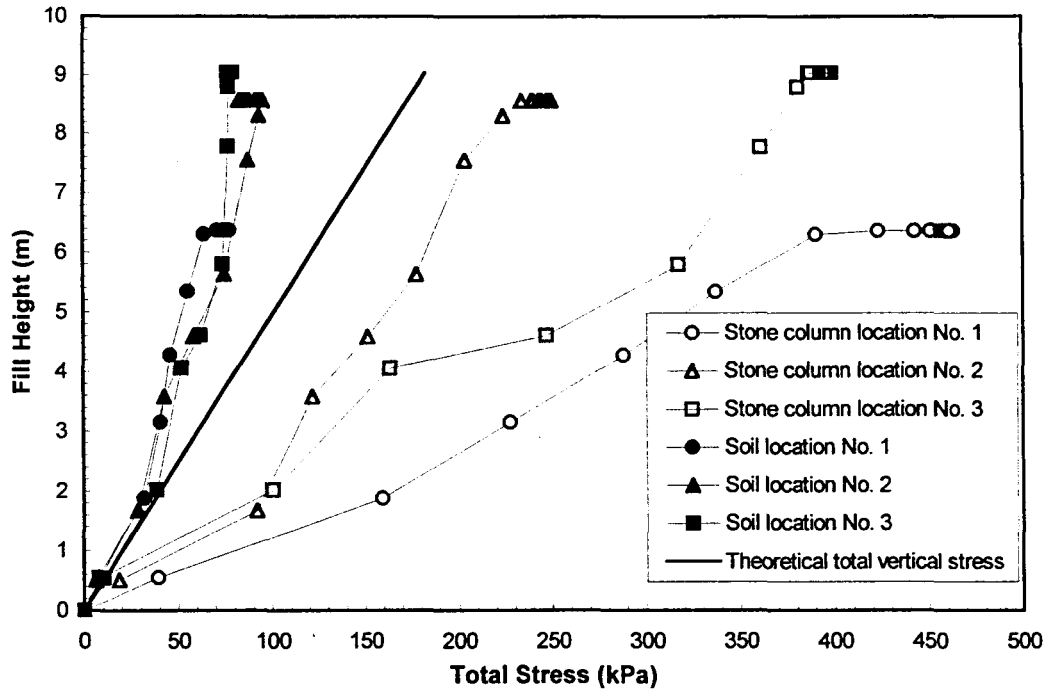
Figure 55. Ramp "B" total stress cell locations 1, 2 and 3

experiencing a stiffening effect because of the piers. As previously suggested, the stone

columns and their matrix soils are behaving independent of each other.

Figure 56 shows the stress concentration ratios for cell locations 1, 2 and 3 at Ramp

"B". The stress concentration ratios indicate that the stone columns are bearing greater load

than the adjacent soil matrix. As consolidation continues, a greater portion of the bearing

load is transferred to the stone columns and the stress concentration ratio increases with time.

The average stress concentration ratio for the total stress cell locations at Ramp "B" is 4.3.

Induced lateral stress

K_o-stepped blade tests were conducted to determine the influence rammed aggregate

piers and stone columns have on lateral stress development in the matrix soil. Initially, tests

were conducted in the far field condition to determine in-situ lateral stress conditions.
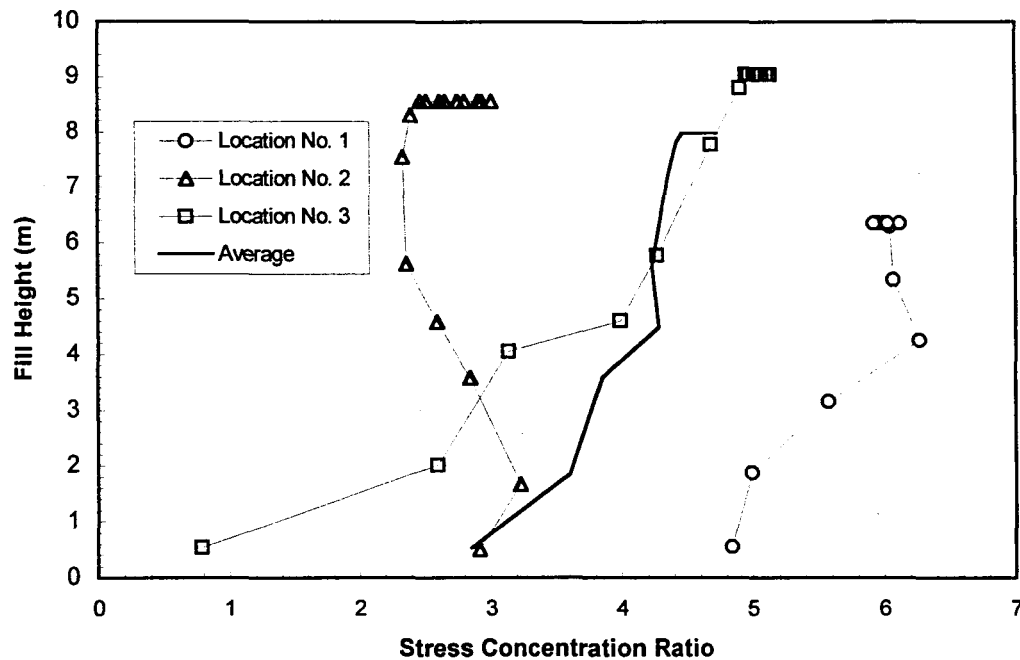
Figure 56. Stone column stress concentration ratios (Ramp "B")

After installation of rammed aggregate piers tests were conducted in the radial stress

direction (σ_r) and in the tangential stress direction (σ_θ). After installation of stone columns

tests were conducted in the radial direction (σ_r) only. Figures 16 and 17 show the locations

of K_o-stepped blade tests at Ramp "C" and "B", respectively.

Rammed aggregate piers

Figure 57 shows the far field lateral stress condition as well as lateral stress

measurements in the radial and tangential directions adjacent to a rammed aggregate pier.

Radial stress measurements were taken 0.85 m (2.8 ft) from the edge of a rammed aggregate

pier, while tangential stress measurements were taken 0.76 m (2.5 ft) from the edge. The

tangential effective stress was higher than the radial effective stress through the top half of
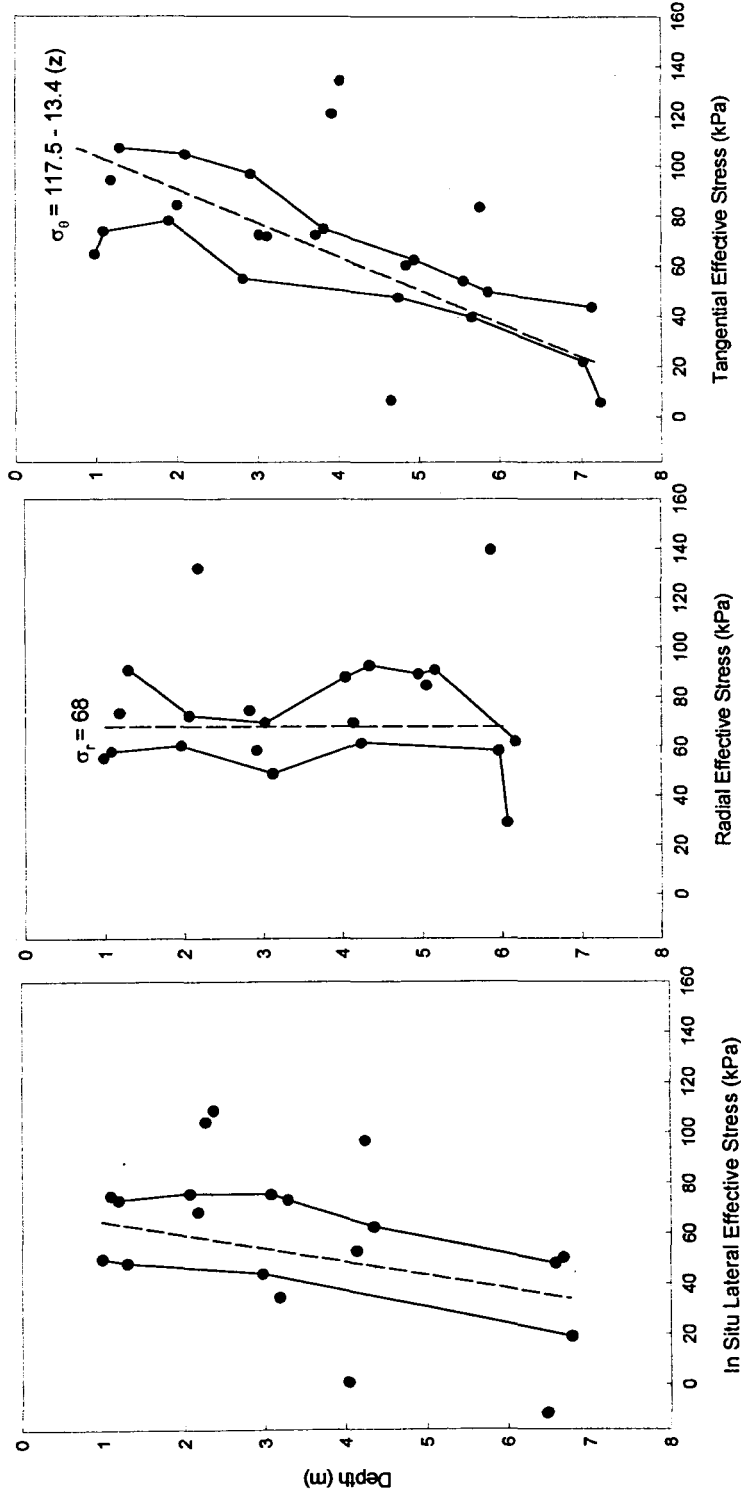
Figure 57. K_0-stepped blade lateral effective stress measurements: (left) lateral effective stress measurements in the far field condition, (middle) radial effective stress measurements 0.85 m from edge of a rammed aggregate pier, (right) tangential effective stress measurements 0.76 m from edge of a rammed aggregate pier

the rammed aggregate pier. This is likely a result of the influence of neighboring rammed aggregate piers since tests were conducted adjacent to several piers.

Figure 58 is a Mohr's circle representation of the results in Figure 57. The Mohr-Coulomb failure line was added based on cohesion and friction angles determined from borehole shear test data. From 0 to 3.7 m (12.1 ft) σ_r and σ_θ are the major and minor principle stresses, respectively. At 3.7 m $\sigma_r = \sigma_\theta$ and σ_v is the minor principal stress. At 3.7 m and deeper σ_r is the major principle stress.

The results of the K_o-stepped blade tests indicate that a group of rammed aggregate piers induces lateral stress in both the radial and tangential directions, and as a result of this, may inhibit settlement (Handy, 2001).

Stone columns

Figure 59 shows radial stress (σ_r) measurements 0.7 m (2.3 ft) from the edge of a stone column. At this location lateral stress development was variable. Note that it has previously been discussed that lateral stresses are typically not induced adjacent to a stone column until deformation and budging under load (Hughes and Withers, 1974).

Load test results

Full-scale load tests were conducted on two rammed aggregate piers and one stone column. Figure 60 shows a photograph of the load test setup. The rammed aggregate piers (one composed of Gradation A and one of Gradation B) were each approximately 6 m (19.7 ft) long. Tests were conducted 3 days after installation of the Gradation A pier and two days after installation of the Gradation B pier. A tell-tale was installed at the bottom of the
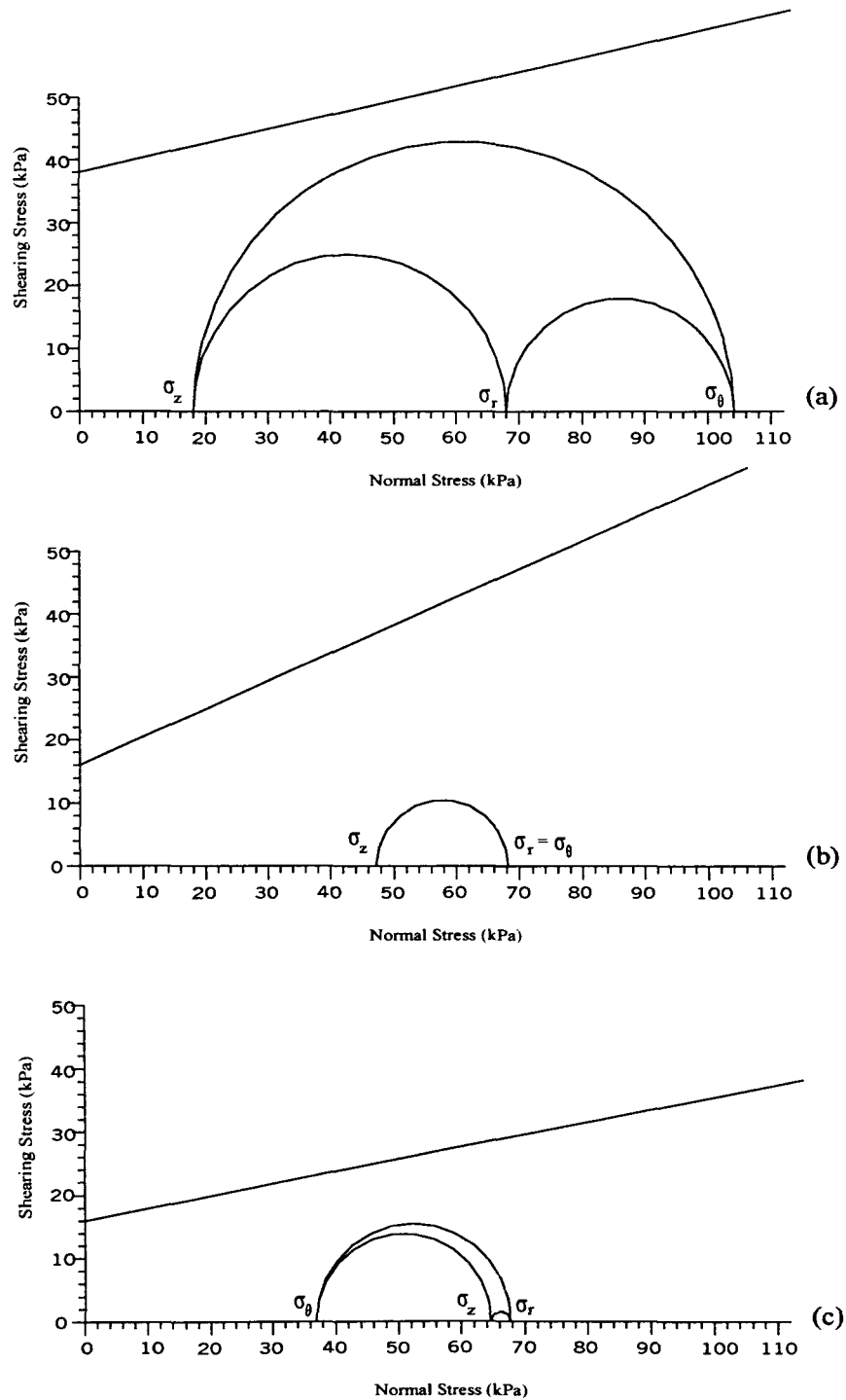
Figure 58. **Mohr's circle representation of radial and tangential stress data from K_o-stepped blade measurements 0.85 m from a rammed aggregate pier (a) $z=$ 1.0 m, (b) z = 3.7 m, (c) z = 6.0 m**
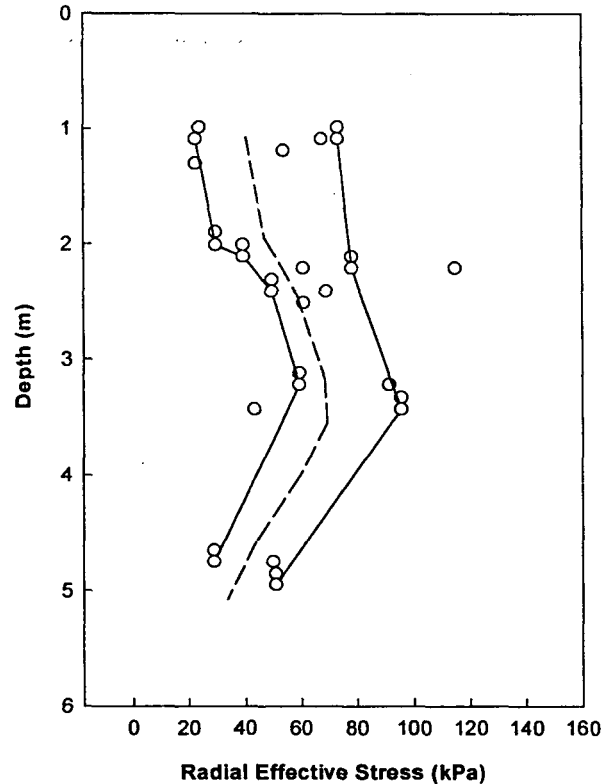
Figure 59. K_o-stepped blade radial effective stress measurements 0.70 m from edge of a stone column

rammed aggregate pier constructed with Gradation A aggregate. Figure 16 shows the

rammed aggregate pier load test locations.

The stone column (Gradation A) was approximately 5.0 m (16.4 ft) long and was

tested 13 days after installation. Figure 17 shows the location of the stone column load test.

The comparative load test results are shown in Figure 61. Results indicate that the rammed

aggregate piers are much stiffer than the stone column. At 200 kPa (4.2 ksf) the stone

column settled 21 mm (0.83 in) while the rammed aggregate piers each settled only 2 to 4

Figure 60. Full-scale load test setup

mm (0.08 to 0.15 in) despite the fact that CPTU results indicate that the stone column upper zone soils are 1.2 time stiffer than the rammed aggregate pier upper zone soils. The tell-tale at the bottom of the Gradation A pier experienced less than 1 mm (< 0.04 in) settlement. There was very little difference between the rammed aggregate pier constructed with Gradation A aggregate and the rammed aggregate pier constructed with Gradation B aggregate.
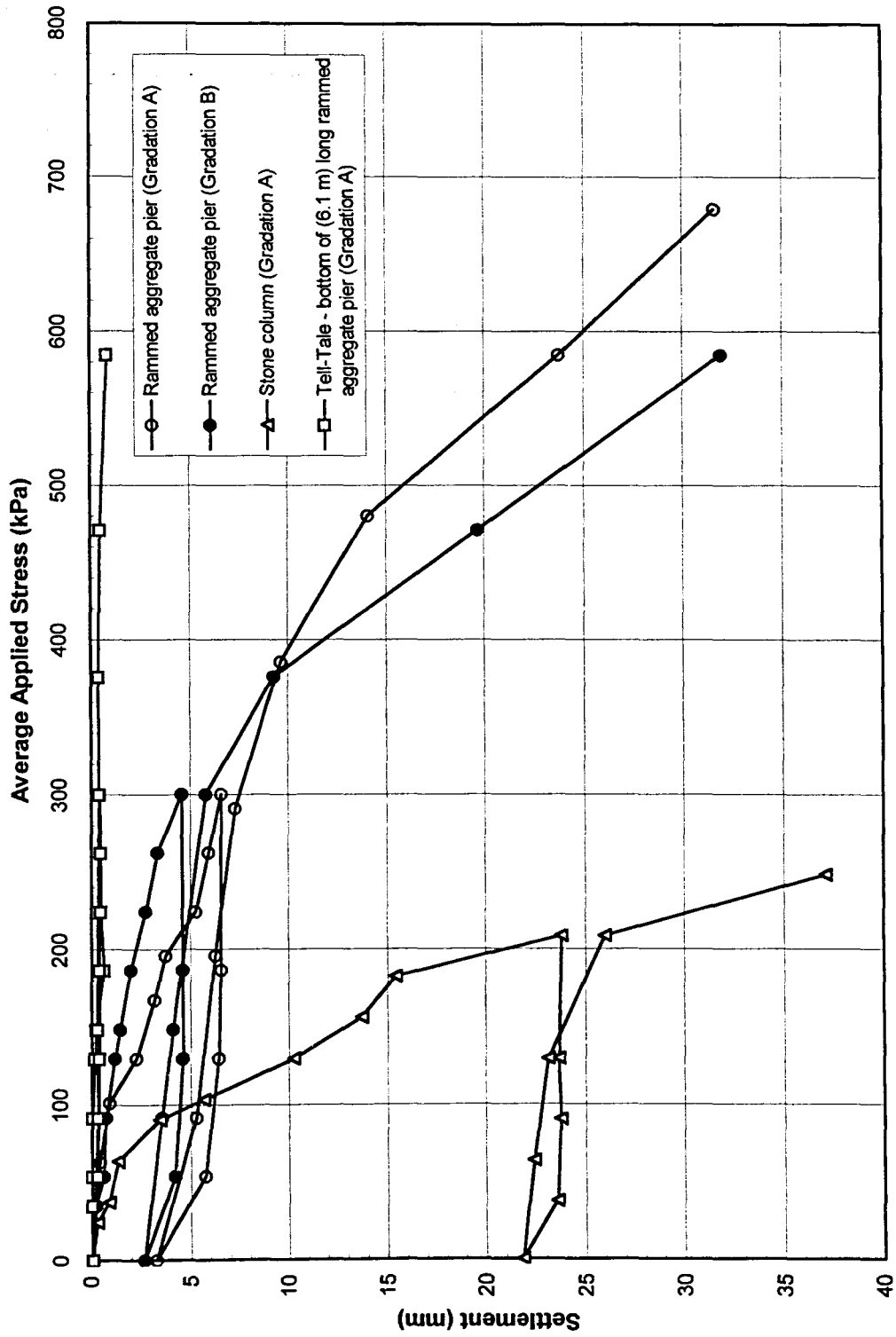
Figure 61. Comparative load test results of a stone column and rammed aggregate pier foundation elements

Comparative stiffness

Modulus values calculated from full-scale load tests are shown in Figure 62. It should be noted that the modulus parameter referred to at this time is not equivalent to the commonly known Young's modulus but is rather a measure of stiffness determined from each load test. The modulus values were calculated by the average applied stress divided by settlement. The unload portion of the data was not considered in this plot. A best-fit hyperbolic decay function was fitted to the data and was used to plot comparative stiffness between the stone column and rammed aggregate piers.

Legend:
- ● 91 cm (36 inch) Stone Column - Gradation A (R^2=0.93)
- ▼ 76 cm (30 inch) Geopier - Gradation A (R^2=0.98)
- ◇ 76 cm (30 inch) Geopier - Gradation B (R^2=0.88)

Y-axis: Modulus (MN/m³) (average applied stress/settlement)
X-axis: Average Applied Stress (kPa)
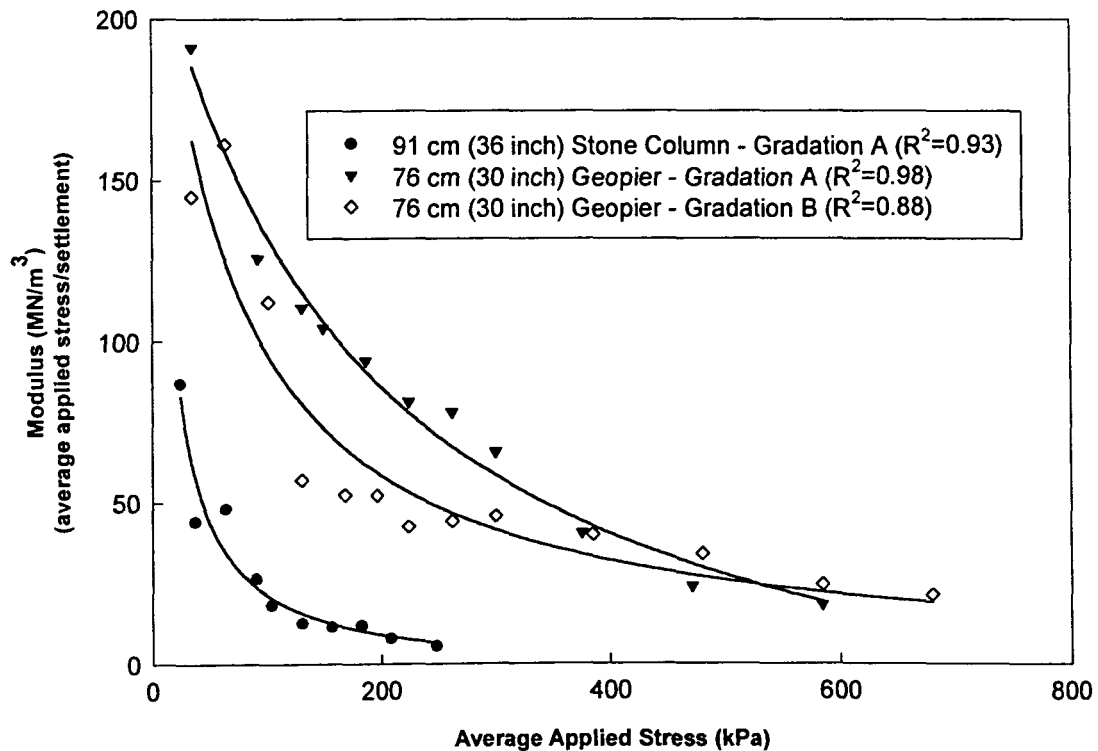
Figure 62. Rammed aggregate pier and stone column modulus verses applied stress (calculated from load test data)

Figure 63 shows the stiffness ratio between the rammed aggregate piers and the stone column. The stiffness ratio is the ratio of modulus values calculated from the load tests then multiplied by the ratio of soil stiffness. As previously mentioned, cone penetration data was used to determine the stiffness of Ramp "C" and "B" soils prior to improvements.

Because the stone column exceeded the displacement capacity of the loading device during testing, the solid line indicating measured stiffness in Figure 63 only extends to 250 kPa. However, the best-fit curves from Figure 62 were used to extend the stiffness ratio to higher loads and are shown as the projected stiffness ratios indicated by dashed lines. The results of the full-scale load tests indicate that the rammed aggregate piers are about 10 to 15 times stiffer than the stone column.
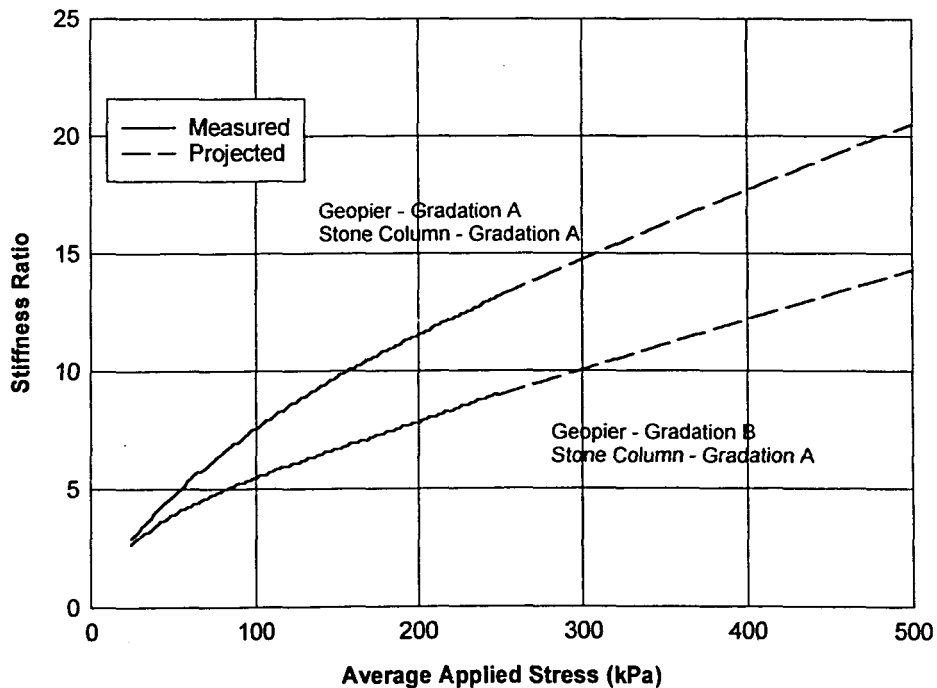
Figure 63. Stiffness ratio of rammed aggregate pier to stone column foundation elements

Comparative standard penetration (SPT) values

SPT soundings were performed through stone columns and rammed aggregate piers

for a measure of comparative density. The tests were performed in stone columns and

rammed aggregate piers constructed with the same aggregate type and gradation (Gradation

A). SPT N-values in stone columns averaged 10.6 ± 5.0 for 42 tests. In comparison N-

values in rammed aggregate piers averaged 16.7 ± 7.7 for 6 tests as shown in Figure 64. The

rammed aggregate piers averaged 58% higher N-values, indicating a stiffer, denser

composite material.

☐ Stone column (Ave=10.6, Std dev=5.0, n=42)
▨ Rammed aggregate pier (Ave=16.7, Std dev=7.7, n=6)
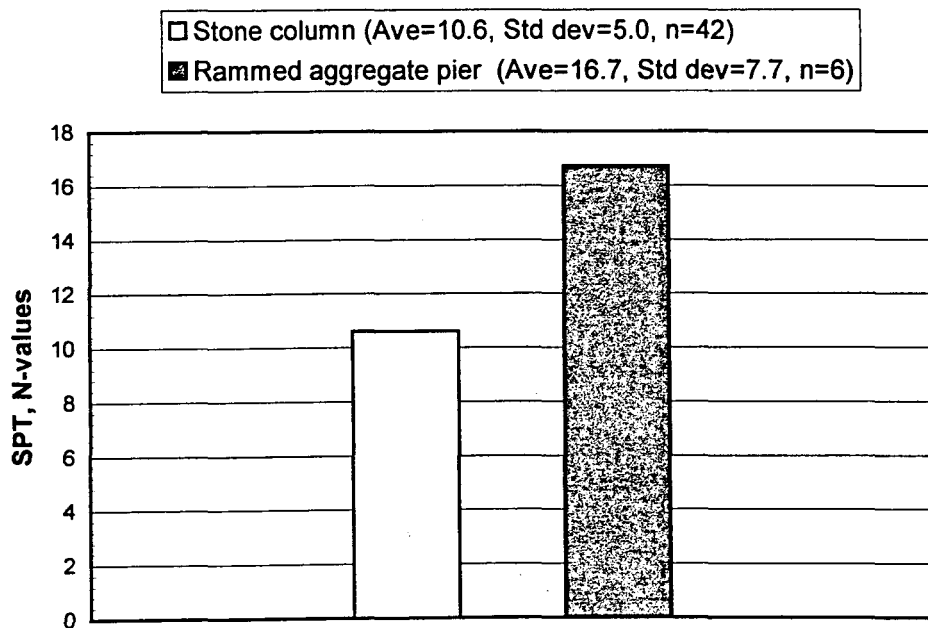
Figure 64. Comparative SPT-N values in stone columns and rammed aggregate piers

SUMMARY AND CONCLUSIONS

The following conclusions have been made based on the information gathered throughout the course of this investigation:

1. At Ramp "C" following completion of Stage 1 embankment construction under approximately 5 m (16 ft) of fill, the unreinforced foundation soils settled on the order of 6.5 to 13 cm (2.6 in to 5.1 in) while the rammed aggregate pier reinforced foundation soils settled only 2.5 cm (1 in). This calculates to settlement ratios (SR) ranging from 0.38 to 0.19 and improvement factors of 2.3 to 5.2, i.e., rammed aggregate piers reduced settlements by as much as 2.3 to 5.2 times that of an unreinforced foundation.

2. Rate of consolidation estimations predicted that up to 250 days would be necessary after embankment construction before subsequent bridge construction could safely begin if the foundation under Ramp "C" were not reinforced. Settlement plate surveys illustrated that settlement of the rammed aggregate pier reinforced foundation was nearly complete three to four weeks after embankment construction. Because of this significant increase in rate of consolidation, delays for subsequent bridge construction could be significantly reduced.

3. Vibrating wire total stress cells indicate that a greater portion of the bearing stress is carried by the stiffer elements of rammed aggregate piers and stone columns than adjacent matrix soils. This load transfer mechanism creates stress concentrations on the piers and columns. Following Stage 1 the average stress concentration ratio for the rammed aggregate piers is 1.7. The average stress concentration ratio for the stone columns is 4.3. Both indicate an increase in stress concentration with time

4. Vibrating wire total stress cells indicate that the rammed aggregate pier matrix soils are carrying a larger percentage of the embankment load than anticipated, while the stone column matrix soils are carrying a smaller percentage than anticipated. Furthermore, stresses on the rammed aggregate pier matrix soils are increasing with time while stresses on the stone column matrix soils and stresses on unreinforced soils are decreasing with time or remain constant. The increasing stresses on the rammed aggregate pier matrix soils are presumed to be due to a stiffening effect created by the piers as a result of soil confinement.

5. The rammed aggregate pier elements and the soft adjacent matrix soils settled nearly identical amounts, this coupled with the fact that the matrix soil is bearing more load than anticipated further suggests that the piers are confining the surrounding soil matrix. As a result the surrounding matrix soils are stiffened under load.

6. At Ramp "B" following completion of approximately 8 m (26 ft) of embankment fill, the stone columns settled 10 cm (3.9 in) while the adjacent matrix soils settled up to 65 cm (25.6 in). This coupled with the fact that the matrix soil is bearing considerable less stress than anticipated suggests that the stone columns and surrounding soils are acting independently of each other.

7. K_o-stepped blade results indicate that the interaction of a group of rammed aggregate piers induces lateral stress in both the radial and tangential directions, as a result, may inhibit settlement. Lateral stress development adjacent to the stone columns was variable.

8. Full-scale load test results indicate that rammed aggregate piers constructed of Gradations A and B are much stiffer than stone columns of Gradation A. At 200 kPa (4.2

ksf) the stone column settled 21 mm (0.83 in) while each rammed aggregate pier settled only 2 to 4 mm (0.08 to 0.15 in) despite the fact that CPTU results indicate that the stone column upper zone soils are approximately 1.2 times stiffer than the rammed aggregate pier upper zone soils. The tell-tale at the bottom of the Gradation A pier experienced less than 1 mm (< 0.04 in) settlement. There was very little difference between the rammed aggregate pier constructed with Gradation A aggregate and the rammed aggregate pier constructed with Gradation B aggregate.

9. Load test modulus values indicate that rammed aggregate piers are about 10 to 15 times stiffer than stone columns.

10. Standard penetration (SPT) blow counts in rammed aggregate piers were an average 58% larger than in stone columns constructed with the same aggregate. This indicates that the piers are a stiffer, denser composite material. N-values in stone columns averaged 10.6 ± 5.0 for 42 tests. In comparison N-values through rammed aggregate piers averaged 16.7 ± 7.7 for 6 tests.

RECOMMENDATIONS FOR FURTHER STUDY

1. Perform standard penetration (SPT) tests in rammed aggregate piers constructed with Gradation B aggregate. This would be beneficial for comparison to piers constructed with Gradation A aggregate as well as further comparison to stone columns.

2. Use the finite element method (FEM) to determine how σ_r and σ_θ interact with changes in depth for various rammed aggregate pier arrangements and spacings.

3. Perform pressuremeter (PMT) tests to determine if there are time dependant changes in p_L and E_o within rammed aggregate pier reinforced soils.

4. Investigate how stress concentrations vary with respect to overlying material type (rigid or soft) for rammed aggregate pier reinforced foundation soils.

5. Investigate how stress concentrations vary with respect to various pier arrangements and spacings.

APPENDIX A:

PIEZOCONE PENETRATION (CPTU) DATA
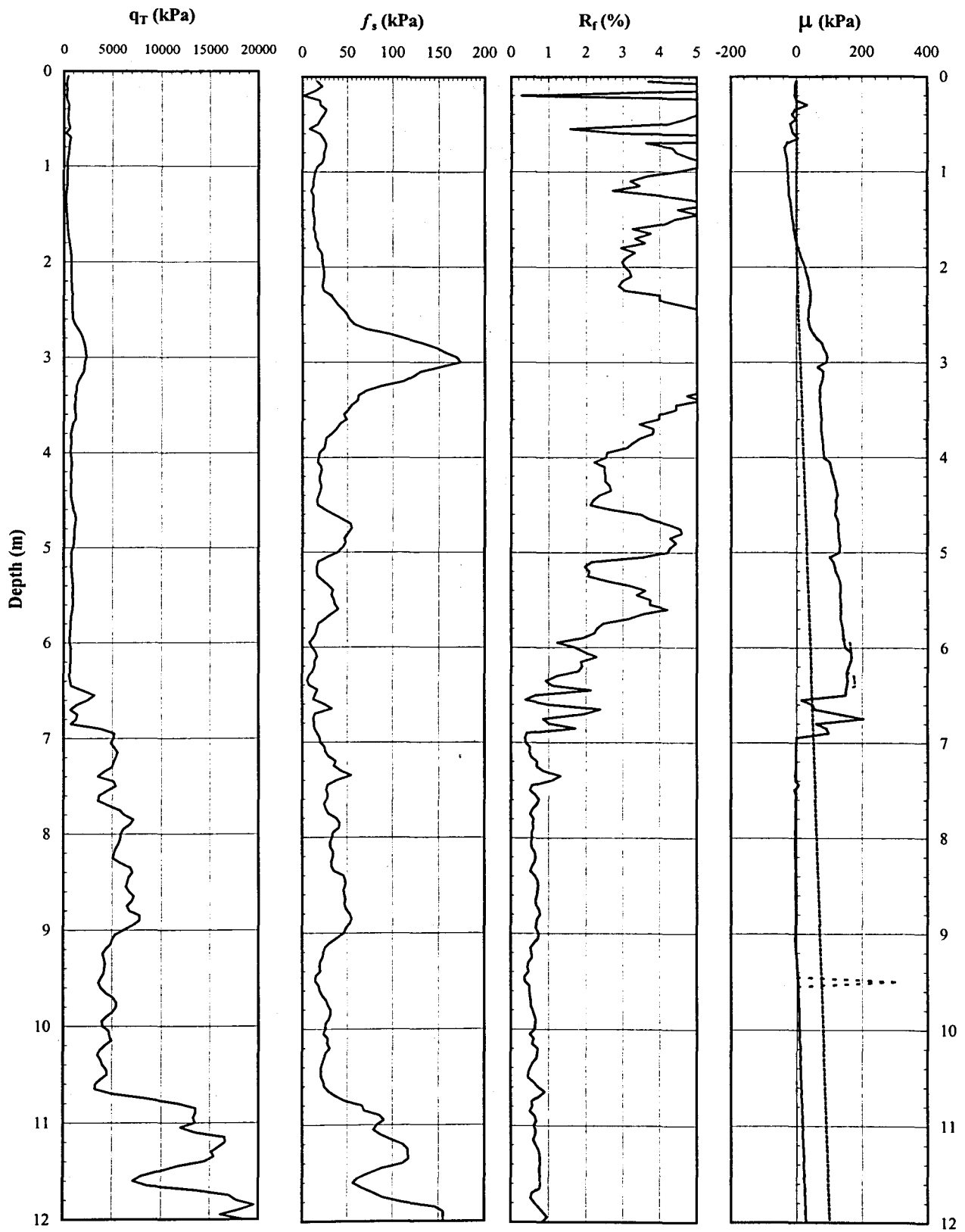
Figure A1. Piezocone penetration data for CPTU-1
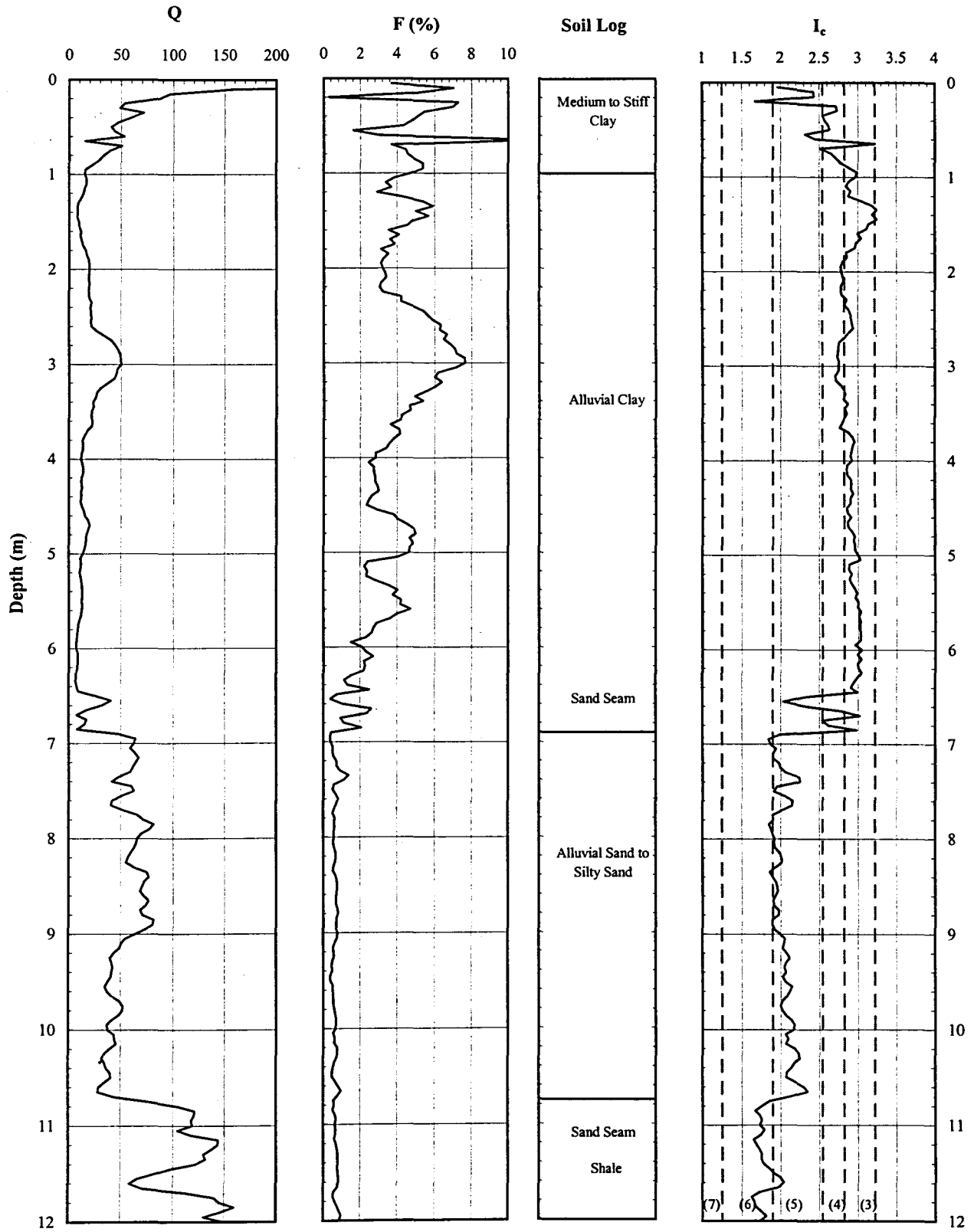
Figure A1. (continued)
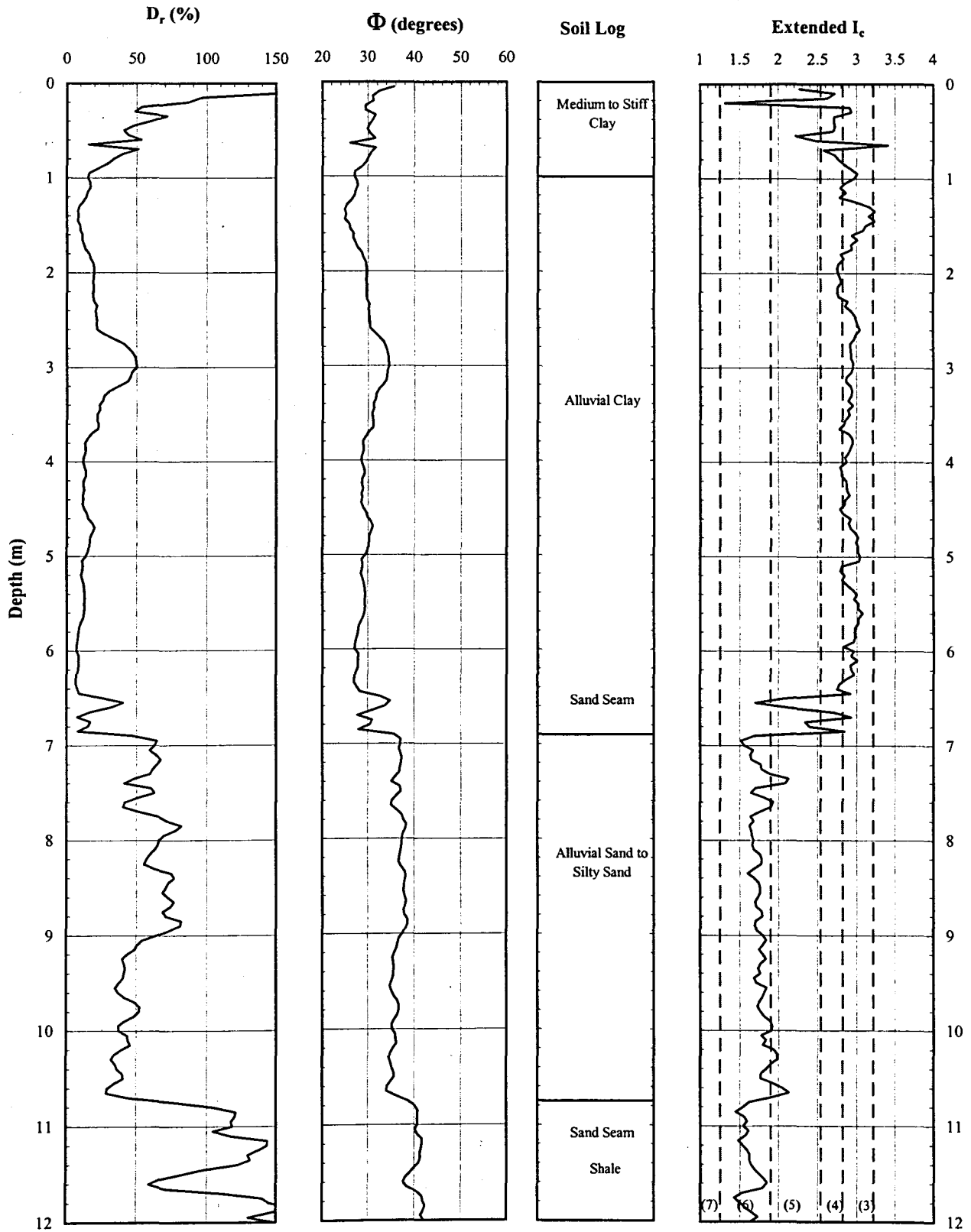
Figure A1. (continued)

Table A1. Piezocone penetration data for CPTU-1

Depth (m)	q_T (kPa)	f_s (kPa)	R_f (%)	f_s/σ'_{vo}	Q
0.15	331	14.6	4.63	7.38	169.0
0.40	421	21.6	5.23	2.88	53.7
0.65	529	20.3	4.68	1.56	40.7
0.90	421	20.1	4.79	1.16	23.4
1.15	355	12.1	3.41	0.54	15.0
1.40	259	12.4	4.82	0.46	8.6
1.65	399	14.4	3.62	0.45	11.6
1.90	685	21.1	3.08	0.59	18.2
2.15	764	23.4	3.06	0.62	19.1
2.40	885	41.0	4.61	1.02	21.0
2.65	1271	78.1	6.09	1.84	28.8
2.90	2193	155.9	7.09	3.51	48.1
3.15	1955	121.0	6.16	2.60	40.8
3.40	1248	59.9	4.79	1.23	24.3
3.65	1097	41.8	3.81	0.82	20.2
3.90	765	23.0	2.99	0.43	13.0
4.15	797	19.5	2.45	0.35	13.0
4.40	777	18.6	2.39	0.32	12.1
4.65	1118	42.3	3.72	0.71	17.3
4.90	1058	46.2	4.36	0.75	15.6
5.15	820	19.3	2.37	0.30	11.3
5.40	940	31.0	3.29	0.47	12.7
5.65	881	30.6	3.42	0.45	11.4
5.90	657	12.4	1.88	0.18	7.8
6.15	704	13.8	1.95	0.19	8.1
6.40	961	10.5	1.22	0.14	11.2
6.65	1864	19.5	1.32	0.25	22.7
6.90	3256	16.5	0.79	0.21	39.5
7.15	5226	30.6	0.59	0.38	63.1
7.40	4631	38.3	0.87	0.46	54.3
7.65	4407	27.6	0.64	0.33	50.3
7.90	6479	37.9	0.58	0.44	73.1
8.15	5446	32.9	0.61	0.37	59.8
8.40	6611	41.9	0.63	0.46	71.3
8.65	6791	47.3	0.70	0.51	71.7
8.90	7141	51.1	0.72	0.54	73.9
9.15	4732	28.7	0.60	0.30	47.4
9.40	4158	17.8	0.43	0.18	40.6
9.65	4466	23.0	0.51	0.23	42.7
9.90	4589	28.9	0.63	0.28	43.2
10.15	4472	27.6	0.62	0.26	41.2
10.40	4095	22.2	0.55	0.21	36.8
10.65	4828	32.8	0.71	0.30	42.8
10.90	13102	79.3	0.60	0.72	116.6
11.15	14891	98.6	0.66	0.87	129.3
11.40	13281	101.7	0.77	0.88	112.5
11.65	10916	70.9	0.69	0.59	89.7
11.90	18005	144.6	0.81	1.19	145.9

Table A1. (continued)

Depth (m)	μ (kPa)	σ_{vo} (kPa)	μ_o (kPa)	σ'_{vo} (kPa)	B_q
0.15	-3.4	2.94	0.0	2.94	-0.01
0.40	-1.5	7.84	0.0	7.84	0.00
0.65	-17.4	12.74	0.0	12.74	-0.03
0.90	-29.8	17.63	0.0	17.63	-0.07
1.15	-23.6	22.32	0.0	22.32	-0.07
1.40	-15.3	26.95	0.0	26.95	-0.07
1.65	-5.7	31.57	0.0	31.57	-0.02
1.90	14.2	36.20	0.6	35.61	0.02
2.15	35.3	40.82	2.9	37.88	0.04
2.40	40.5	45.45	5.4	40.06	0.04
2.65	45.9	50.07	7.8	42.23	0.03
2.90	86.9	54.70	10.3	44.41	0.04
3.15	75.4	59.32	12.7	46.58	0.03
3.40	71.2	63.95	15.2	48.76	0.05
3.65	75.4	68.57	17.6	50.93	0.06
3.90	81.1	73.20	20.1	53.11	0.09
4.15	107.4	77.82	22.5	55.28	0.12
4.40	120.2	82.45	25.0	57.46	0.14
4.65	121.6	87.07	27.4	59.63	0.09
4.90	128.7	91.70	29.9	61.81	0.10
5.15	114.3	96.32	32.3	63.98	0.11
5.40	132.4	100.95	34.8	66.16	0.12
5.65	134.2	105.57	37.2	68.33	0.13
5.90	142.6	110.20	39.7	70.51	0.19
6.15	160.8	114.82	42.1	72.68	0.20
6.40	152.2	119.44	44.6	74.85	0.13
6.65	90.5	123.89	47.0	76.85	0.02
6.90	48.5	128.29	49.5	78.80	0.00
7.15	-2.6	132.69	51.9	80.75	-0.01
7.40	-2.8	137.09	54.4	82.70	-0.01
7.65	-2.6	141.49	56.8	84.65	-0.01
7.90	-3.9	145.89	59.3	86.60	-0.01
8.15	-5.0	150.29	61.7	88.55	-0.01
8.40	-3.7	154.69	64.2	90.50	-0.01
8.65	-3.4	159.09	66.6	92.45	-0.01
8.90	-3.0	163.49	69.1	94.40	-0.01
9.15	-3.2	167.89	71.5	96.35	-0.02
9.40	1.5	172.29	74.0	98.30	-0.02
9.65	5.1	176.69	76.4	100.25	-0.02
9.90	7.3	181.09	78.9	102.20	-0.02
10.15	9.2	185.49	81.3	104.15	-0.02
10.40	12.3	189.89	83.8	106.10	-0.02
10.65	14.8	194.32	86.2	108.08	-0.02
10.90	17.1	199.37	88.7	110.68	-0.01
11.15	19.2	204.62	91.1	113.48	0.00
11.40	21.8	209.87	93.6	116.28	-0.01
11.65	24.7	215.12	96.0	119.08	-0.01
11.90	26.8	220.37	98.5	121.88	0.00

Table A1. (continued)

| Depth (m)	F (%)	I_c	ϕ (Degrees)	D_r (%)
0.15	4.44	2.35	31.7	52.8
0.40	5.24	2.61	30.5	45.7
0.65	3.93	2.60	30.5	45.3
0.90	4.98	2.85	28.6	34.1
1.15	3.62	2.90	27.2	25.8
1.40	5.36	3.20	25.3	14.1
1.65	3.91	3.01	27.0	24.2
1.90	3.25	2.81	29.3	37.9
2.15	3.23	2.79	29.6	40.2
2.40	4.88	2.87	30.2	43.6
2.65	6.40	2.85	31.8	53.2
2.90	7.29	2.74	34.3	68.1
3.15	6.38	2.75	33.6	64.2
3.40	5.06	2.84	31.4	50.6
3.65	4.06	2.83	30.7	46.3
3.90	3.32	2.93	28.8	35.4
4.15	2.72	2.88	28.9	36.0
4.40	2.68	2.90	28.7	34.7
4.65	4.11	2.89	30.4	44.6
4.90	4.78	2.96	30.0	42.5
5.15	2.67	2.92	28.7	34.7
5.40	3.70	2.97	29.3	38.1
5.65	3.95	3.02	28.9	35.8
5.90	2.28	3.02	27.4	27.0
6.15	2.34	3.01	27.7	28.5
6.40	1.25	2.75	29.1	37.0
6.65	1.12	2.47	32.2	55.6
6.90	0.53	2.09	34.8	71.3
7.15	0.60	1.95	37.0	84.5
7.40	0.85	2.08	36.4	80.7
7.65	0.65	2.05	36.1	78.9
7.90	0.60	1.89	37.9	89.6
8.15	0.62	1.97	37.0	84.3
8.40	0.65	1.92	37.9	89.6
8.65	0.71	1.94	37.9	90.0
8.90	0.73	1.93	38.1	91.2
9.15	0.63	2.06	36.1	79.1
9.40	0.45	2.06	35.4	75.1
9.65	0.54	2.07	35.7	76.9
9.90	0.66	2.11	35.8	77.4
10.15	0.64	2.12	35.7	76.4
10.40	0.57	2.14	35.2	73.6
10.65	0.71	2.13	35.9	78.0
10.90	0.61	1.73	40.6	106.3
11.15	0.67	1.71	41.2	109.6
11.40	0.78	1.80	40.6	106.0
11.65	0.66	1.84	39.6	100.0
11.90	0.81	1.73	41.9	114.0
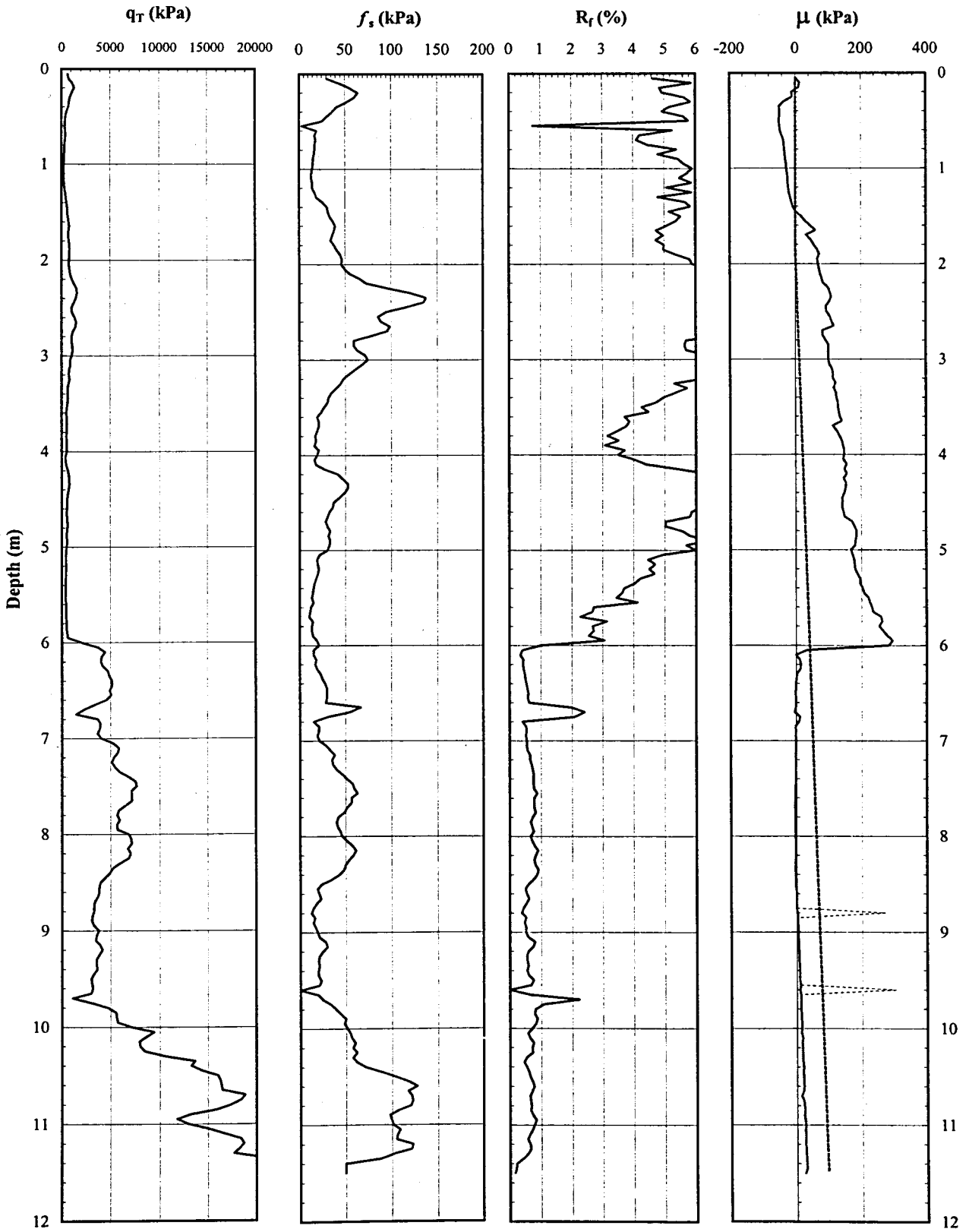
Figure A2. Piezocone penetration data for CPTU-2
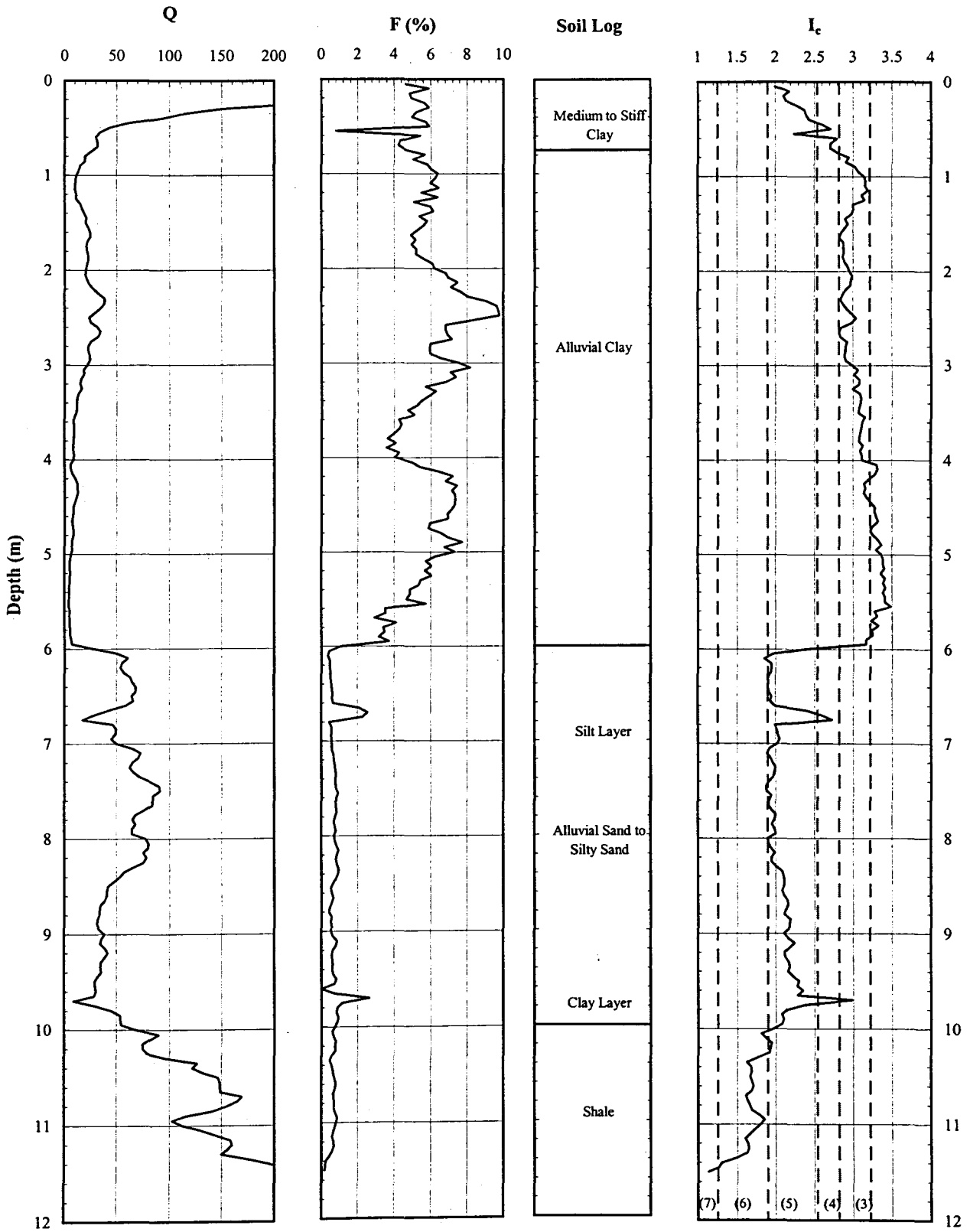
Figure A2. (continued)
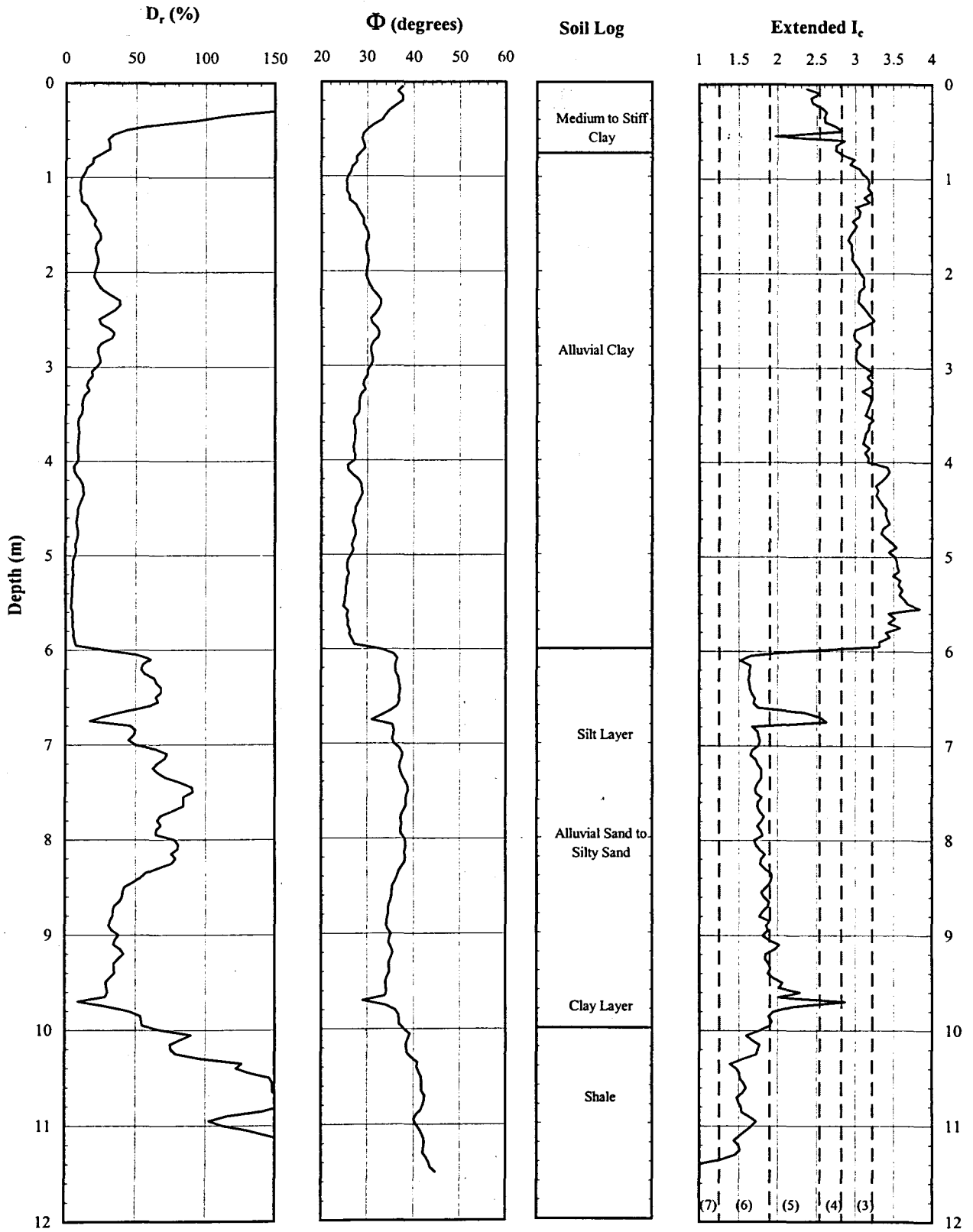
Figure A2. (continued)

Table A2. Piezocone penetration data for CPTU-2

Depth (m)	q_T (kPa)	f_s (kPa)	R_f (%)	f_s/σ'_{vo}	Q
0.15	985	50.9	5.19	20.26	398.1
0.40	679	37.0	5.47	5.09	92.2
0.65	395	14.9	3.76	1.15	30.3
0.90	291	15.7	5.44	0.91	15.9
1.15	260	14.6	5.61	0.66	10.8
1.40	520	28.2	5.39	1.05	18.4
1.65	748	37.2	4.98	1.19	22.9
1.90	804	43.5	5.41	1.23	21.8
2.15	984	68.4	6.89	1.81	25.0
2.40	1361	120.9	8.94	3.04	33.2
2.65	1303	89.6	6.93	2.14	29.9
2.90	1081	65.7	6.08	1.49	23.3
3.15	846	55.5	6.55	1.20	17.0
3.40	653	32.8	5.00	0.68	12.2
3.65	541	20.9	3.86	0.41	9.3
3.90	540	18.4	3.40	0.35	8.8
4.15	551	30.3	5.27	0.55	8.6
4.40	723	46.9	6.48	0.82	11.2
4.65	572	31.8	5.57	0.54	8.2
4.90	551	32.4	5.88	0.53	7.5
5.15	440	20.5	4.66	0.32	5.4
5.40	407	15.5	3.81	0.24	4.6
5.65	436	12.8	2.99	0.19	4.8
5.90	852	16.3	2.40	0.23	10.5
6.15	4096	17.0	0.42	0.24	55.1
6.40	4983	27.0	0.54	0.36	65.6
6.65	3352	42.1	1.54	0.55	42.5
6.90	3861	19.7	0.51	0.25	47.8
7.15	5477	34.5	0.63	0.43	66.8
7.40	6680	50.9	0.76	0.62	79.8
7.65	6783	55.4	0.82	0.66	79.2
7.90	5979	42.7	0.72	0.50	67.9
8.15	6983	56.5	0.81	0.64	77.8
8.40	4925	39.8	0.80	0.44	53.2
8.65	3604	19.2	0.53	0.21	37.6
8.90	3312	15.9	0.48	0.17	33.6
9.15	3788	24.9	0.66	0.26	37.9
9.40	3401	20.9	0.62	0.21	33.1
9.65	2693	19.9	0.94	0.20	25.3
9.90	5770	46.5	0.81	0.46	55.0
10.15	8497	58.2	0.69	0.56	79.9
10.40	13552	76.8	0.56	0.72	124.9
10.65	17301	121.4	0.70	1.11	155.9
10.90	14291	105.3	0.75	0.94	125.4
11.15	17451	113.0	0.65	0.98	149.5
11.40	23696	68.0	0.31	0.58	198.6

Table A2. (continued)

Depth (m)	μ (kPa)	σ$_{vo}$ (kPa)	μ$_o$ (kPa)	σ'$_{vo}$ (kPa)	B$_q$
0.15	0.6	2.94	0.0	2.94	0.00
0.40	-45.4	7.84	0.0	7.84	-0.07
0.65	-41.1	12.73	0.0	12.73	-0.11
0.90	-29.9	17.42	0.0	17.42	-0.11
1.15	-22.3	22.05	0.0	22.05	-0.09
1.40	-4.0	26.67	0.0	26.67	-0.01
1.65	43.2	31.30	0.0	31.30	0.06
1.90	66.3	35.92	0.6	35.33	0.09
2.15	82.3	40.55	2.9	37.61	0.08
2.40	100.4	45.17	5.4	39.78	0.07
2.65	99.2	49.80	7.8	41.96	0.07
2.90	98.0	54.42	10.3	44.13	0.09
3.15	112.7	59.05	12.7	46.31	0.13
3.40	124.8	63.67	15.2	48.48	0.19
3.65	129.6	68.30	17.6	50.66	0.24
3.90	143.0	72.92	20.1	52.83	0.26
4.15	150.4	77.55	22.5	55.01	0.27
4.40	148.0	82.17	25.0	57.18	0.19
4.65	157.3	86.80	27.4	59.36	0.27
4.90	180.6	91.42	29.9	61.53	0.33
5.15	180.2	96.05	32.3	63.71	0.43
5.40	204.4	100.67	34.8	65.88	0.55
5.65	243.3	105.30	37.2	68.06	0.62
5.90	276.4	109.91	39.7	70.22	0.32
6.15	13.7	114.37	42.1	72.23	-0.01
6.40	-0.6	118.77	44.6	74.18	-0.01
6.65	0.3	123.17	47.0	76.13	-0.01
6.90	0.3	127.57	49.5	78.08	-0.01
7.15	-1.7	131.97	51.9	80.03	-0.01
7.40	-2.2	136.37	54.4	81.98	-0.01
7.65	-4.4	140.77	56.8	83.93	-0.01
7.90	-3.6	145.17	59.3	85.88	-0.01
8.15	-2.9	149.57	61.7	87.83	-0.01
8.40	-3.7	153.97	64.2	89.78	-0.01
8.65	-0.6	158.37	66.6	91.73	-0.02
8.90	3.2	162.77	69.1	93.68	-0.02
9.15	5.7	167.17	71.5	95.63	-0.02
9.40	8.0	171.57	74.0	97.58	-0.02
9.65	11.0	175.97	76.4	99.53	-0.03
9.90	13.5	180.40	78.9	101.51	-0.01
10.15	15.9	185.45	81.3	104.11	-0.01
10.40	18.5	190.70	83.8	106.91	0.00
10.65	19.2	195.95	86.2	109.71	0.00
10.90	23.4	201.20	88.7	112.51	0.00
11.15	25.5	206.45	91.1	115.31	0.00
11.40	27.6	211.70	93.6	118.11	0.00

Table A2. (continued)

| Depth (m)	F (%)	I_c	ϕ (Degrees)	D_r (%)
0.15	5.19	2.15	36.9	84.1
0.40	5.51	2.49	32.8	59.4
0.65	3.91	2.69	29.1	36.9
0.90	5.74	3.01	26.9	23.7
1.15	6.12	3.16	25.8	17.0
1.40	5.71	2.96	28.6	34.2
1.65	5.18	2.86	30.0	42.3
1.90	5.66	2.91	30.0	42.7
2.15	7.25	2.94	30.9	47.5
2.40	9.19	2.93	32.3	56.0
2.65	7.15	2.88	31.9	54.0
2.90	6.40	2.92	30.9	47.9
3.15	7.06	3.05	29.6	40.2
3.40	5.56	3.09	28.3	32.2
3.65	4.42	3.12	27.3	26.1
3.90	3.94	3.11	27.2	25.5
4.15	6.39	3.24	27.2	25.5
4.40	7.32	3.19	28.4	32.7
4.65	6.56	3.27	27.2	25.4
4.90	7.04	3.32	26.9	23.9
5.15	5.96	3.39	25.8	16.9
5.40	5.07	3.40	25.3	14.2
5.65	3.89	3.32	25.5	15.7
5.90	2.19	2.90	28.7	34.5
6.15	0.43	1.93	36.1	79.1
6.40	0.56	1.91	37.0	84.3
6.65	1.31	2.28	35.0	72.6
6.90	0.53	2.02	35.6	76.3
7.15	0.64	1.94	37.3	85.9
7.40	0.78	1.92	38.1	91.3
7.65	0.83	1.94	38.2	91.4
7.90	0.73	1.96	37.5	87.4
8.15	0.83	1.95	38.2	91.6
8.40	0.83	2.08	36.5	81.2
8.65	0.56	2.13	34.9	72.0
8.90	0.50	2.15	34.5	69.3
9.15	0.69	2.17	35.1	72.8
9.40	0.65	2.21	34.5	69.4
9.65	0.79	2.35	33.3	62.5
9.90	0.83	2.07	36.9	84.0
10.15	0.70	1.90	38.7	94.8
10.40	0.57	1.69	40.9	107.8
10.65	0.71	1.67	42.0	114.4
10.90	0.75	1.75	41.0	108.5
11.15	0.66	1.66	41.9	113.9
11.40	0.29	1.36	43.3	122.3
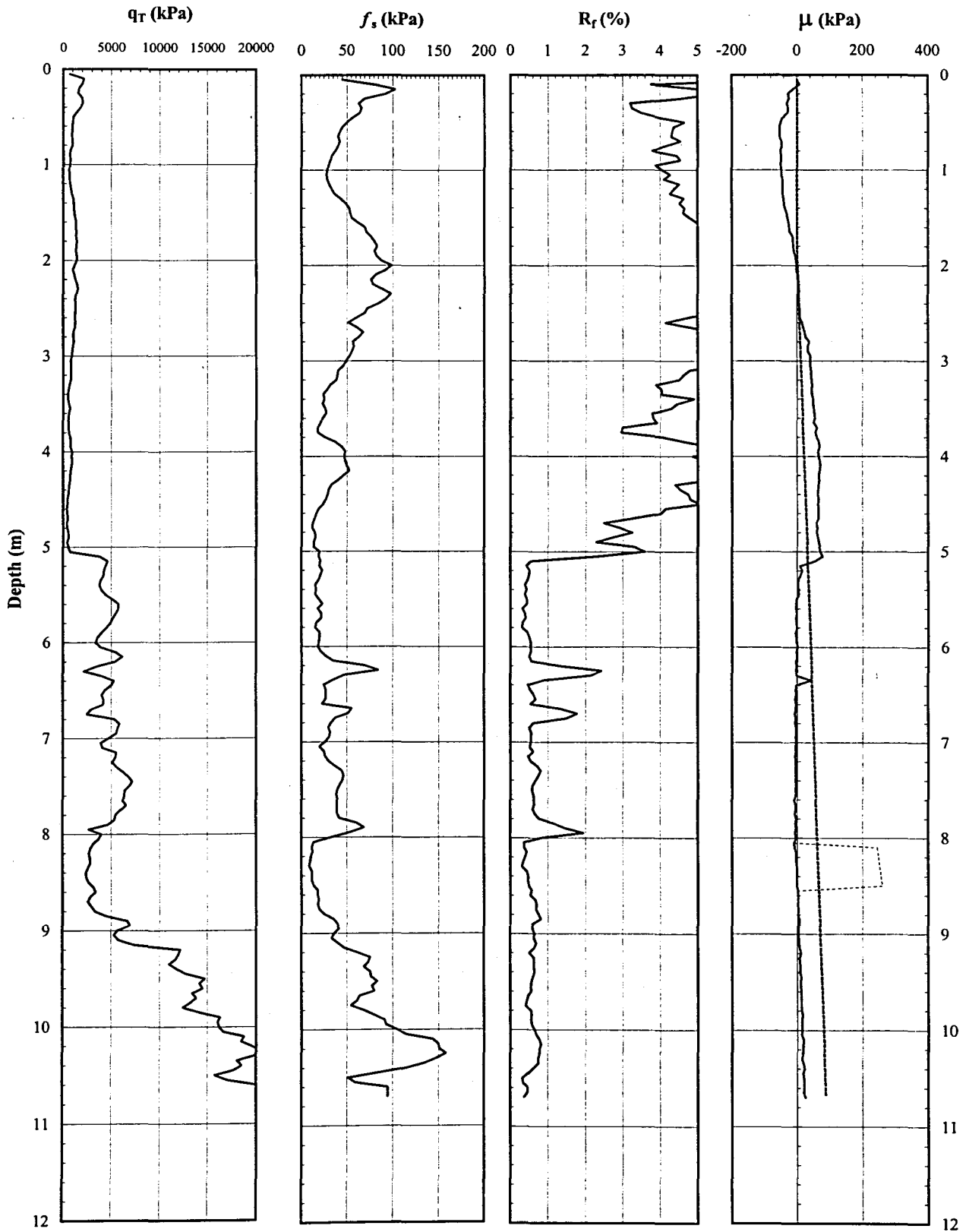
Figure A3. Piezocone penetration data for CPTU-3
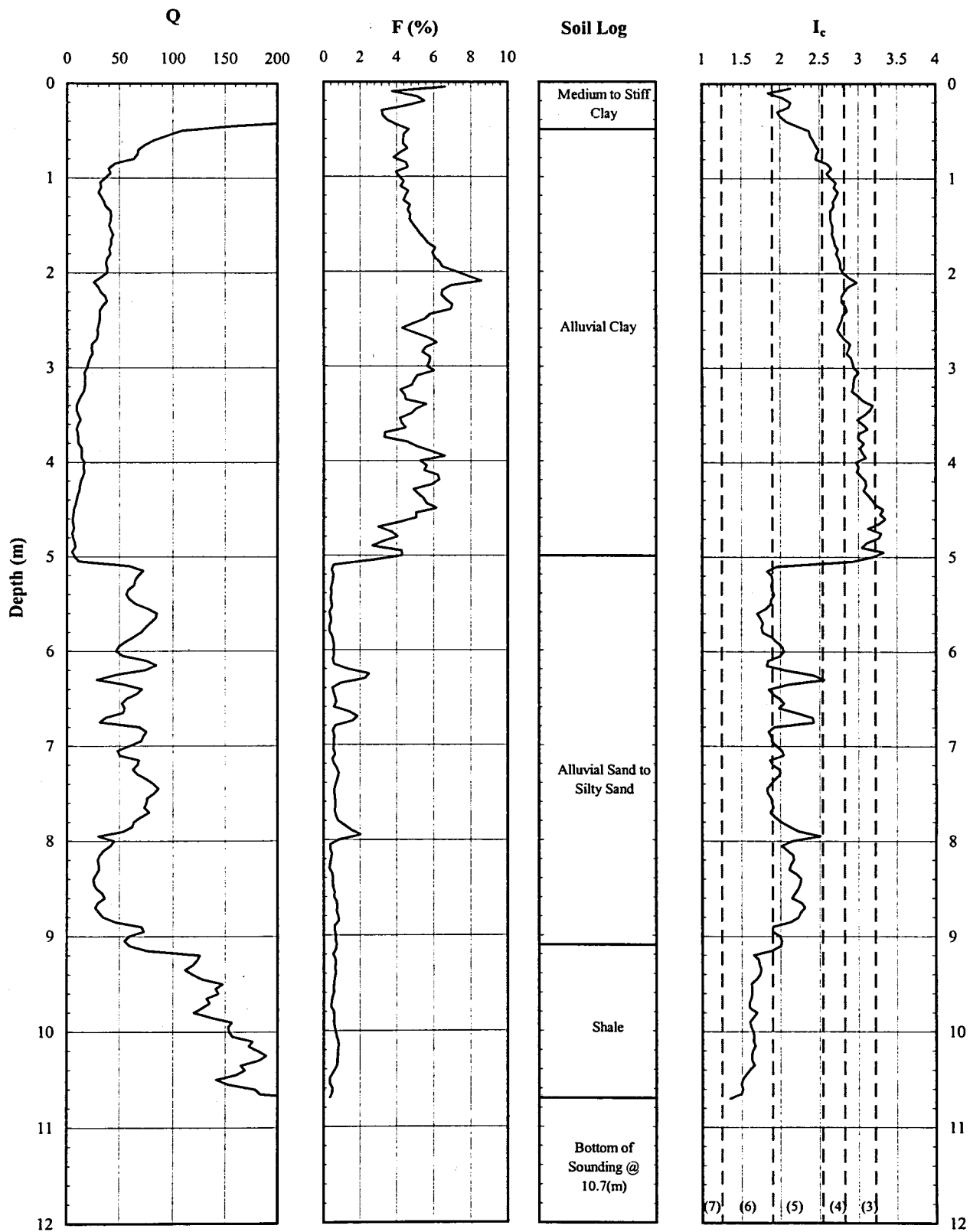
Figure A3. (continued)
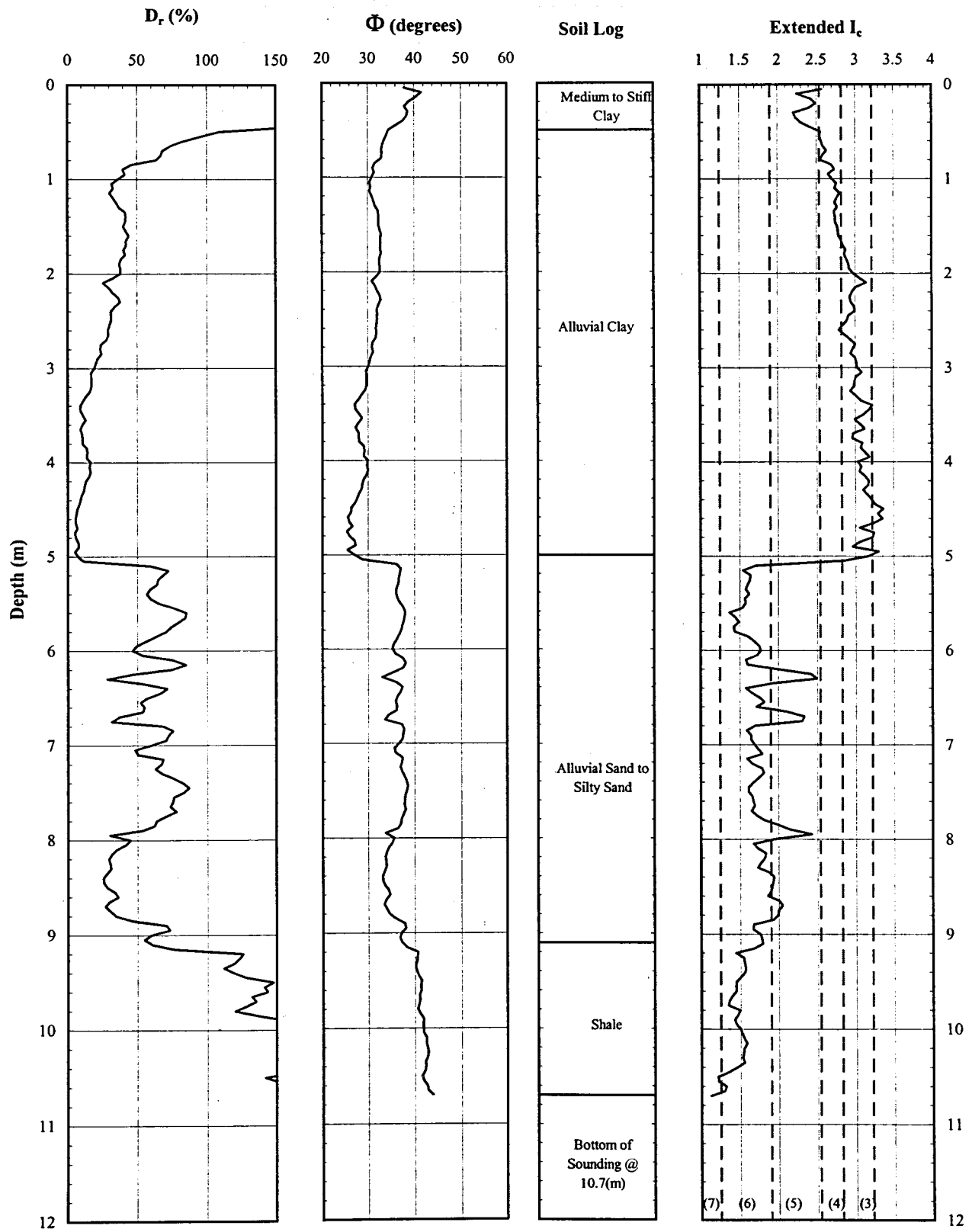
Figure A3. (continued)

Table A3. Piezocone penetration data for CPTU-3

Depth (m)	q_T (kPa)	f_s (kPa)	R_f (%)	f_s/σ'_{vo}	Q
0.15	1610	78.0	5.10	31.91	641.2
0.40	1669	59.9	3.71	8.02	226.7
0.65	970	41.9	4.32	3.40	77.6
0.90	783	32.2	4.13	1.90	45.3
1.15	730	31.4	4.30	1.44	32.5
1.40	1094	50.8	4.64	1.92	40.4
1.65	1335	72.2	5.40	2.32	42.1
1.90	1389	86.6	6.23	2.47	38.6
2.15	1205	83.5	7.01	2.24	31.2
2.40	1350	83.7	6.19	2.12	33.1
2.65	1224	60.9	5.00	1.46	28.2
2.90	1015	54.2	5.35	1.24	21.9
3.15	836	39.1	4.67	0.85	16.9
3.40	582	25.1	4.34	0.52	10.8
3.65	614	21.5	3.49	0.43	10.9
3.90	802	40.4	5.00	0.77	13.9
4.15	880	47.3	5.39	0.87	14.7
4.40	607	28.3	4.71	0.50	9.2
4.65	440	14.7	3.37	0.25	6.0
4.90	511	15.3	3.03	0.25	6.9
5.15	3588	20.9	0.87	0.33	55.1
5.40	4059	17.0	0.42	0.26	60.7
5.65	5454	20.3	0.37	0.30	79.7
5.90	4058	18.6	0.47	0.27	57.2
6.15	4864	47.3	1.06	0.66	66.9
6.40	4167	32.2	0.93	0.44	55.4
6.65	3561	38.9	1.16	0.52	45.9
6.90	5433	30.1	0.55	0.39	69.0
7.15	4808	27.4	0.57	0.35	59.3
7.40	6503	43.3	0.67	0.54	78.8
7.65	6292	39.1	0.62	0.47	74.4
7.90	4446	51.5	1.23	0.61	50.9
8.15	3050	11.5	0.38	0.13	33.5
8.40	2610	11.3	0.44	0.13	27.7
8.65	3000	18.8	0.63	0.21	31.4
8.90	5406	35.4	0.67	0.38	56.6
9.15	8528	51.7	0.62	0.54	88.0
9.40	12399	75.7	0.61	0.77	125.2
9.65	13829	67.6	0.49	0.67	136.0
9.90	15059	87.5	0.58	0.85	144.1
10.15	18788	143.3	0.76	1.35	175.4
10.40	17986	106.9	0.58	0.98	163.6

Table A3. (continued)

Depth (m)	μ (kPa)	σ_{vo} (kPa)	μ_o (kPa)	σ'_{vo} (kPa)	B_q
0.15	-11.4	2.94	0.0	2.94	-0.01
0.40	-36.4	7.83	0.0	7.83	-0.02
0.65	-51.0	12.52	0.0	12.52	-0.05
0.90	-49.1	17.15	0.0	17.15	-0.06
1.15	-44.5	21.77	0.0	21.77	-0.06
1.40	-35.9	26.40	0.0	26.40	-0.03
1.65	-20.0	31.02	0.0	31.02	-0.02
1.90	-6.9	35.65	0.6	35.06	-0.01
2.15	2.1	40.27	2.9	37.33	0.00
2.40	7.2	44.90	5.4	39.51	0.00
2.65	18.5	49.52	7.8	41.68	0.01
2.90	36.5	54.15	10.3	43.86	0.03
3.15	42.7	58.77	12.7	46.03	0.04
3.40	47.3	63.40	15.2	48.21	0.06
3.65	55.0	68.02	17.6	50.38	0.07
3.90	65.6	72.65	20.1	52.56	0.06
4.15	69.1	77.27	22.5	54.73	0.06
4.40	64.3	81.90	25.0	56.91	0.07
4.65	62.9	86.52	27.4	59.08	0.10
4.90	65.5	91.14	29.9	61.25	0.08
5.15	33.5	95.59	32.3	63.25	0.00
5.40	2.5	99.99	34.8	65.20	-0.01
5.65	-3.6	104.39	37.2	67.15	-0.01
5.90	-2.8	108.79	39.7	69.10	-0.01
6.15	-3.4	113.19	42.1	71.05	-0.01
6.40	6.1	117.59	44.6	73.00	-0.01
6.65	-5.8	121.99	47.0	74.95	-0.02
6.90	-4.8	126.39	49.5	76.90	-0.01
7.15	-5.9	130.79	51.9	78.85	-0.01
7.40	-5.9	135.19	54.4	80.80	-0.01
7.65	-6.8	139.59	56.8	82.75	-0.01
7.90	-5.2	143.99	59.3	84.70	-0.01
8.15	-5.9	148.39	61.7	86.65	-0.02
8.40	-1.2	152.79	64.2	88.60	-0.03
8.65	1.9	157.19	66.6	90.55	-0.02
8.90	4.3	161.59	69.1	92.50	-0.01
9.15	7.3	166.33	71.5	94.79	-0.01
9.40	9.4	171.58	74.0	97.59	-0.01
9.65	11.4	176.83	76.4	100.39	0.00
9.90	14.3	182.08	78.9	103.19	0.00
10.15	16.7	187.33	81.3	105.99	0.00
10.40	18.9	192.58	83.8	108.79	0.00

Table A3. (continued)

Depth (m)	F (%)	I_c	ϕ (Degrees)	D_r (%)
0.15	4.85	2.04	39.3	98.2
0.40	3.61	2.11	37.1	85.2
0.65	4.38	2.45	33.4	62.9
0.90	4.20	2.59	31.6	52.3
1.15	4.43	2.70	30.7	46.8
1.40	4.75	2.66	32.2	55.7
1.65	5.54	2.70	32.8	59.1
1.90	6.40	2.77	32.7	58.4
2.15	7.17	2.87	31.8	53.5
2.40	6.41	2.81	32.3	55.9
2.65	5.19	2.80	31.7	52.3
2.90	5.64	2.90	30.6	46.2
3.15	5.03	2.95	29.6	40.0
3.40	4.84	3.09	27.8	28.9
3.65	3.93	3.04	27.9	29.9
3.90	5.54	3.05	29.1	36.9
4.15	5.90	3.04	29.4	39.0
4.40	5.40	3.18	27.6	27.8
4.65	4.18	3.26	25.9	18.0
4.90	3.65	3.18	26.6	21.8
5.15	0.60	1.99	35.8	77.2
5.40	0.43	1.89	36.3	80.3
5.65	0.38	1.76	37.7	88.3
5.90	0.47	1.93	36.2	79.4
6.15	1.00	2.05	37.0	84.2
6.40	0.79	2.06	36.2	79.4
6.65	1.13	2.21	35.4	74.5
6.90	0.57	1.90	37.3	86.3
7.15	0.59	1.96	36.7	82.4
7.40	0.68	1.89	38.1	90.7
7.65	0.64	1.90	37.8	89.4
7.90	1.20	2.19	36.1	79.1
8.15	0.40	2.11	34.3	68.0
8.40	0.46	2.21	33.5	63.2
8.65	0.66	2.23	34.1	66.9
8.90	0.68	2.01	36.8	83.5
9.15	0.62	1.83	39.0	96.2
9.40	0.62	1.70	40.7	106.5
9.65	0.50	1.62	41.1	109.2
9.90	0.59	1.64	41.5	111.3
10.15	0.77	1.65	42.5	117.2
10.40	0.60	1.60	42.2	115.6
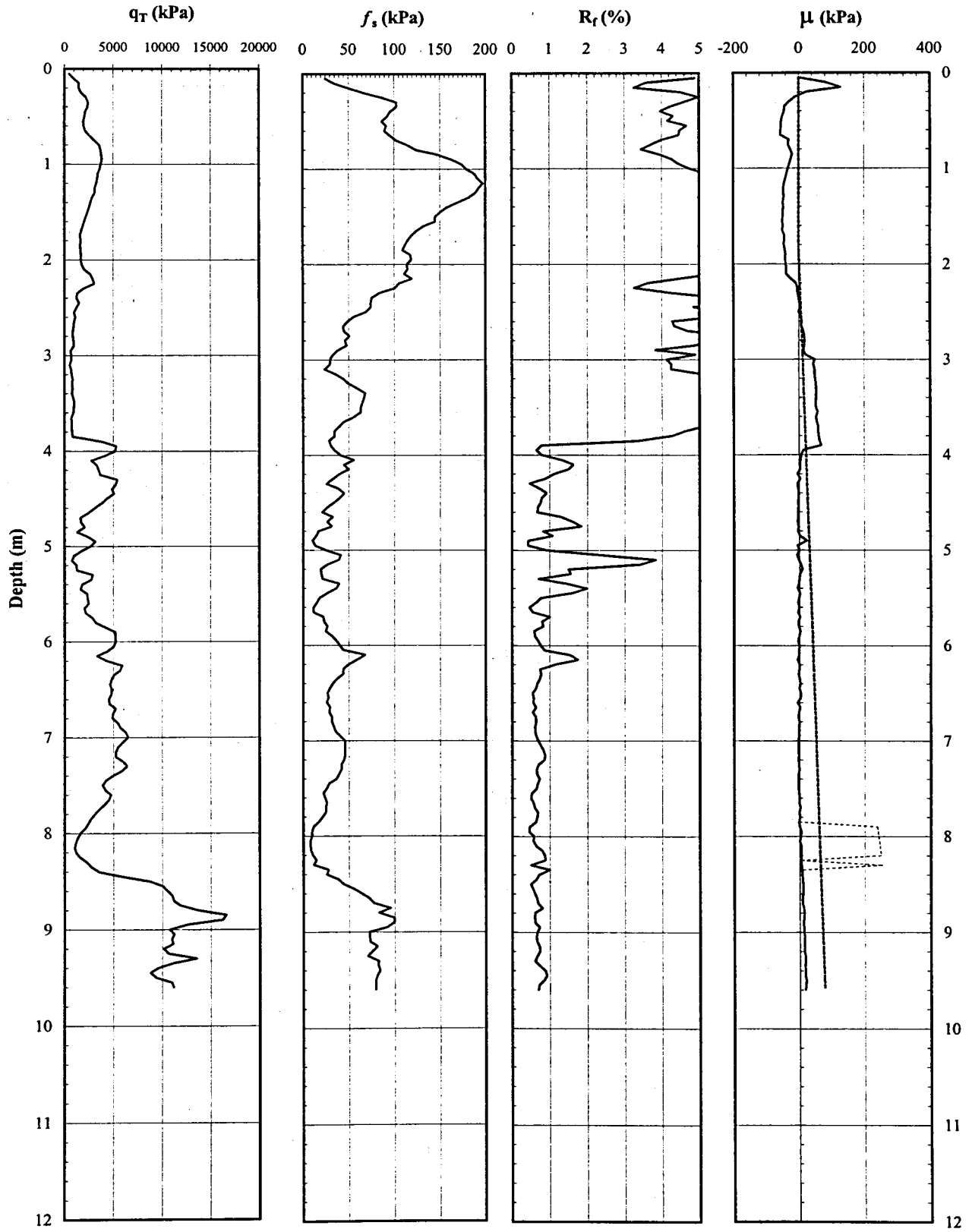
Figure A4. Piezocone penetration data for CPTU-4

118
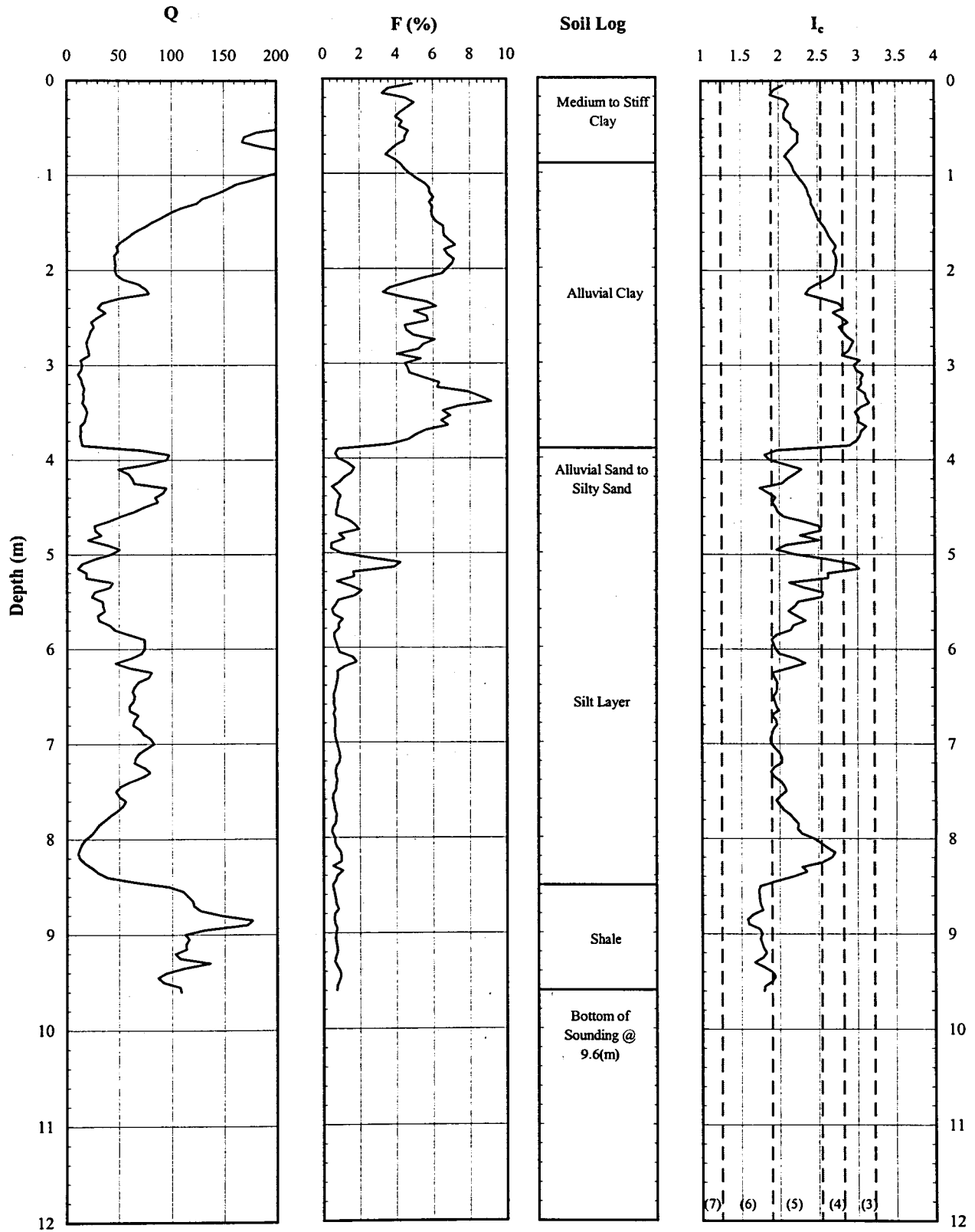
Figure A4. (continued)
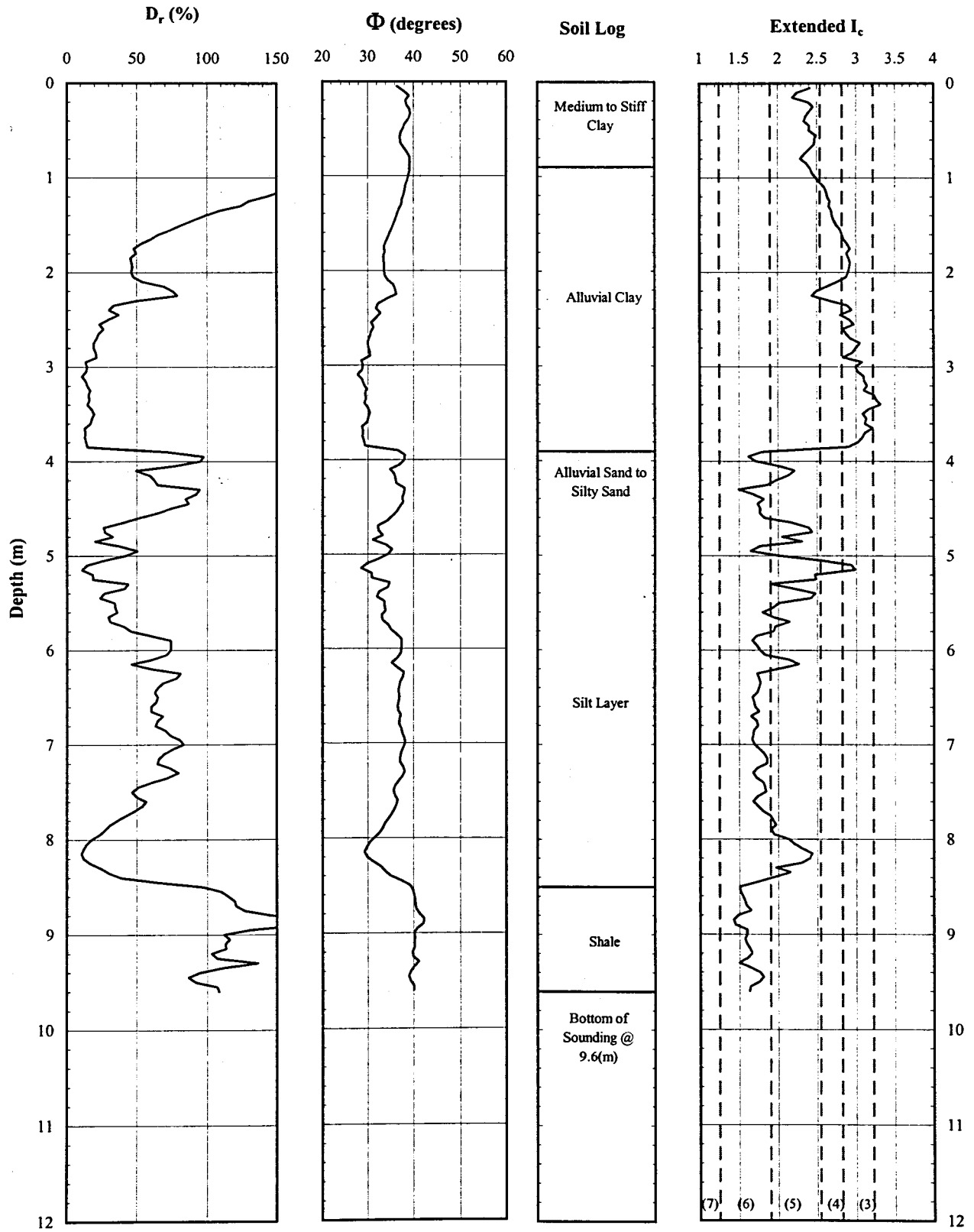
Figure A4. (continued)

Table A4. Piezocone penetration data for CPTU-4

Depth (m)	q_T (kPa)	f_s (kPa)	R_f (%)	f_s/σ'_{vo}	Q
0.15	1248	52.7	4.24	18.96	452.6
0.40	2261	96.1	4.26	12.80	298.2
0.65	2358	99.0	4.26	7.80	183.0
0.90	3774	157.4	4.16	8.93	214.7
1.15	3404	191.5	5.64	8.65	153.3
1.40	2722	160.7	5.91	6.03	101.1
1.65	1913	127.0	6.66	4.06	60.2
1.90	1700	114.3	6.73	3.22	46.9
2.15	2502	110.3	4.63	2.92	65.0
2.40	1488	75.7	5.19	1.90	36.2
2.65	1004	48.8	4.90	1.16	22.7
2.90	849	38.9	4.59	0.88	18.0
3.15	716	36.6	5.03	0.78	14.1
3.40	889	64.5	7.33	1.33	17.0
3.65	831	47.5	5.66	0.94	15.0
3.90	3195	33.9	1.98	0.64	58.6
4.15	3509	44.4	1.29	0.81	62.5
4.40	4991	36.6	0.74	0.64	86.4
4.65	2560	27.8	1.23	0.47	42.2
4.90	2333	16.1	0.74	0.26	36.9
5.15	1226	29.3	2.53	0.47	18.1
5.40	2300	28.3	1.30	0.44	34.1
5.65	2403	16.7	0.69	0.25	34.5
5.90	4614	32.0	0.70	0.47	65.6
6.15	4625	53.1	1.21	0.75	64.0
6.40	5026	34.1	0.67	0.47	67.8
6.65	4842	28.7	0.59	0.39	63.4
6.90	5776	37.3	0.64	0.49	74.0
7.15	5582	45.0	0.81	0.57	69.6
7.40	5081	34.5	0.68	0.43	61.7
7.65	4252	24.3	0.58	0.30	50.1
7.90	2417	13.8	0.56	0.16	27.1
8.15	1293	9.8	0.75	0.11	13.3
8.40	4665	29.5	0.68	0.33	51.1
8.65	10921	73.2	0.67	0.81	118.6
8.90	13955	89.4	0.65	0.96	147.7
9.15	10826	74.9	0.69	0.78	110.7
9.40	10490	82.0	0.80	0.83	104.3

Table A4. (continued)

Depth (m)	μ (kPa)	σ_{vo} (kPa)	μ_o (kPa)	σ'_{vo} (kPa)	B_q
0.15	45.6	2.94	0.0	2.94	0.04
0.40	-44.0	7.84	0.0	7.84	-0.02
0.65	-45.8	12.74	0.0	12.74	-0.02
0.90	-25.6	17.57	0.0	17.57	-0.01
1.15	-43.0	22.21	0.0	22.21	-0.01
1.40	-47.9	26.84	0.0	26.84	-0.02
1.65	-47.6	31.46	0.0	31.46	-0.03
1.90	-41.6	36.09	0.6	35.50	-0.03
2.15	-23.0	40.71	2.9	37.77	-0.01
2.40	0.1	45.34	5.4	39.95	0.00
2.65	10.2	49.96	7.8	42.12	0.00
2.90	23.0	54.59	10.3	44.30	0.02
3.15	47.9	59.21	12.7	46.47	0.05
3.40	51.6	63.84	15.2	48.65	0.04
3.65	55.6	68.46	17.6	50.82	0.05
3.90	41.8	73.03	20.1	52.94	0.01
4.15	1.0	77.44	22.5	54.90	-0.01
4.40	-3.3	81.84	25.0	56.85	-0.01
4.65	-3.4	86.24	27.4	58.80	-0.01
4.90	2.6	90.64	29.9	60.75	-0.01
5.15	1.1	95.04	32.3	62.70	-0.03
5.40	-1.5	99.44	34.8	64.65	-0.02
5.65	-2.2	103.84	37.2	66.60	-0.02
5.90	-1.2	108.24	39.7	68.55	-0.01
6.15	-1.9	112.64	42.1	70.50	-0.01
6.40	0.4	117.04	44.6	72.45	-0.01
6.65	-1.4	121.44	47.0	74.40	-0.01
6.90	-1.7	125.84	49.5	76.35	-0.01
7.15	-2.8	130.24	51.9	78.30	-0.01
7.40	-2.6	134.64	54.4	80.25	-0.01
7.65	-0.6	139.04	56.8	82.20	-0.01
7.90	1.2	143.44	59.3	84.15	-0.03
8.15	3.3	147.84	61.7	86.10	-0.05
8.40	7.4	152.27	64.2	88.08	-0.01
8.65	9.4	157.32	66.6	90.68	-0.01
8.90	12.3	162.57	69.1	93.48	0.00
9.15	14.8	167.82	71.5	96.28	-0.01
9.40	17.0	173.07	74.0	99.08	-0.01

Table A4. (continued)

| Depth (m)	F (%)	I_c	ϕ (Degrees)	D_r (%)
0.15	4.23	2.03	38.1	90.9
0.40	4.27	2.11	38.6	93.9
0.65	4.22	2.20	37.6	88.1
0.90	4.19	2.17	39.1	97.0
1.15	5.66	2.36	38.0	90.7
1.40	5.96	2.48	36.5	81.6
1.65	6.75	2.66	34.5	69.2
1.90	6.87	2.73	33.6	64.1
2.15	4.48	2.50	35.3	74.2
2.40	5.24	2.72	32.7	58.5
2.65	5.12	2.86	30.7	46.5
2.90	4.89	2.93	29.8	41.0
3.15	5.57	3.04	28.8	35.4
3.40	7.82	3.08	29.8	41.0
3.65	6.23	3.05	29.3	38.4
3.90	1.09	2.11	35.7	76.4
4.15	1.29	2.14	36.0	78.6
4.40	0.75	1.88	37.6	88.2
4.65	1.12	2.24	34.4	68.6
4.90	0.72	2.19	33.8	65.4
5.15	2.59	2.75	30.7	46.5
5.40	1.29	2.35	33.6	64.1
5.65	0.72	2.21	33.8	65.0
5.90	0.71	1.97	36.8	83.2
6.15	1.18	2.11	36.8	82.9
6.40	0.69	1.95	37.1	84.9
6.65	0.61	1.95	36.8	83.4
6.90	0.66	1.91	37.6	88.1
7.15	0.83	1.98	37.4	86.8
7.40	0.70	1.99	36.9	83.7
7.65	0.59	2.03	36.0	78.3
7.90	0.61	2.27	33.2	61.8
8.15	0.85	2.61	30.2	43.5
8.40	0.65	2.04	36.3	80.0
8.65	0.68	1.75	40.3	103.9
8.90	0.65	1.66	41.4	110.5
9.15	0.70	1.78	40.1	102.8
9.40	0.79	1.83	39.9	101.5
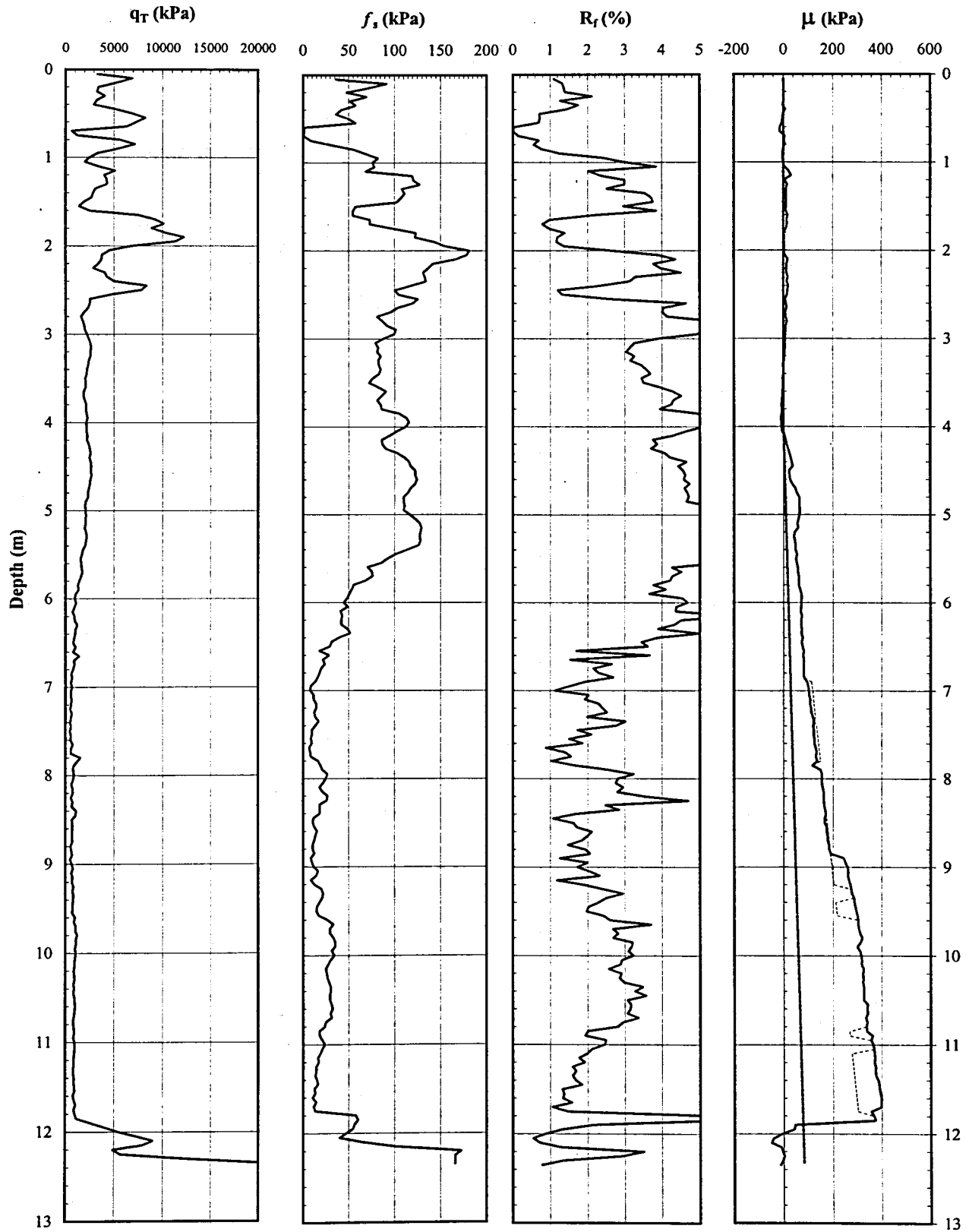
Figure A5. Piezocone penetration data for CPTU-5
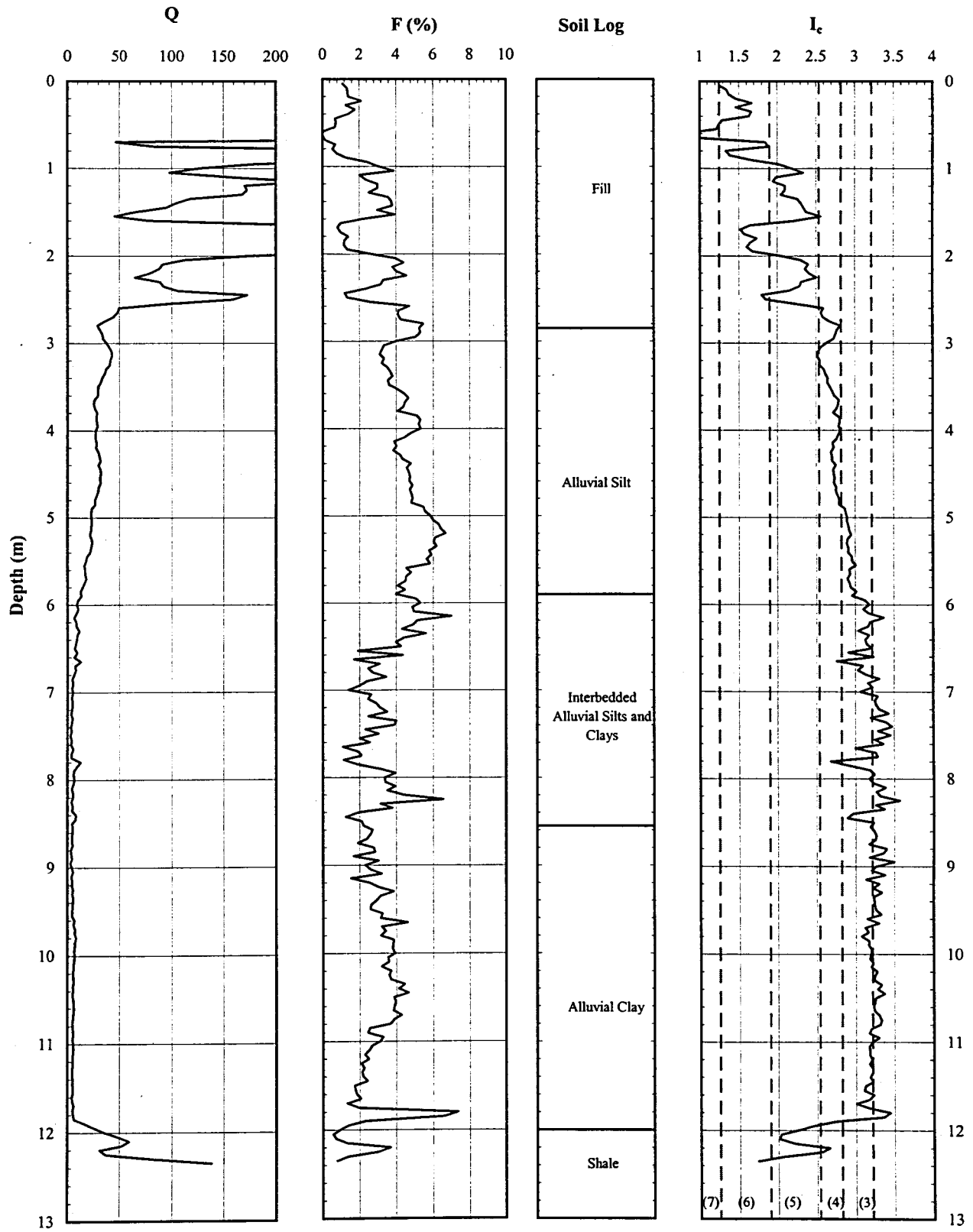
Figure A5. (continued)
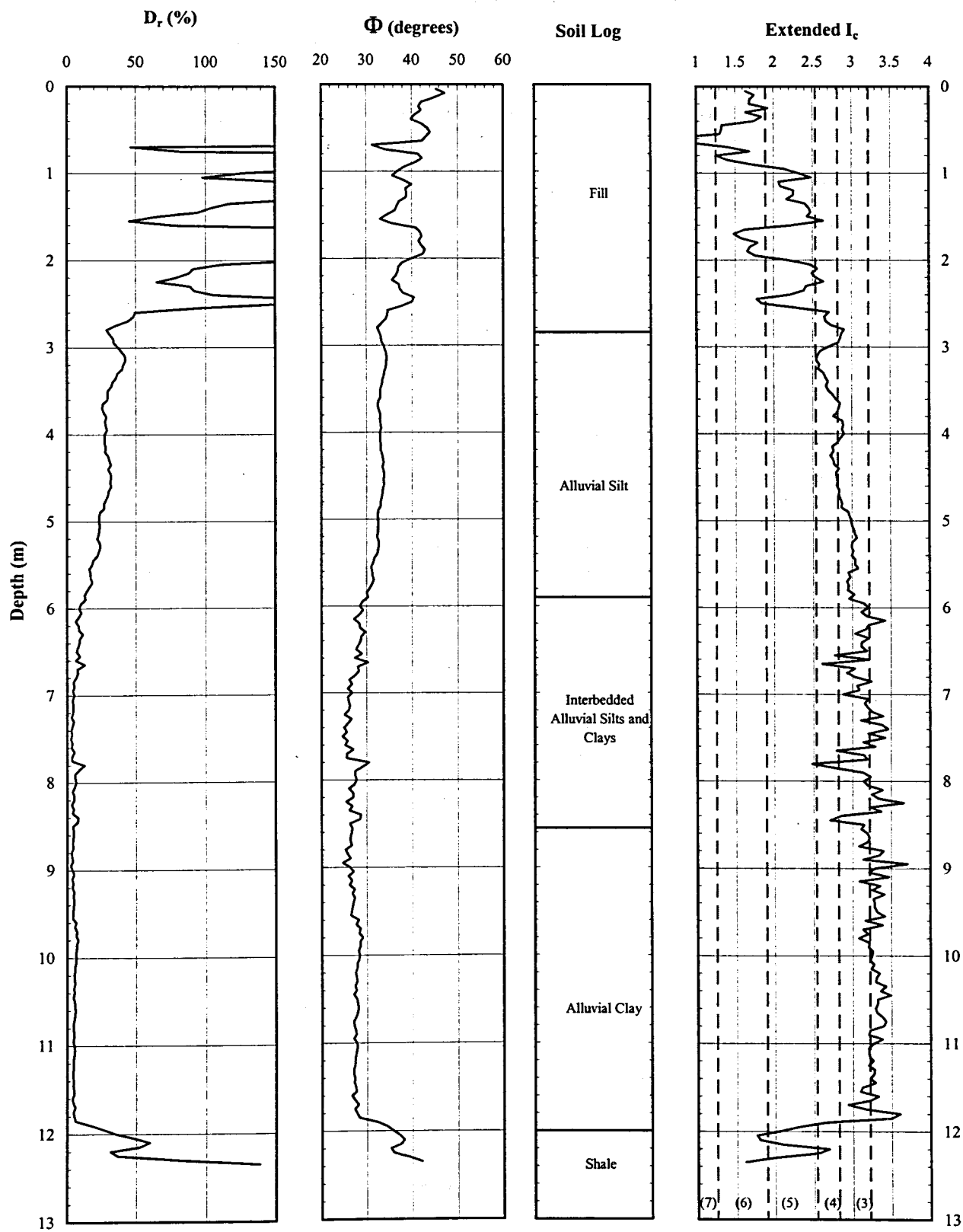
Figure A5. (continued)

Table A5. Piezocone penetration data for CPTU-5

Depth (m)	q_T (kPa)	f_s (kPa)	R_f (%)	f_s/σ'_{vo}	Q
0.15	4455	63.6	1.46	26.99	2055.1
0.40	4465	47.5	1.17	6.35	565.4
0.65	4751	14.0	0.32	1.24	401.6
0.90	4840	63.0	1.61	3.52	281.3
1.15	3770	103.0	2.84	4.53	164.9
1.40	2998	97.3	3.30	3.58	109.9
1.65	6153	71.1	1.76	2.18	185.0
1.90	9916	145.0	1.55	3.88	266.0
2.15	3695	150.7	4.10	3.59	87.2
2.40	5910	118.0	2.26	2.52	123.7
2.65	2858	105.1	3.89	2.03	54.5
2.90	1936	93.7	4.88	1.65	33.1
3.15	2590	82.2	3.17	1.34	41.2
3.40	2273	80.3	3.53	1.22	33.5
3.65	2008	85.2	4.25	1.21	27.5
3.90	2199	106.5	4.84	1.41	28.2
4.15	2281	92.3	4.06	1.18	28.1
4.40	2607	114.2	4.38	1.42	31.3
4.65	2601	120.5	4.63	1.46	30.4
4.90	2198	111.7	5.10	1.31	24.8
5.15	2114	127.0	6.01	1.46	23.1
5.40	2002	112.6	5.61	1.26	21.3
5.65	1670	75.7	4.54	0.83	17.1
5.90	1239	50.8	4.15	0.54	12.1
6.15	939	43.5	4.70	0.45	8.6
6.40	1007	40.2	3.97	0.41	9.0
6.65	1024	22.6	2.35	0.23	9.0
6.90	666	12.8	1.92	0.13	5.2
7.15	575	12.8	2.24	0.12	4.2
7.40	547	12.6	2.32	0.12	3.8
7.65	589	8.2	1.44	0.08	4.1
7.90	1053	21.6	2.26	0.19	8.2
8.15	695	22.8	3.35	0.20	4.8
8.40	838	15.3	1.94	0.13	5.9
8.65	704	12.8	1.82	0.11	4.6
8.90	595	10.5	1.80	0.09	3.6
9.15	726	14.4	1.98	0.12	4.5
9.40	774	18.2	2.35	0.15	4.8
9.65	959	27.4	2.85	0.22	6.2
9.90	1110	34.1	3.08	0.27	7.2
10.15	961	27.2	2.83	0.21	5.9
10.40	916	29.9	3.28	0.23	5.4
10.65	963	30.3	3.14	0.22	5.7
10.90	906	21.1	2.34	0.15	5.1
11.15	934	17.6	1.88	0.13	5.2
11.40	885	14.4	1.63	0.10	4.7
11.65	934	12.6	1.36	0.09	5.0
11.90	2860	55.4	3.08	0.38	18.0
12.15	6969	109.0	1.80	0.74	45.6

Table A5. (continued)

Depth (m)	μ (kPa)	σ_{vo} (kPa)	μ_o (kPa)	σ'_{vo} (kPa)	B_q
0.15	0.1	2.94	0.0	2.94	0.00
0.40	0.3	7.84	0.0	7.84	0.00
0.65	-5.4	12.74	0.0	12.74	0.00
0.90	-0.7	17.64	0.0	17.64	0.00
1.15	15.6	22.54	0.0	22.54	0.00
1.40	11.3	27.44	0.0	27.44	0.00
1.65	13.5	32.34	0.0	32.34	0.00
1.90	3.0	37.24	0.0	37.24	0.00
2.15	12.3	42.14	0.0	42.14	0.00
2.40	16.5	47.04	0.0	47.04	0.00
2.65	9.9	51.94	0.0	51.94	0.00
2.90	10.2	56.73	0.0	56.73	0.01
3.15	4.8	61.36	0.0	61.36	0.00
3.40	-0.8	65.98	0.0	65.98	0.00
3.65	-4.7	70.61	0.0	70.61	0.00
3.90	-7.9	75.23	0.0	75.23	0.00
4.15	7.9	79.86	1.5	78.39	0.00
4.40	29.5	84.48	3.9	80.56	0.01
4.65	37.8	89.11	6.4	82.74	0.01
4.90	64.8	93.73	8.8	84.91	0.03
5.15	53.0	98.36	11.3	87.09	0.02
5.40	49.8	102.98	13.7	89.26	0.02
5.65	58.6	107.61	16.2	91.44	0.03
5.90	68.4	112.23	18.6	93.61	0.04
6.15	70.7	116.86	21.1	95.79	0.06
6.40	74.3	121.48	23.5	97.96	0.06
6.65	80.9	126.11	26.0	100.14	0.06
6.90	92.4	130.73	28.4	102.31	0.12
7.15	109.1	135.36	30.9	104.49	0.18
7.40	121.2	139.98	33.3	106.66	0.22
7.65	128.8	144.61	35.8	108.84	0.21
7.90	142.5	149.23	38.2	111.01	0.12
8.15	160.1	153.86	40.7	113.19	0.22
8.40	167.1	158.48	43.1	115.36	0.18
8.65	178.2	163.11	45.6	117.54	0.25
8.90	226.0	167.73	48.0	119.71	0.42
9.15	267.7	172.36	50.5	121.89	0.39
9.40	288.1	176.98	52.9	124.06	0.39
9.65	305.9	181.61	55.4	126.24	0.32
9.90	312.8	186.23	57.8	128.41	0.28
10.15	323.0	190.86	60.3	130.59	0.34
10.40	327.0	195.48	62.7	132.76	0.37
10.65	340.9	200.11	65.2	134.94	0.36
10.90	352.5	204.73	67.6	137.11	0.41
11.15	371.9	209.36	70.1	139.29	0.42
11.40	383.2	213.98	72.5	141.46	0.46
11.65	389.2	218.61	75.0	143.64	0.44
11.90	164.9	223.23	77.4	145.81	0.03
12.15	-20.3	227.86	79.9	147.99	-0.01

Table A5. (continued)

Depth (m)	F (%)	I_c	ϕ (Degrees)	D_r (%)
0.15	1.43	1.41	44.2	127.4
0.40	1.07	1.44	41.8	113.4
0.65	0.30	1.13	41.0	108.2
0.90	1.31	1.69	40.3	104.1
1.15	2.75	2.08	38.5	93.4
1.40	3.28	2.25	36.9	84.0
1.65	1.16	1.75	40.0	102.3
1.90	1.47	1.74	41.9	113.9
2.15	4.13	2.39	36.9	83.8
2.40	2.01	2.05	38.9	95.7
2.65	3.75	2.50	35.2	73.5
2.90	4.98	2.73	33.1	61.1
3.15	3.25	2.54	34.3	68.3
3.40	3.64	2.64	33.5	63.5
3.65	4.40	2.76	32.8	59.0
3.90	5.01	2.79	33.0	60.7
4.15	4.19	2.74	33.1	61.1
4.40	4.53	2.72	33.7	64.6
4.65	4.80	2.75	33.6	64.1
4.90	5.31	2.84	32.8	58.9
5.15	6.30	2.92	32.5	57.4
5.40	5.93	2.93	32.2	55.5
5.65	4.84	2.94	31.3	50.0
5.90	4.50	3.04	29.8	41.1
6.15	5.29	3.20	28.4	32.8
6.40	4.54	3.14	28.7	34.5
6.65	2.52	2.99	28.7	34.6
6.90	2.40	3.18	26.6	22.0
7.15	2.92	3.31	25.9	17.5
7.40	3.10	3.36	25.6	15.8
7.65	1.85	3.22	25.9	17.6
7.90	2.39	3.02	28.6	34.0
8.15	4.21	3.35	26.6	21.8
8.40	2.26	3.12	27.4	26.9
8.65	2.37	3.23	26.5	21.6
8.90	2.47	3.33	25.7	16.5
9.15	2.60	3.25	26.6	22.0
9.40	3.05	3.27	26.9	23.6
9.65	3.52	3.21	27.8	29.5
9.90	3.69	3.17	28.5	33.4
10.15	3.53	3.23	27.8	29.0
10.40	4.15	3.30	27.5	27.4
10.65	3.97	3.27	27.7	28.6
10.90	3.01	3.24	27.4	26.6
11.15	2.43	3.19	27.5	27.3
11.40	2.14	3.20	27.2	25.5
11.65	1.77	3.14	27.4	26.9
11.90	2.10	2.70	32.7	58.7
12.15	1.62	2.31	36.9	84.0

APPENDIX B:

SETTLEMENT ESTIMATES USING CPTU DATA

Sanglerat (1972) proposed:

$$S = \Sigma H_0 \frac{\Delta \sigma}{\alpha q_c}$$

where:

S   = total settlement, including short term and long term settlement

$\Delta \sigma$ = expected change in stress at mid-depth of the soil layer

α = soil compressibility coefficient.
For low to medium plasticity clay (CL): $q_c < 7$ bar, $3 < \alpha < 8$; $7 < q_c < 20$ bar, $2 < \alpha < 5$

q_c = average tip resistance for each soil layer

Table B1. Embankment parameters

	H, Fill Height (ft)	H, Fill Height (m)	Load[a] (psf)	L, Embankment width (m)	L/H
Stage 1	15	4.6	1800	13	2.8
Total (1 & 2)	30	9.1	3600	13	1.4

[a] $\gamma = 120$ pcf assumed

Table B2. $\Delta \sigma$ calculations

Z, Depth to Mid of layer (m)	Z/H Stage 1	Z/H Stage 2	Influence Factor[b] Stage 1	Influence Factor[b] Stage 2	$\Delta \sigma$ Stage 1 (kpa)	$\Delta \sigma$ Total (1 & 2) (kpa)
0.95	0.21	0.10	0.95	0.90	81.88	155.13
1.25	0.27	0.14	0.95	0.89	81.88	153.41
1.55	0.34	0.17	0.94	0.89	81.01	153.41
1.85	0.40	0.20	0.93	0.87	80.15	149.96
2.25	0.49	0.25	0.93	0.87	80.15	149.96
2.75	0.60	0.30	0.92	0.86	79.29	148.24
3.25	0.71	0.36	0.92	0.85	79.29	146.51
3.75	0.82	0.41	0.91	0.84	78.43	144.79
4.25	0.93	0.46	0.91	0.83	78.43	143.07
4.75	1.04	0.52	0.90	0.82	77.57	141.34
5.25	1.15	0.57	0.90	0.81	77.57	139.62
5.75	1.26	0.63	0.89	0.80	76.70	137.90

[b] Influence factors from Winterkorn and Fang (1975), pg 167

Table B3. Settlement calculations

Depth to Top of Layer (m)	Depth to Mid of layer (m)	H_o Layer (m)	q_c Layer Ave (kPa)	q_c Layer Ave (bar)	α
0.8	0.95	0.3	291	2.91	5.8
1.1	1.25	0.3	360	3.60	5.8
1.4	1.55	0.3	634	6.34	5.8
1.7	1.85	0.3	804	8.04	5.8
2.0	2.25	0.5	1173	11.73	5.8
2.5	2.75	0.5	1192	11.92	5.8
3.0	3.25	0.5	750	7.50	5.8
3.5	3.75	0.5	541	5.41	5.8
4.0	4.25	0.5	637	6.37	5.8
4.5	4.75	0.5	561	5.61	5.8
5.0	5.25	0.5	424	4.24	5.8
5.5	5.75	0.5	644	6.44	5.8

Table B4. Results of settlement estimates using CPTU data

	Settlement	
	(m)	(in)
Stage 1	0.120	4.7
Stage 2	0.101	4.0
Total	0.221	8.7

APPENDIX C:

PRESSUREMETER (PMT) TEST DATA
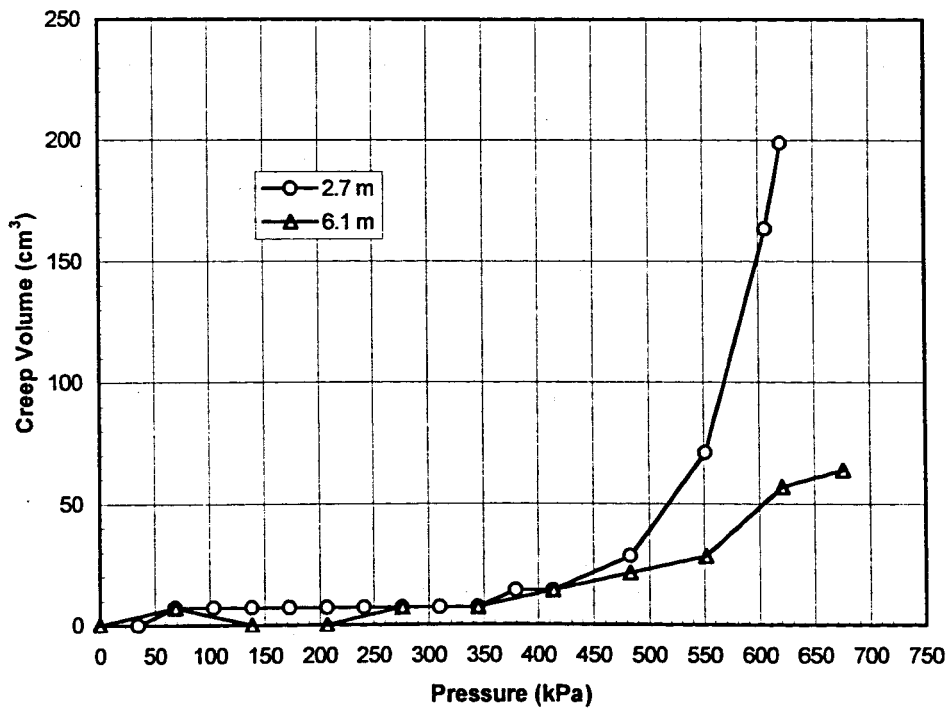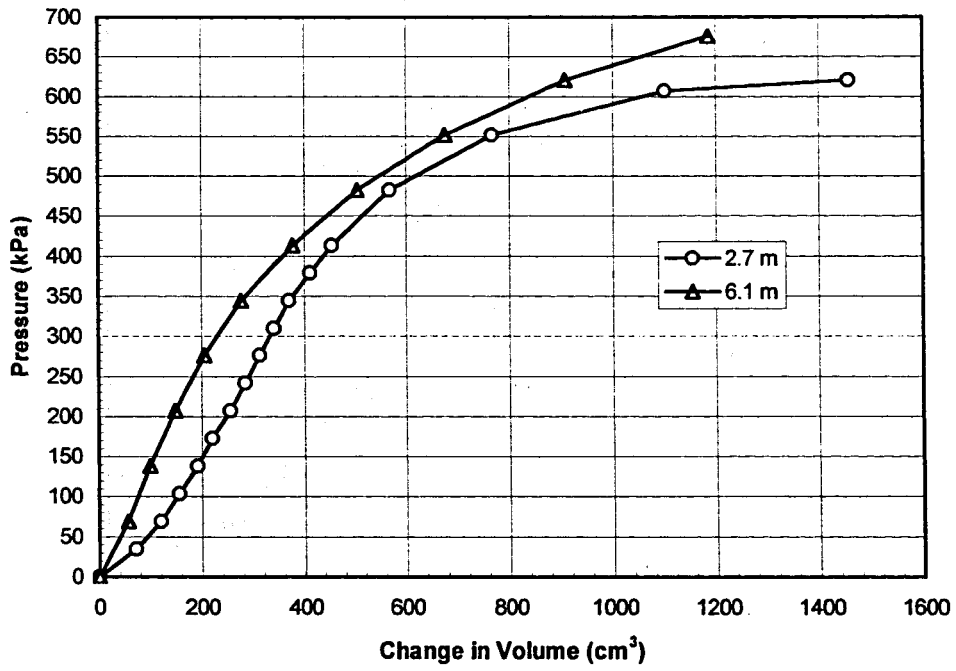
Figure C1. PMT-1 (Prior to rammed aggregate pier installation) (top) pressuremeter curve, (bottom) creep curve
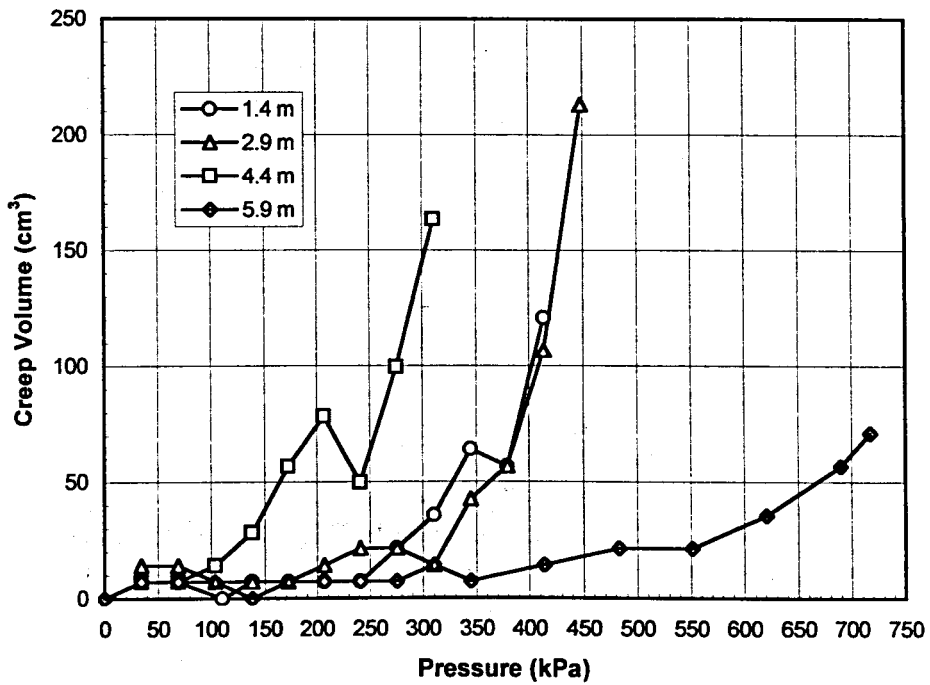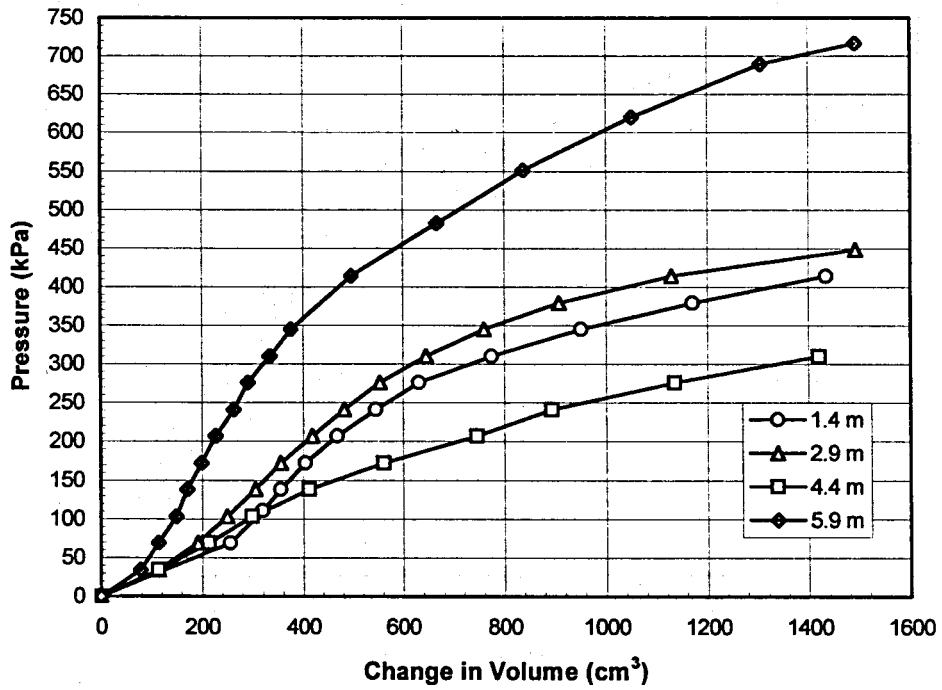
Figure C2. PMT-2 (Prior to rammed aggregate pier installation) (top) pressuremeter curve, (bottom) creep curve
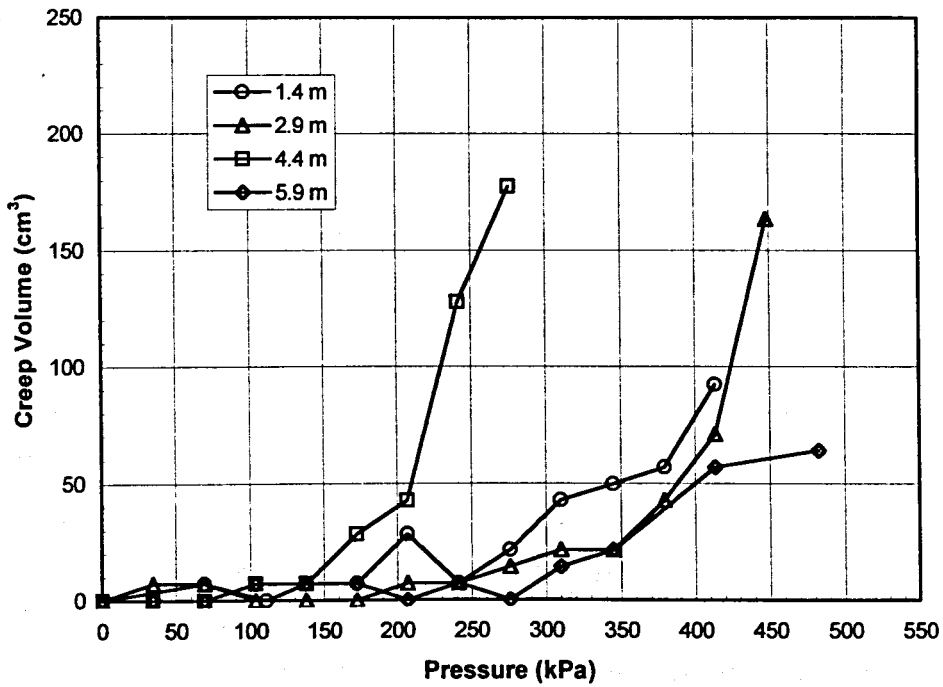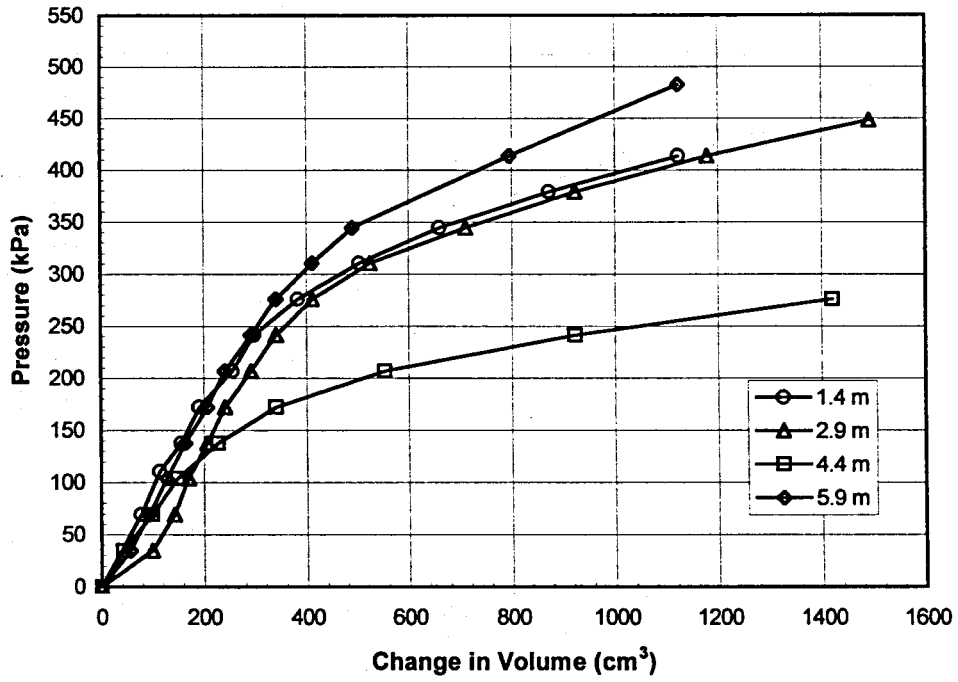
Figure C3. PMT-3 (7 days after installation of rammed aggregate piers) (top)
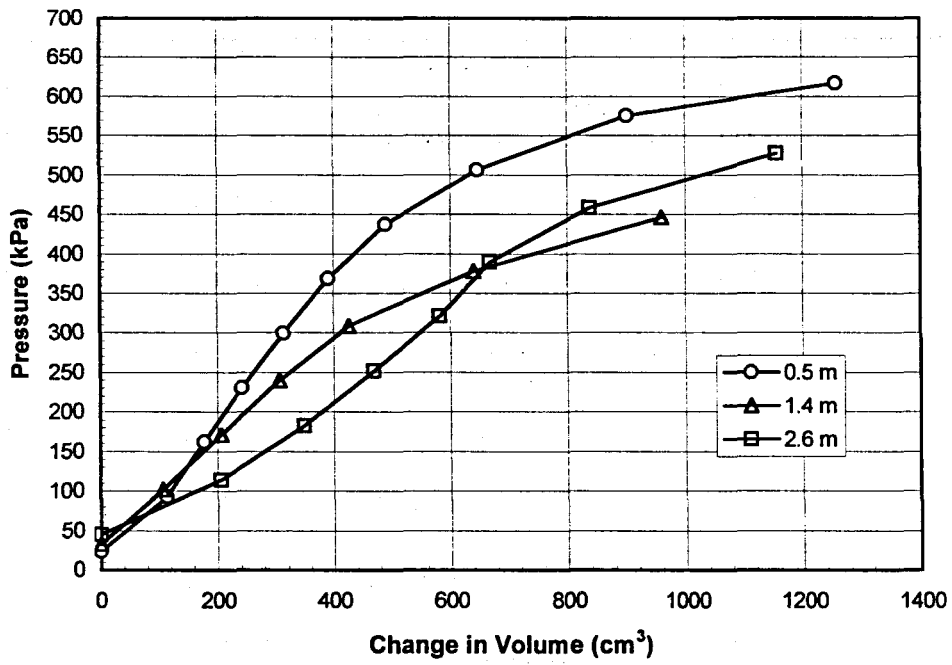pressuremeter curve, (bottom) creep curve
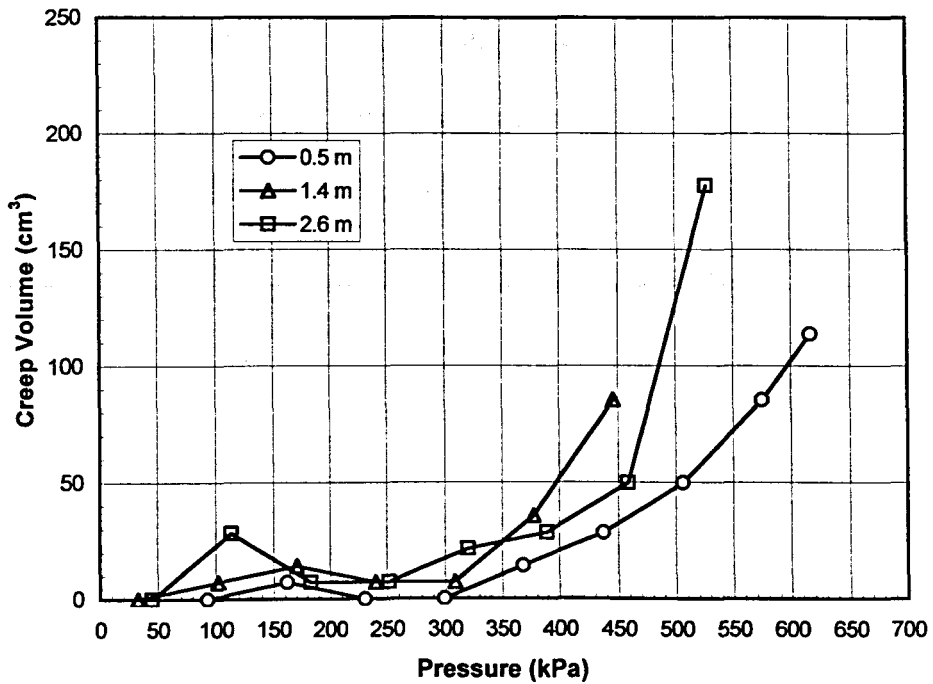
Figure C4. PMT-4 (73 days after installation of rammed aggregate piers) (top)
pressuremeter curve (bottom) creep curve

Table C1. Results of pressuremeter tests 1-4

Depth (m)	Test No.	Time of test	E_o (kPa)	p_L (kPa)
0.5	PMT-4	73 days after piers	5387	620
1.4	PMT-2	Prior to piers	4053	425
1.4	PMT-3	7 days after piers	4288	440
1.4	PMT-4	73 days after piers	3478	475
2.6	PMT-4	73 days after piers	2594	550
2.7	PMT-1	Prior to piers	6508	620
2.9	PMT-2	Prior to piers	3194	475
2.9	PMT-3	7 days after piers	4789	480
4.4	PMT-2	Prior to piers	1884	325
4.4	PMT-3	7 days after piers	3640	300
5.9	PMT-2	Prior to piers	6044	750
5.9	PMT-3	7 days after piers	4667	530
6.1	PMT-1	Prior to piers	7790	700

APPENDIX D:

BOREHOLE SHEAR (BHST) TEST DATA
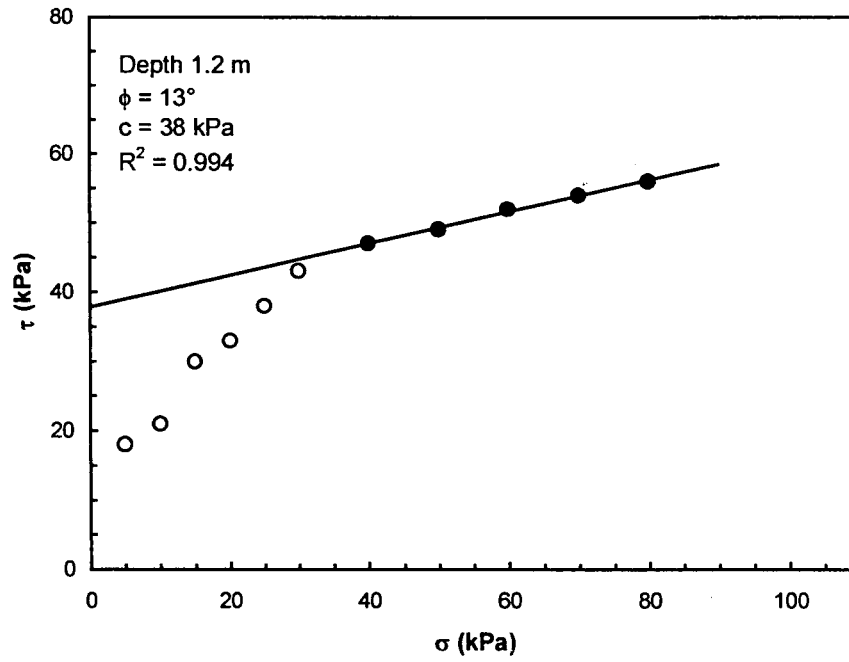
Figure D1. BHST-1 at depth 1.2 m
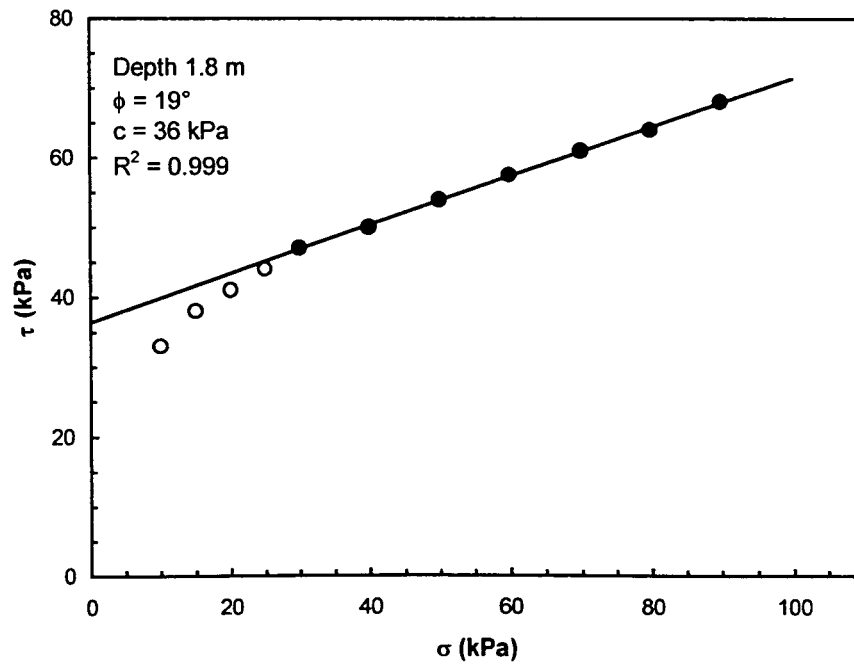
Figure D2. BHST-1 at depth 1.8 m
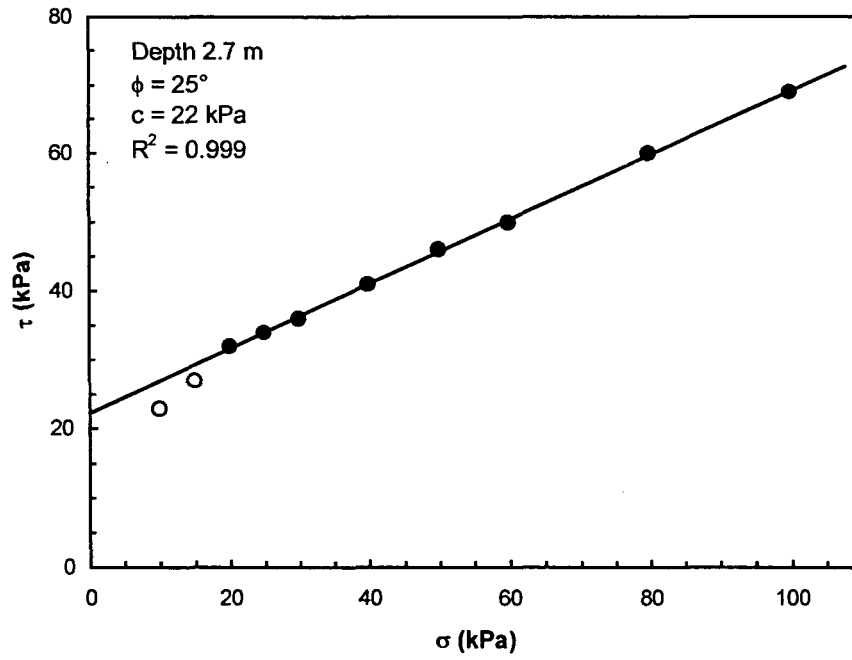
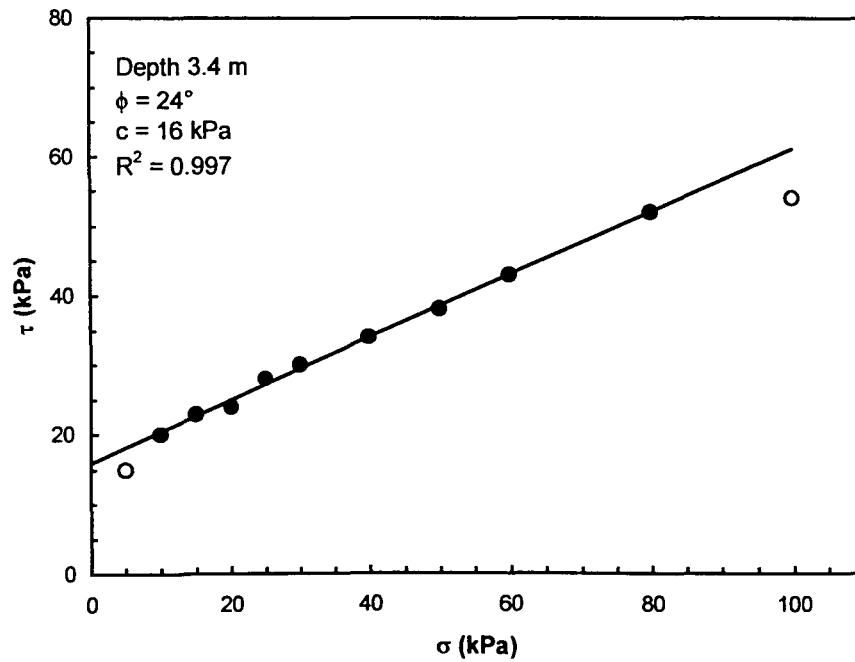**Figure D3. BHST-1 at depth 2.7 m**

Figure D4. BHST-1 at depth 3.4 m
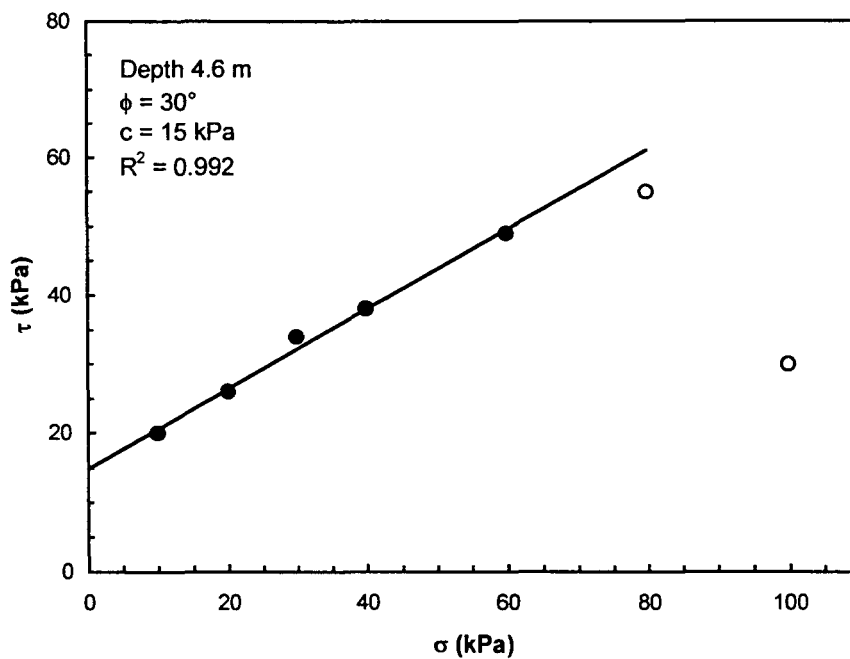
Figure D5. BHST-1 at depth 4.6 m
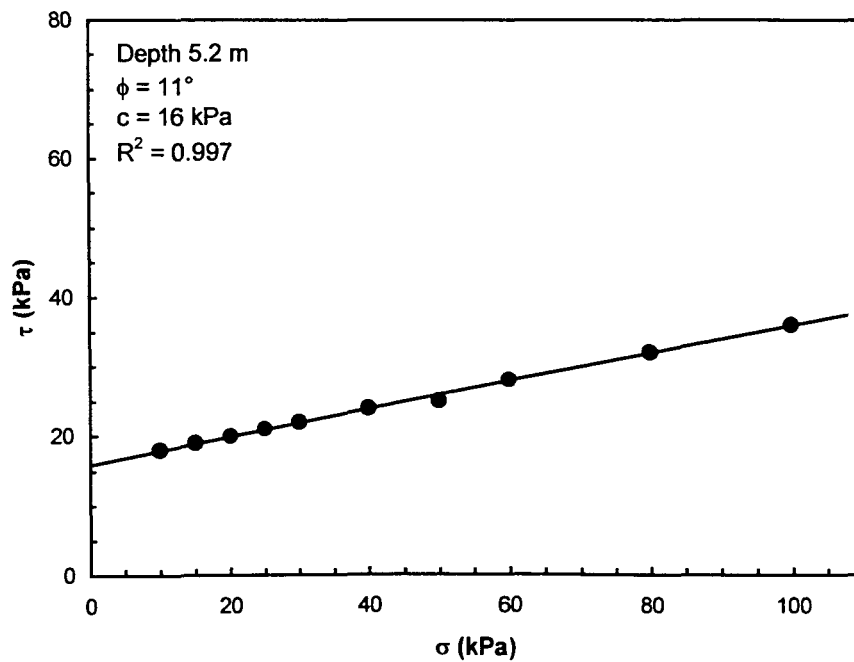
Figure D6. BHST-1 at depth 5.2 m

Table D1. Results of BHST-1

Depth (m)	ϕ (degrees)	c (kPa)	R^2
1.2	13	38	0.994
1.8	19	36	0.999
2.7	25	22	0.999
3.4	24	16	0.997
4.6	30	15	0.992
5.2	11	16	0.997

APPENDIX E:

SQUARE-ROOT-OF-TIME COMPRESSION CURVES
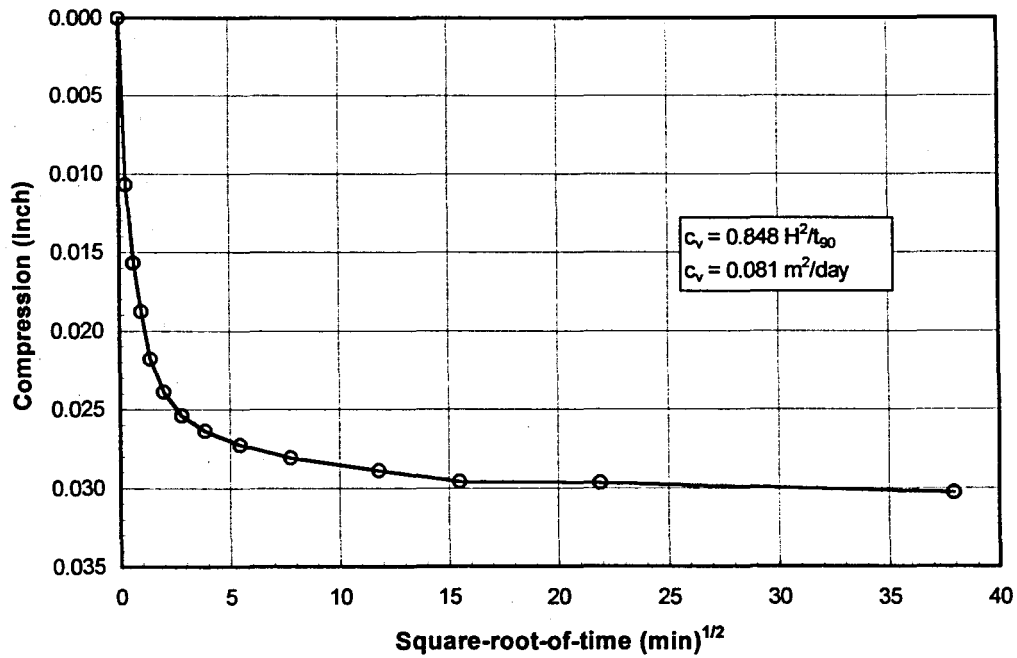
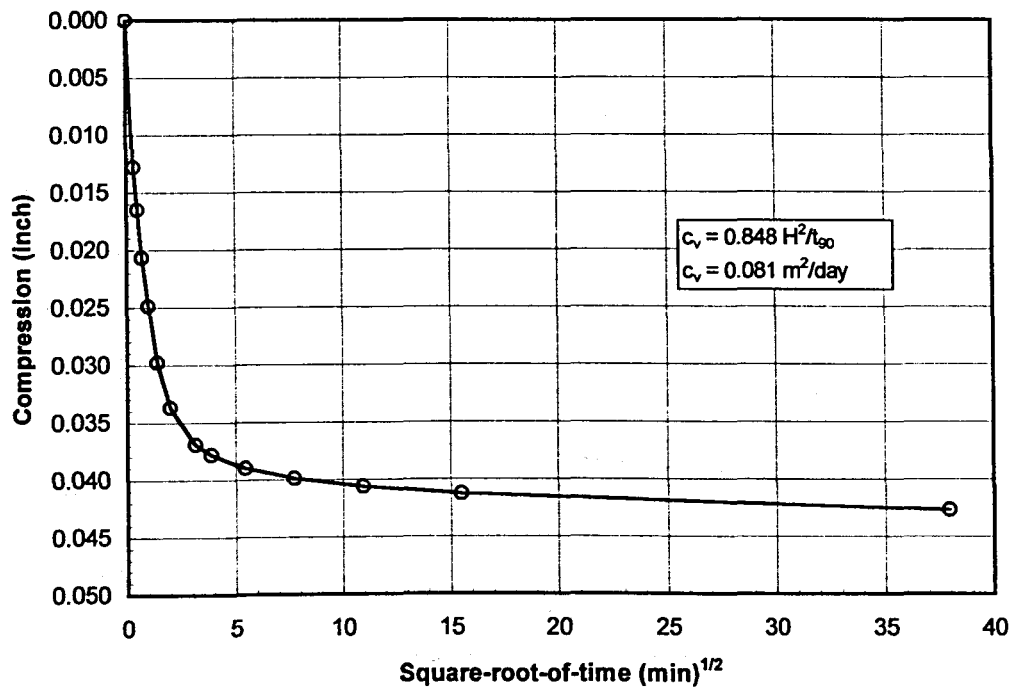**Figure E1. Square-root-of-time compression curve for 100 kPa load increment**

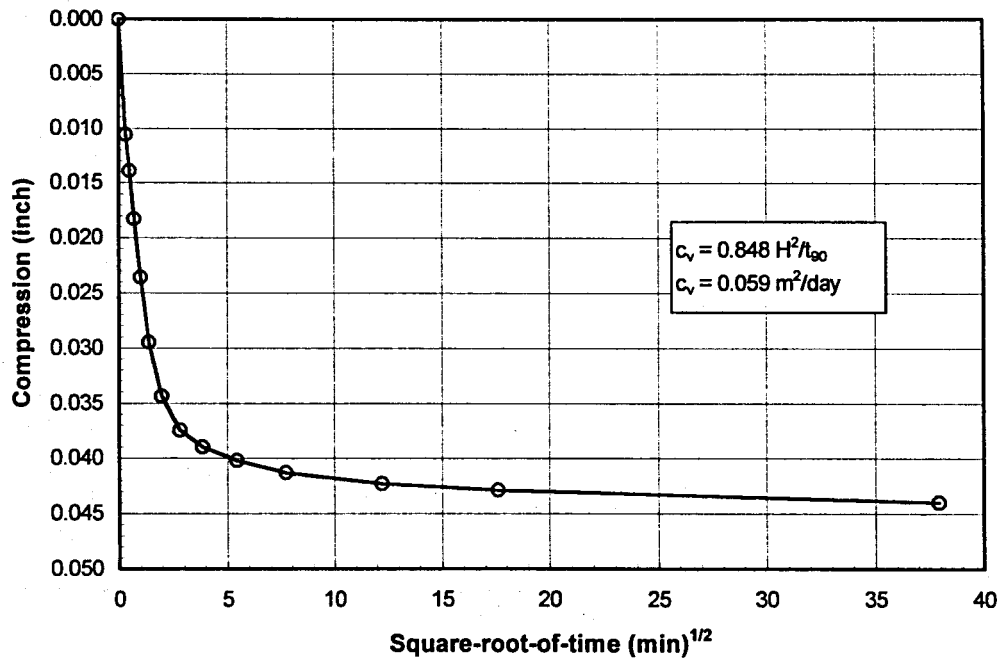**Figure E2. Square-root-of-time compression curve for 200 kPa load increment**

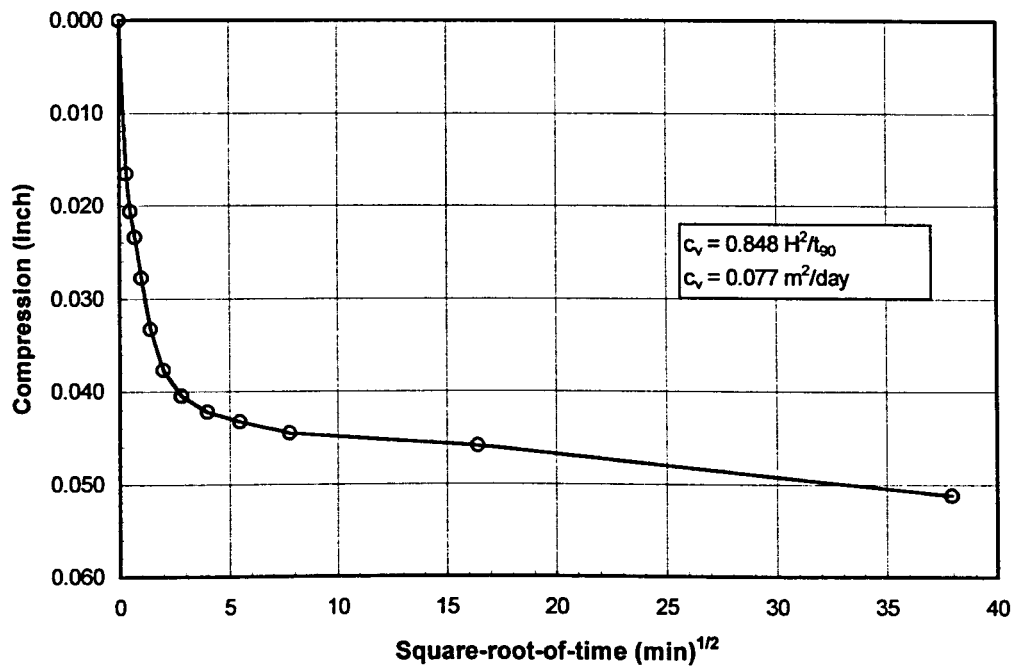**Figure E3. Square-root-of-time compression curve for 400 kPa load increment**

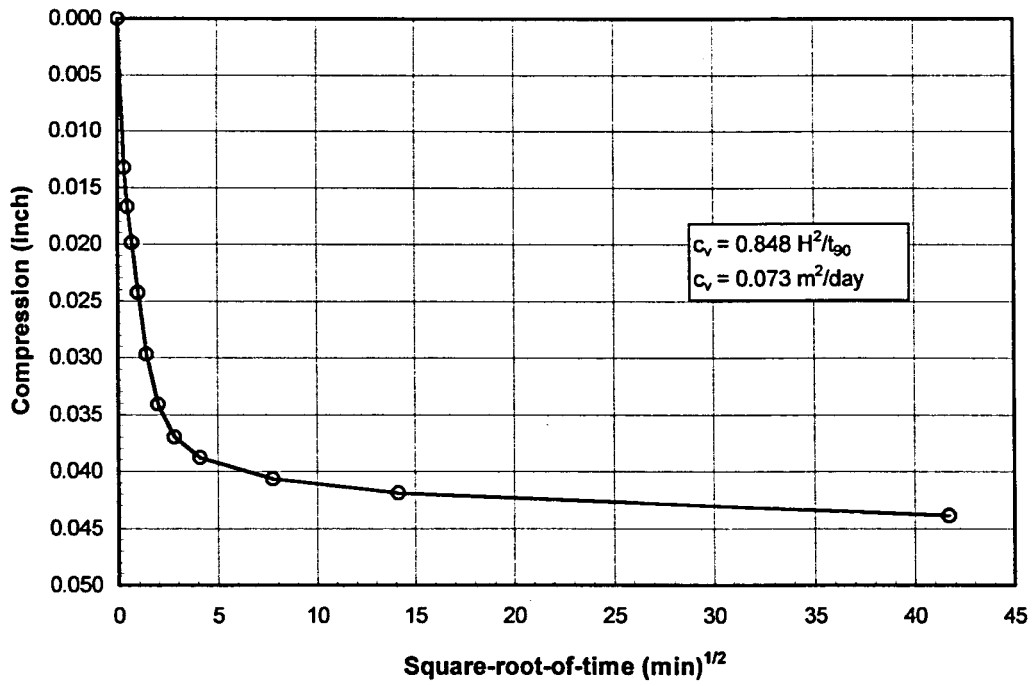**Figure E4. Square-root-of-time compression curve for 800 kPa load increment**

Figure E5. Square-root-of-time compression curve for 1600 kPa load increment

APPENDIX F:

SETTLEMENT ESTIMATES USING CONFINED
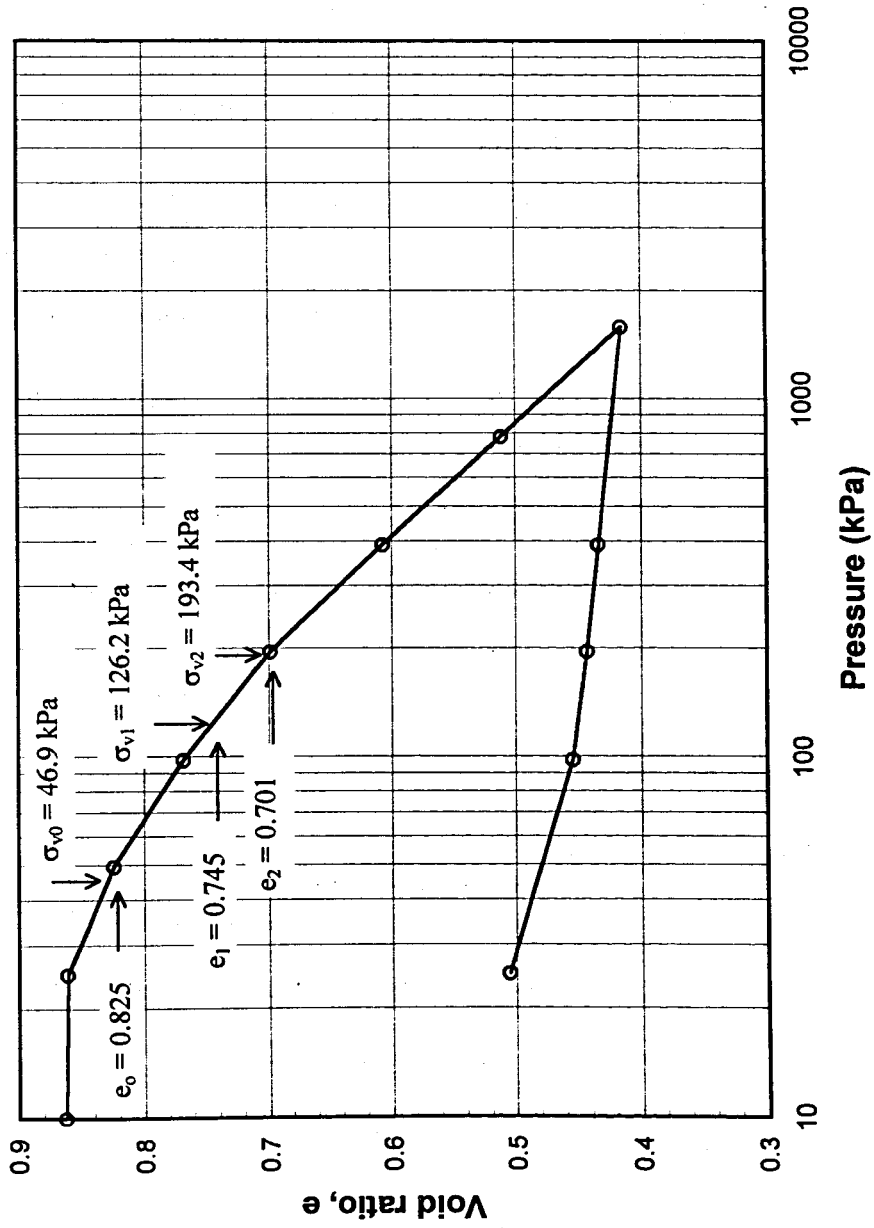
COMPRESSION (OEDOMETER) DATA

Figure F1. e-log-p curve for the compressible clay at 2.7 m depth showing effective stresses at mid-depth of the compressible layer for each stage of construction

Table F1. Stress calculations for the compressible layer

Initial stresses:

Depth		Description	$\Delta\sigma_v$, depth x γ^a	σ_v	u^b	$\sigma_{v, \text{effective}}$
(m)	(ft)		(psf)	(psf)	(psf)	(psf)
0.0	0.0	Ground surface		0.0		
			1259.8			
3.2	10.5	Mid-depth clay layer		1259.8	280.7	979.1
			1102.3			
6.0	19.7	Clay/sand barrier		2362.2	853.9	1508.2

[a] γ = 120 pcf assumed
[b] phreatic surface at 6 ft depth

Increment of stress at mid-depth of the clay layer:

Stage 1 (15 ft fill height)

Depth		L/H	Z/H	Influence	$\Delta\sigma_v$, load[b] x I.F.
(m)	(ft)			Factor, I.F.[a]	(psf)
3.2	10.5	2.8	0.66	0.92	1656

[a] Influence factors from Winterkorn and Fang (1975, p. 167)
[b] γ = 120 pcf assumed

Stage 2 (30 ft fill height)

Depth		L/H	Z/H	Influence	$\Delta\sigma_v$, load[b] x I.F.
(m)	(ft)			Factor, I.F.[a]	(psf)
3.2	10.5	1.4	0.34	0.85	3060

[a] Influence factors from Winterkorn and Fang (1975, p. 167)
[b] γ = 120 pcf assumed

Summary of effective stresses at mid-depth of the clay layer:

$$\sigma_{vo} = 979.1 \text{ psf} \quad = \quad 46.9 \text{ kPa}$$

$$\sigma_{v1} = 2635.1 \text{ psf} \quad = 126.2 \text{ kPa}$$

$$\sigma_{v2} = 4039.1 \text{ psf} \quad = 193.4 \text{ kPa}$$

Table F2. Primary consolidation settlement calculations

$$\rho = \frac{\sum H_0}{1 + e_0} \Delta e$$

where:

ρ = primary consolidation settlement

H_0 = depth of the consolidating soil layer

e_0 = initial in-situ void ratio

Δe = change in void ratio as a result of changes in effective stress

Stage 1 settlement:

$$\rho = \frac{5.6\,m}{1 + 0.825}(0.825 - 0.745) = 0.245\,m = 9.66\,in$$

Stage 2 settlement:

$$\rho = \frac{5.6\,m}{1 + 0.745}(0.745 - 0.701) = 0.141\,m = 5.56\,in$$

Total estimated settlement for unreinforced soil = 0.387 m = 15.22 in

Table F3. Results of settlement estimates using confined compression data

	Settlement	
	(m)	(in)
Stage 1	0.245	9.7
Stage 2	0.141	5.6
Total	0.386	15.2

REFERENCES

Balaam, N. P., and Booker, J. R. (1985). "Effect of stone column yield on settlement of rigid foundations in stabilized clay." *Int. J. Num. Anal. Methods in Geomechanics*, 9(4), p. 331-351.

Barksdale, R. D. and Brachus R. C. (1983). "Design and construction of stone column." Federal Highway Administration, Washington, D. C.

Bowles, J. E. (1996). *Foundation analysis and design*, 5th Edition. McGraw-Hill, New York, New York.

Briaund, Jean-Louis. (1989). "The pressuremeter test for highway applications." Federal Highway Administration Report No. FHWA –IP-89-008.

Brinoli, Enrico, Garassino, Angelo, and Renzo, Pietro. (1994). "The usefulness of stone columns to reduce settlements and distortions – A Case History." *Vertical and Horizontal Deformations of Foundations and Embankments*, Vol. 1, Geotechnical Special Publication No. 40, ASCE, New York, New York, p. 561-570.

Buggy, Fintan J., Martinez, Ramon E., Hussin, James D., and Deschamps, Richard J. (1994). "Performance of oil storage tanks on vibroflotation improved hydraulic fill in the Port of Tampa, Florida." *Vertical and Horizontal Deformations of Foundations and Embankments*, Vol. 1, Geotechnical Special Publication No. 40, ASCE, New York, New York, p. 561-570.

Fox, N. S., and Lawton, E. C. (1993). "Short aggregate piers and method and apparatus for producing same." U.S. Patent No. 5,249,892 issued October 5.

Goughnour, R. R. (1983). "Settlement of vertically loaded stone columns in soft ground." *Improvement of Ground*, Rotterdam, p. 235-240.

Greenwood, D. A. (1970). Mechanical improvement of soils below ground surface." *Proc. Conf. On Ground Engineering*, London, ICE, p. 11-22.

Greenwood, D.A. and Kirsch, K. (1983). "Specialized ground treatment by vibratory and dynamic methods." *Proc. Conf. On Advances in Piling and Ground Treatment for Foundations*, London, Institution of Civil Engineers, p. 17-45.

Handy, R.L. (1976). "Discussion: Measurement of in-situ shear strength, in-situ measurement of soil properties." ASCE, Vol. II, p. 143-149.

Handy, R.L., Remmes, B., Moldt, S., Lutenegger, A.J., and Trott, G. (1982). "In-situ stress determination by Iowa stepped blade." Journal of the Geotechnical Engineering Division, ASCE 108, No. GT11, p. 1405-1422.

Handy, Richard L. (2001). "Does lateral stress really influence settlement?" ASCE Journal of Geotechnical Engineering (Accepted for Publication).

Handy, Richard L., Fox, Nathaniel S., and Wissman, Kord J. (1999). "Short aggregate piers reinforce soils near tunnels." *Geo-Engineering for Underground Facilities,* Geotechnical Special Publication No. 90, ASCE, New York, New York, p. 1039-1047.

Hughes, J.M.O., and Withers, N.J. (1974). "Reinforcing of soft cohesive soils with stone columns." *Ground Engineering,* Vol. 7, No. 3, May, p. 42-49.

Jamiolkowshi, M., Baldi, G., Bellotti, R., Ghionna, V., and Pasqualini, E. (1985). "Penetration resistance and liquefaction of sand." *Proceedings, 11th International Conference on Soil Mechanics and Foundation Engineering,* Vol. 4, San Francisco, p. 1891-1896.

Kulhawy, F.H., and Mayne, P.W. (1990). "Manuel on estimating soil properties for foundation design." EL-6800 Electric Power Research Institute, Palo Alto, California.

Lambe, T. W. and Whitman, Robert V. (1969). *Soil mechanics.* John Wiley & Sons, New York, New York.

Lawton, Evert C., and Fox, Nathaniel S. (1994). "Settlement of structures supported on marginal or inadequate soils stiffened with short aggregate piers." *Vertical and Horizontal Deformations of Foundations and Embankments,* Vol. 2, Geotechnical Special Publication No. 40, ASCE, New York, New York, 962-974.

Lawton, Evert C., Fox, Nathaniel S., and Handy, Richard L. (1994). "Control of settlement and uplift of structures using short aggregate piers." *In-Situ Deep Soil Improvement,* Geotechnical Special Publication No. 45, ASCE, New York, New York, p. 121-132.

Lunne, T., Robertson, P.K., and Powell, J.M. (1997). *Cone penetration testing in geotechnical practice.* Blackie Academic and Professional, New York, New York.

Menard Soltraitement International. (2000). Installation of stone columns. Retrieved October 20, 2000 from the World Wide Web: http://www.menard-soltraitement.com/

Mitchell, J.K. (1981). "Soil improvement: State-of-the-art report." *Proc. 10th ICSMFE,* Stockholm, 4, p. 509-565.

Nagaraj, T.S. (1993). *Principles of testing soils, rocks and concreters.* Elsevier Publishing Co., Amsterdam, Netherlands.

Riaund, Jean-Louis, and Miran, Jerome. (1992). "The cone penetrometer test." Federal Highway Administration Report No. FHWA-SA-91-043.

Robertson, P.K, and Campanella, R.G. (1986). "Guidelines for use, interpretation, and application of the CPT and CPTU." 3rd ed., Hogentogler and Co., Inc.

Robertson, P.K., Campanella, R.G., Gillespie, D., and Grieg, J. (1986). "Use of pressuremeter cone data." *Proceedings of In-situ 86,* ASCE Specialty Conference, Blacksburg, Virginia.

Sanglerat, G. (1972). *The penetrometer and soil exploration.* Elsevier Publishing Co., Amsterdam, Netherlands.

Schmertmann J. H. (1970). "Static cone to compute settlements over sand." *J. Soil Mech. Found. Div.,* Proc. ASCE, 96(SM3), p. 1011-1043.

Schmertmann, J. H., Hartman, J. P., and Brown. P. R. (1978). "Improved strain influence factor diagrams." *J. Geotech. Eng. Div.,* ASCE, 104(GT8), p. 1131-1135.

Schmertmann, J.H. (1976). "Measurement of in-situ shear strength, in-situ measurement of soil properties." ASCE, Vol. II, p. 57-138.

Stewart, Doug, and Fahey, Martin. (1984). "An investigation of the reinforcing effect of stone columns in soft clay." *Vertical and Horizontal Deformations of Foundations and Embankments,* Vol. 1, Geotechnical Special Publication No. 40, ASCE, New York, New York, p. 513-524.

Van Impe, W. F. (1989). *Soil Improvement Techniques and Their Evolution,* Balkema, Rotterdam, The Netherlands.

White, David J., and Handy, R.L. (2001). "Preconsolidation Pressures and Soil Modulii form Borehole Shear Tests." *International Conference on In-situ Measurement of Soil Properties and Case Histories,* May, Bali, Indonesia.

White, David J., Lawton, Evert C., and Pitt, John M. (2000). "Lateral earth pressure induced by rammed aggregate piers." *Proceedings of the 53rd Canadian Geotechnical Conference,* Montreal, Vol. 2, p. 871-876.

Wineland, J.D. (1976). "Borehole shear device, in-situ measurement of soil properties." ASCE, Vol. II, p. 57-138.

Winterkorn, H.F., and Fang, H. (1975). *Foundation engineering handbook.* Van Nostrand Reinhold Co., New York, New York.

ACKNOWLEDGMENTS